DOI:10.14753/SE.2022.2552

MECHANISM OF MODULATED ELECTRO-HYPERTHERMIA INDUCED TUMOR GROWTH SUPPRESSION IN B16F10 MELANOMA PULMONARY METASTASES

PhD thesis

Thomas Mbuotidem Jeremiah

Theoretical and Translational Medicine Doctoral School

Semmelweis University

Supervisor: Zoltán Benyó, MD, D.Sc.

Official reviewers: Eleonóra Nardainé Imrédi, MD, Ph.D.
Zoltán Lohinai, MD, Ph.D.

Head of the Complex Examination Committee: György Losonczy, MD, D.Sc.

Members of the Complex Examination Committee: Lajos Géczi, MD, Ph.D.
Kulka Janina, MD, D.Sc.

Budapest

2021

DOI:10.14753/SE.2022.2552

Table of Contents

DOI:10.14753/SE.2022.2552

DOI:10.14753/SE.2022.2552

List of Abbreviations

(6-4)PPs:	(6-4) Pyrimidone Photoproducts
[^{18}F]FDG:	2-Fluoro[18F]-2-Deoxy-D-Glucose
8-oxodG:	8-Oxo-7,8-Dihydro-2'-Deoxyguanosine
ATM:	Ataxia Telangiectasia-Mutative
ATR:	Ataxia Telangiectasia and Rad3-Related Protein
APAF1:	Mouse Apoptotic Protease Activating Factor 1
ATP:	Adenosine Triphosphate
BID:	BH3 Interacting-Domain Death Agonist
BAK:	Bcl-2 Homologous Antagonist Killer
BRAF:	V-Raf Murine Sarcoma Viral Oncogene Homolog B1
BRAFi:	V-Raf Murine Sarcoma Viral Oncogene Homolog B1 Inhibitor
BSA:	Bovine Serum Albumin
Bcl-2:	B-cell lymphoma 2
Bcl-xL	B-cell lymphoma-extra-large
C57BL/6:	C57 Black 6
Casp3:	Caspase 3
Casp6:	Caspase 6
Casp7:	Caspase 7
Casp8:	Caspase 8
Casp9:	Caspase 9
CCasp3:	Cleaved Caspase-3
CCL5:	Chemokine Ligand 5
CD28:	Cluster of Differentiation 28
CD16:	Cluster of Differentiation 16
CD25:	Cluster of Differentiation 25
CD4:	Cluster of Differentiation 4
CD40:	Cluster of Differentiation 40
CD8:	Cluster of Differentiation 8
CD80:	Cluster of Differentiation 80
CD86:	Cluster of Differentiation 86
CD95:	Cluster of Differentiation 95
CDK:	Cyclin-Dependent Kinase
CDKN2A:	Cyclin-Dependent Kinase 2A
CHPP:	Continuous Hyperthermic Peritoneal Perfusion
CPDs:	Cis-Syn Cyclobutane Pyrimidine Dimers
CRAF:	RAF Proto-Oncogene Serine/Threonine-Protein Kinase
CSD:	Chronically Sun Damaged
CAD:	Caspase-Activated DNase

CTLA-4:	Cytotoxic T-Lymphocyte-Associated Protein-4
CXCL10:	C-X-C Motif Chemokine Ligand 10
CXCL9:	C-X-C Motif Chemokine Ligand 9
dATP:	Deoxyadenosine Triphosphate
DAB:	3,3'-Diaminobenzidine
DAMP:	Damage-Associated Molecular Pattern
DCs:	Dendritic Cells
DD:	Death Domain
DED:	Death Effector Domain
DISC:	Death-Inducing Signaling Complex
DIABLO:	Direct Inhibitor of Apoptosis-Binding Protein with Low pI
DNA:	Deoxyribonucleic Acid
DNMT3a:	DNA (cytosine-5)-Methyltransferase 3a
DSS:	Disease-Specific Survival
DTIC:	Dacarbazine
DR:	Direct
dATP:	Deoxyadenosine Triphosphate
E2F:	Elongation Factor 2
EDTA:	Ethylenediaminetetraacetic Acid
EMA:	European Medicines Agency
ERK:	Extracellular Signal-Regulated Kinase
FADD:	Fas-Associated Death Domain
FasL:	Fas Ligand
FOXP3:	Forkhead Box P3
GM-CSF:	Granulocyte-Macrophage Colony Stimulating Factor
GTP:	Guanosine-5'-triphosphate
H&E:	Hematoxylin and Eosin
H2AX:	H2A Histone Family Member X
HIPEC:	Hyper Thermic Intraperitoneal Chemotherapy
HMGB1:	High-Mobility Group Protein B1
Hsp70:	Heat Shock Protein 70
ICAM-1:	Intercellular Adhesion Molecule 1
ICAD:	Inhibitor of Caspase-Activated DNase
IFNα:	Interferon Alfa
IFNγ:	Interferon Gamma
IgG:	Immunoglobulin G
IHC:	Immunohistochemistry
IAP:	Inhibitors of Apoptosis Proteins
IL-1:	Interleukin-1
IL-10:	Interleukin-10
IL-12:	Interleukin-12

IL-13:	Interleukin-13
IL-2 :	Interleukin-2
IL-35:	Interleukin-35
IL-4:	Interleukin-4
IL-6:	Interleukin-6
INF-α:	Interferon Alfa
iNOS:	Inducible Nitric Oxide Synthase
iTregs:	Induced Regulatory T Cells
JTK:	Janus Tyrosine Kinase
KIRs:	Killer Immunoglobulin-Like Receptors
LIR:	Leukocyte Inhibitory Receptors
MAGE:	Melanoma-Associated Antigens
MAGE-A3:	Melanoma Associated Antigen A3
MAPK:	Mitogen-Activated Protein Kinase
MC1R:	Melanocortin 1 Receptor
M-CSF:	Macrophage Colony Stimulating Factor
MDM2:	Mouse Double Minute 2
MDSCs:	Myeloid-Derived Suppressor Cells
mEHT:	Modulated Electro-Hyperthermia
MEK:	Mitogen-Activated Protein Kinase Kinase
MEM:	Minimum Essential Medium
MHC:	Major Histocompatibility Complex
MITF:	Microphthalmia-Associated Transcription Factor
MPO:	Myeloperoxidase
NCSD:	Non-Chronically Sun Damaged
NEAAs:	Nonessential Amino Acids
NF1:	Neurofibromin 1
NF-kappa B:	Nuclear Factor Kappa-Light-Chain-Enhancer of Activated B Cells
NK Cells:	Natural Killer Cells
NKG2D:	Natural Killer Group 2D
NKT-cells:	Natural Killer T-Cells
NRAS:	Neuroblastoma RAS Viral Oncogene Homolog
NOXA:	Phorbol-12-Myristate-13-Acetate-Induced Protein 1
nTregs:	Natural Regulatory T cells
OS:	Overall Survival
P:	Phosphate
PCNA:	Proliferating Cell Nuclear Antigen
PD-1:	Programmed Cell Death-1
PDGFRA:	Platelet-Derived Growth Factor Receptor Alpha
PD-L1:	Programmed Death-Ligand 1
PD-L2:	Programmed Death-Ligand 2

PET:	Positron Emission Tomography
PFS:	Progression-Free Survival
POT1:	Protection of Telomeres 1 Protein
Procasp8:	Procaspase 8
Procasp9:	Procaspase 9
PUMA:	p53 Upregulated Modulator of Apoptosis
pRb:	Retinoblastoma Protein
RF:	Radiofrequency
RTK:	Receptor Tyrosine Kinase
RIP:	Receptor-Interacting Protein
SCF:	Stem Cell Factor
SEM:	Standard Error of Mean
SASP:	Senescence-associated secretory phenotype
SMAC:	Second Mitochondria-Derived Activator of Caspase
STAT 1:	Signal Transducer and Activator of Transcription 1
STAT3:	Signal Transducer and Activator of Transcription 3
STAT6:	Signal Transducer and Activator of Transcription 6
SUR:	Standardized Uptake Ratio
SURmax:	Maximum Standardized Uptake Ratio
SUV:	Standardized Uptake Values
SUVmax:	Maximum Standardized Uptake Values
TBS:	Tris-Buffered Saline
TBST:	Tris-Buffered Saline With Tween 20
TCR:	T-Cell Receptor
TERF2IP:	Telomeric Repeat-Binding Factor 2 Interacting Protein
TERT:	Telomerase Reverse Transcriptase
TGFβ:	Transforming Growth Factor Beta
TLRs:	Toll-Like Receptors
TNF:	Tumor Necrotic Factor
TNFR:	Tumor Necrosis Factor Receptor
TNF-α:	Tumor Necrosis Factor Alpha
TRADD:	Tumor Necrosis Factor Receptor-Associated Death Domain
TRAF:	Tumor Necrosis Factor Receptor–Associated Factor
Tregs:	Regulatory T-cells
Triple-WT:	Triple-Wild Type
T-VEC:	Talimogene Laherparepvec
UV:	Ultraviolet
UVA:	Ultraviolet A
UVB:	Ultraviolet B
UVC:	Ultraviolet C
UVR:	Ultraviolet Radiation

DOI:10.14753/SE.2022.2552

VEGF:	Vascular Endothelial Growth Factor
VEGFR2:	Vascular Endothelial Growth Factor Receptor 2
αMSH:	α Melanocyte-Stimulating Hormone
γ-H2AX:	Phosphorylated H2A Histone Family Member X

DOI:10.14753/SE.2022.2552

1. Introduction

1.1. Epidemiology

Melanoma is a type of cancer arising from the unregulated proliferation of pigment-producing melanocytes (1-3). Melanoma of the skin, leptomeninges, and uveal tract have been extensively described, although, cutaneous melanoma remains the most prevalent and most lethal form of skin cancer (4, 5) and thus will be the subject of focus of this chapter. Over the past 50 years, a significant increase in the incidence of melanoma has been observed in comparison to almost any other type of cancer (6-8). It is a highly aggressive cancer with a tendency to metastasize beyond the primary site relatively early (4, 9). Over the last several decades, a steady increase in the incidence of melanoma has been observed worldwide (10, 11). A significant increase in the annual incidence of 4-6 % has been observed in Caucasian populations that predominate regions such as New Zealand, Northern Europe, North America, and Australia (12-14) (Figure 1). This is most prominently due to the decrease in melanin and the consequential decrease in photoprotection seen in these populations (15). In contrast, darker skin populations show significant photoprotection from ultraviolet (UV) A and B radiation due to the significantly higher melanin in the skin (12, 13, 15). Ultraviolet radiation is considered the most important risk factor of melanoma due to its ability to induce malignant transformation of skin cells (14, 16, 17).

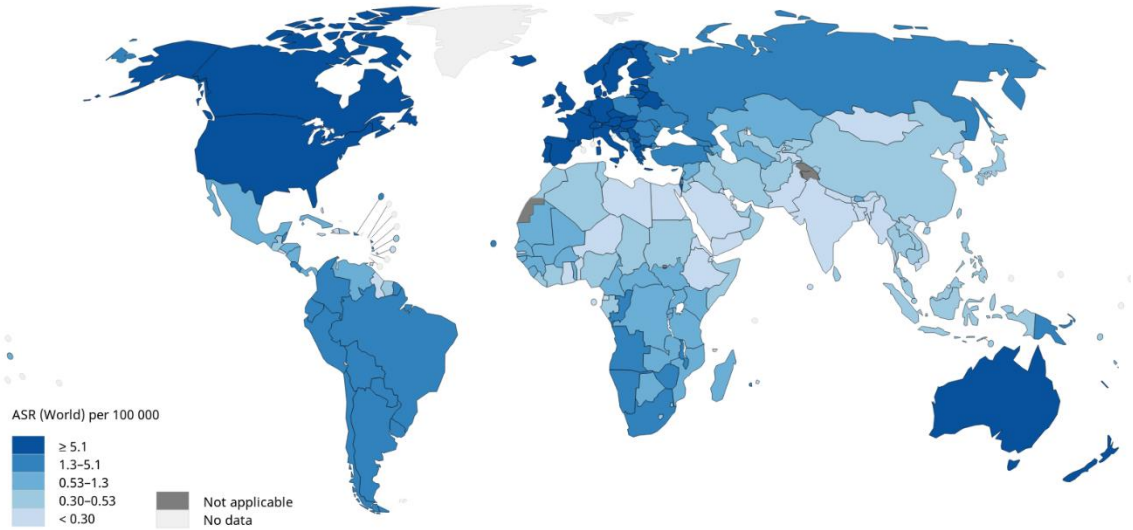

Figure 1. Worldwide melanoma age-standardized incidence rate (2020), both sexes, age 0-74, by geography. Modified from the original figure of Cancer Today (18).

Fair-skinned populations can attenuate UVB radiation by only 50 % compared to the darker-skinned population (15). Differences in geography play a significant role in the incidence of melanoma among people with similar ethnicity (19). Geographical differences can result in variations in seasons, altitude, atmospheric absorption, latitude, and cloud cover which as a result influences the amount of UV radiation in contact with the skin. Melanoma incidence has been reported to increase with increasing proximity to the equator (19). In Australia, populations living close to the equator with higher exposure to sunlight experience an increased incidence of melanoma compared to populations farther from the equator (20). For example, a higher incidence of melanoma is observed in the predominantly tropical state of Queensland (latitude 27 °S) compared to the non-tropical region of New South Wales (latitude 34°S) in Australia (21, 22).

From a public health perspective, melanoma presents a unique problem with a considerable burden to public health and a substantial annual cost of management (23). In the United States alone, the annual cost of melanoma management is estimated to have increased by 288% over the last decade and out of the $8.1 billion direct annual costs of skin cancer, melanoma comprised a total of $3.3 billion (23), while the indirect cost of melanoma is estimated to be over $3.5 billion annually (24). Subsequently, the cost of treatment is significantly high and is projected to increase as the incidence of melanoma increases (23). The direct and indirect cost of melanoma management may subsequently be reduced if adequate population-based control strategies are implemented. With the help of epidemiological studies, investigators can now identify populations at risk which helps in developing population-based control of melanoma incidence through preventive methods, management strategies, and treatments (21).

1.2. Pathogenesis and risk factors of melanoma

1.2.1. Exogenous factors in the development of melanoma

Ultraviolet radiation (UVR) can be classified into UVA, UVB, and UVC. UVR is well-known to be the main environmental risk factor for developing primary cutaneous melanoma in the world. Of the three types of UVR, UVC is thought to be a minor contributor to skin cancer since the atmospheric ozone layer blocks most of it from reaching the earth's surface (22). Ultraviolet radiation can induce significant DNA damage directly or indirectly in living organisms. The dimerization of pyrimidines in

DNA is a common after-effect of UV irradiation resulting in the formation of pyrimidine (6-4) pyrimidone photoproducts ((6-4) PPs) and cis-syn cyclobutane pyrimidine dimers (CPDs) as major products (Figure 2).

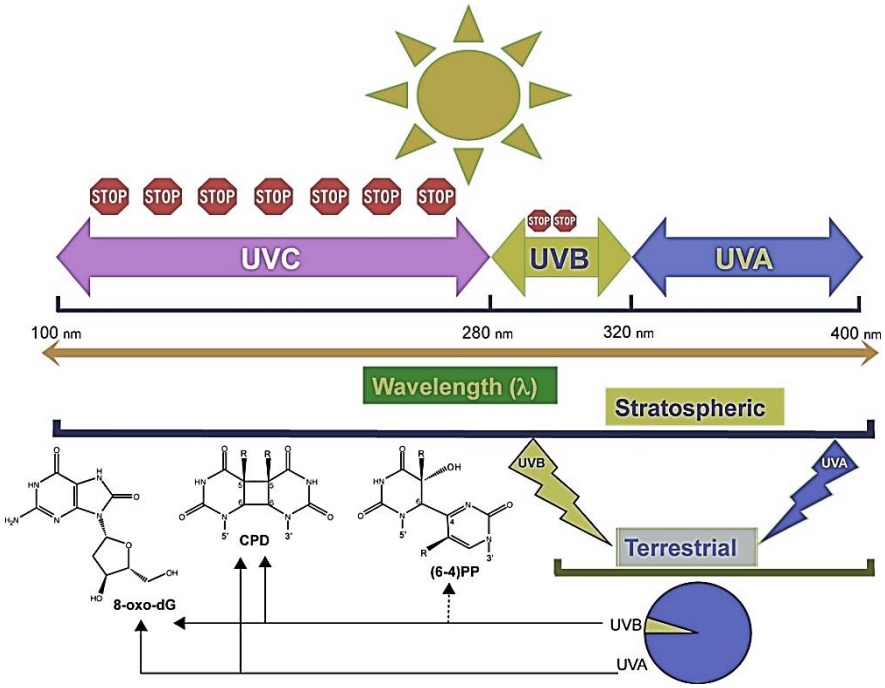

Figure 2. Photoproducts of UVB and UVC irradiation on DNA at different wavelengths (UVA: ultraviolet A, UVB: ultraviolet B, UVC: ultraviolet C, 8-oxo-dG: 8-oxo-7,8-dihydro-2'-deoxyguanosine, CPD: cis-syn cyclobutane pyrimidine dimers, (6-4)pp: (6-4) pyrimidone photoproducts). Modified from the original figure of Pfeifer GP et al. (2012) (25)

In comparison to UVB and UVC, UVA irradiation can also induce CPDs although at a low level making it less mutagenic (26, 27). UVA and UVB further promote indirectly the formation of oxidized DNA bases such as 8-oxodG (8-oxo-7,8-dihydro-2'-deoxyguanosine) (28-32). The DNA damage and formation of corresponding photoproducts following UVA and UVB irradiation occur at different wavelengths as indicated in Figure 2. However, UV radiation with shorter wavelengths is blocked by oxygen and the ozone layer in the atmosphere, and thus not a major risk factor for developing melanoma (Figure 2, "stop" sign) (25).

1.2.2. Endogenous factors in the development of melanoma

Genetic factors play a significant role in the occurrence of melanoma. In contrary to many other cancer types, multiple genes of different penetrance affects the lifetime risk and susceptibility of developing melanoma as described in Table 1.

Table 1. Genetic mutations involved in the development of melanoma (33)

Gene Penetrance	Gene	Encoded Protein	Role
High-penetrance	CDKN2A	$p16^{INK4a}$	Cell cycle regulator
		$p14^{ARF}$	Cell cycle regulator
	CDK4	CDK4	Cell cycle regulator
	TERT	Catalytic subunit of telomerase	Telomere elongation
	POT1	POT1	Telomere maintenance
Intermediate-penetrance	MC1R	MC1R	Melanin synthesis and melanocyte proliferation
	MITF	MITF	Melanocyte development and differentiation

(CDKN2A: cyclin-dependent kinase 2A, CDK4: cyclin-dependent kinase 4, TERT: telomerase reverse transcriptase, POT1: protection of telomeres 1, MC1R: melanocortin 1 receptor, MITF: microphthalmia-associated transcription factor)

1.2.2.1. High-penetrance genes

CDKN2A is a high-penetrance gene that results in a significant predisposition to melanoma. It is found in about 20% - 40% of high-risk families for melanoma (38, 39). CDKN2A is a tumor suppressor gene that encodes the cell cycle regulator proteins p14ARF (p14) and p16INK4A (p16) (Table 1). p14 in its self is also a tumor suppressor capable of inducing cell cycle arrest leading to apoptosis via the p53 pathway. p16 on the other hand inhibits protein phosphorylation of retinoblastoma (RB) *via* a cyclin-dependent kinase 4 (CDK4) leading to cell cycle arrest in the G1 phase (34).

Another high-penetrance gene is the CDK4 oncogene which encodes the binding partners of p16, mutation of which results in an increased risk of developing melanoma. Mutation in CDK4 leads to uninhibited CDK4 kinase activity due to the inability of p16 to bind and regulates its activity, resulting in increased phosphorylation of retinoblastoma bound to elongation factor 2 (E2F) transcription factors. As a result, E2F release is

increased leading to pro-S phase cell cycle genes activation that promotes the transition from G1 to S phase of the cell cycle (34).

Additionally, TERT genes have been demonstrated to play a significant role in melanoma development and like CDKN2A and CDK4, is a high-penetrance gene. TERT encodes the ribonucleoprotein complex, a catalytic subunit of telomerase responsible for maintaining telomere length. Mutations in TERT result in higher telomerase expression leading to telomere stabilization with an effect on cell senescence, aging, and turnover (35, 36). POT1 is another high-penetrance gene, necessary for the maintenance of telomere. POT1 alongside TERF2IP and ACD are members of the shelterin complex genes and early-onset melanoma has been demonstrated to be significantly higher in families carrying POT1, TERF2IP, and ACD gene mutations (37-39).

1.2.2.2. Intermediate-penetrance genes

As described in Table 1, MCIR and MITF are two genes with intermediate penetrance, mutations of which increase significantly the risk of developing melanoma. MCIR gene is involved in cutaneous pigmentation *via* encoding of G-protein coupled receptor that binds α melanocyte-stimulating hormone (αMSH). cAMP-induced tyrosinase activity is increased when αMSH binds to melanocortin 1 receptor (MC1R). The cumulative effect of this results in the synthesis of eumelanin. R alleles of MCIR variants notably are involved with an increased risk of melanoma development (40). The ability of MCIR to influence the risk of melanoma development is mediated *via* its effect on UV sensitivity, pigmentation, DNA repair mechanisms, cell differentiation, proliferation, and regulation of melanocytes (41). On the other hand, MITF is another gene with intermediate penetrance that plays a role in the regulation of melanocytes homeostasis and influences cell proliferation, survival, and differentiation (42). Increase susceptibility to familial melanoma has been demonstrated in families with MITF gene mutation (43, 44).

1.3. Molecular subtypes of melanoma

1.3.1. BRAF subtype

Due to its role in cellular growth control, survival, and invasion, the mitogen-activated protein kinase (MAPK) pathway is involved in the pathogenesis of several cancers. MAPK signaling pathway starts when receptor tyrosine kinase (RTK) activates the protein RAS. Activated RAS causes the recruitment of specific RAF proteins into the

membrane, following which RAF phosphorylates the mitogen-activated protein kinase kinase (MEK), a prominent protein kinase that phosphorylates extracellular signal-regulated kinase (ERK). ERK is responsible for the direct and indirect activation of multiple transcription factors necessary for cell survival and proliferation (45-48). Activation of these pathways mostly occurs in the presence of BRAF (V-Raf Murine Sarcoma Viral Oncogene Homolog B1) mutation of which results in the uncontrollable proliferation and survival of melanoma cells (49) (Figure 3). BRAF mutations in the case of non-chronically sun damaged (NCSD) melanomas have been demonstrated to be more frequent than in chronically sun-damaged (CSD) melanoma, acral melanoma, and UV-activated mucosal melanoma. The BRAF subtype is also more prevalent in younger patients compared to other subtypes of melanoma (50).

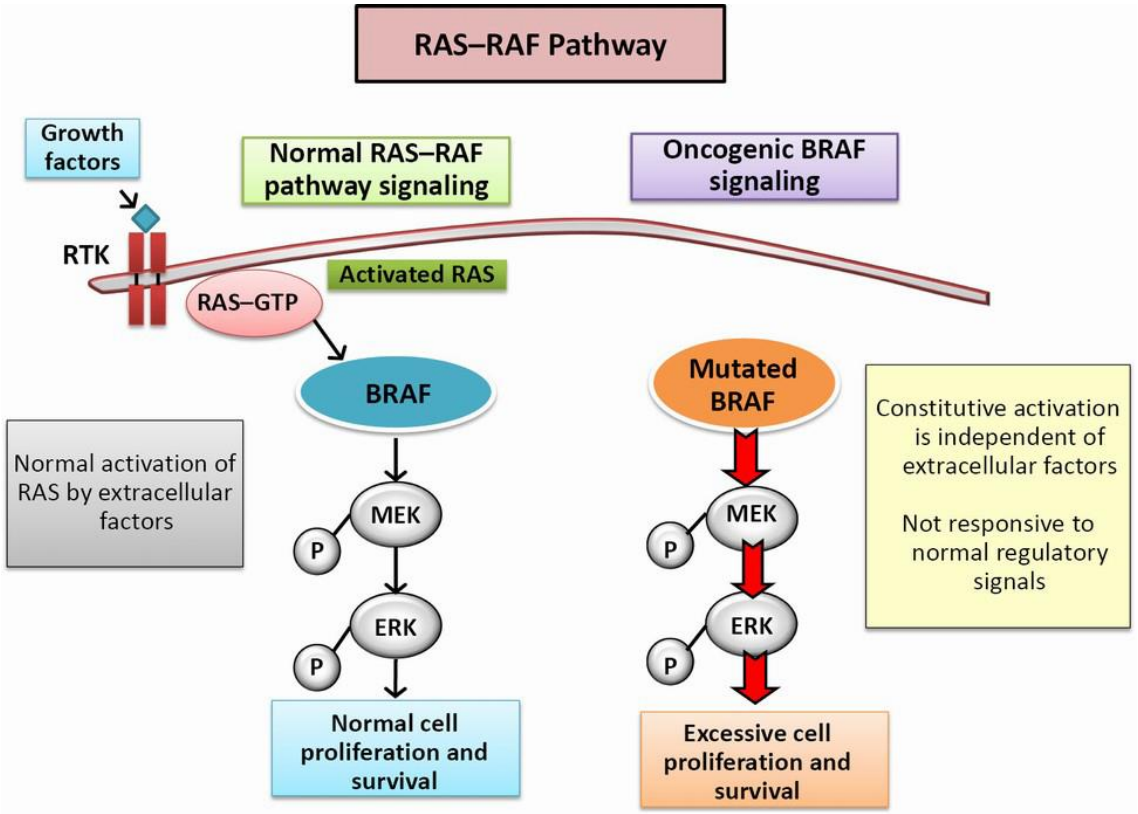

Figure 3. Genetic alterations in the MAPK pathway that constitutes the molecular subtypes of melanoma (RAS: rat sarcoma virus protein, RAF: rapidly accelerated fibrosarcoma, GTP: guanosine-5'-triphosphate, BRAF: V-Raf murine sarcoma viral oncogene homolog B1, MEK: mitogen-activated protein kinase kinase, ERK: extracellular signal-regulated kinase, P: phosphate). Modified from the original figure of Munoz-Couselo E et al. (2015) (51)

1.3.2. RAS subtype

The second major melanoma subtype consists of RAS mutations, which mostly include NRAS Q61K/L/R or NRASG121D. These are missense mutations that lead to a substitution of an amino acid at 12, 13, or 61 positions. The presence of somatic mutations in NRAS locus has been demonstrated in 13-25% of all malignant melanomas. The consequence of these mutations is a major NRAS activation and subsequent MAPK signal pathways activation (52-54). Interestingly, RAS mutations in congenital nevi are common, and in inherited nevi are absent. However, in CSD skin melanomas, NRAS mutations are more common (55).

1.3.3. NF1 subtype

Mutations in Neurofibromin 1 (NF1) protein that negatively regulate RAS proteins are the third most frequent mutation in the MAPK signaling pathway. NF1 is a Guanosine Triphosphatase (GTPase)-activating a protein known to reduce RAS activity *via* GTPase activation. NF1 loss of function is an alternative way to activate the MAPK signaling pathway (56). The mutations in NF1 define some subtypes of melanoma, primarily desmoplastic melanoma (57).

1.3.4. Triple wild-type subtype

Triple wild type (Triple-WT) melanoma is characterized by the absence of BRAF, NRAS, or NF1 mutations. Somatic copy-number alteration studies have shown that Triple-WT melanoma had significantly more alterations in the copy-number which was enhanced with critical amplifications targeting known oncogenes (58). Oncogenes such as transmembrane receptor tyrosine kinase (KIT), platelet-derived growth factor receptor alpha (PDGFRA), and vascular endothelial growth factor receptor 2 (VEGFR2) have been demonstrated to be often amplified. Some of the BRAF/NRAS/NF1 wild-type melanomas also show amplification in vital oncogenes such as cyclin D1 and Cyclin-dependent kinase 4 (CDK4), mouse double minute 2 (MDM2), and Telomerase Reverse Transcriptase (TERT) (59).

DOI:10.14753/SE.2022.2552

1.4. Therapeutic options in the management of melanoma

1.4.1. Surgical management of melanoma

Local excision is the standard treatment for primary skin melanoma and can often cure localized small tumors without metastases. Because abnormal melanocytes frequently occur in the epidermis around the tumor, extensive local excision is often required (60). Depending on the tumor thickness and site, the scar is excised with a margin of 1-2 cm and sentinel node biopsy is performed for staging where appropriate. A complete lymphadenectomy of the affected region is indicated in cases of clinically detected regional lymph node metastases or metastatic sentinel nodes. Resectable metastases with narrow, yet clear margins are excised. Surgical treatment in the case of distant metastases of cancer can be considered as either a life prolongation procedure or strictly as a palliative therapy (61).

1.4.2. Chemotherapeutic management of melanoma

Chemotherapy was the treatment option for metastatic melanoma before 2011 when ipilimumab and vemurafenib were introduced. Dacarbazine (DTIC) is an alkylating agent that incorporates alkyl groups into guanine bases in DNA and induces apoptosis as a consequence. For decades, DTIC was used to treat metastatic melanoma at a 10-20 % response rate. However, in a phase III trial, the DTIC was never shown to raise overall survival (OS). There have been efforts to improve the OS by chemotherapy but without success. Temozolomide is often favored as it is an oral DTIC analog that demonstrates similar effects in metastatic melanoma treatment (62).

1.4.3. Targeted therapy in the management of melanoma

In 2011, the first orally available selective antagonists of BRAF (BRAFi), vemurafenib, were approved nine years after the discovery of common BRAF mutations in melanoma. It attaches to BRAF proteins induced by V600 mutations (63). In 2012 the European Medicines Agency (EMA) approved vemurafenib for use in unresectable stage III or IV melanoma. The second BRAFi, dabrafenib, was authorized in 2013 after sustained progression-free survival (PFS) interaction in BRAFV600-mutant melanoma was demonstrated (64). However, BRAFi therapy demonstrates significant adverse effects such as headache, hyperkeratosis, pyrexia, fatigue, and arthralgia. New dermal

neoplasms, particularly skin squamous cell carcinoma, are also a common side effect. The new dermal neoplasms are formed due to paradoxical activation of RAF proto-oncogene serine/threonine-protein kinase (CRAF) in the BRAF-wild type cells which promote the development of premalignant RAS-mutant cells (63).

1.4.4. Immunotherapy in the management of melanoma

1.4.4.1. Immunotherapeutic effects of cytokines

Interferons are a family of white blood cells-derived molecules produced to react with pathogenic agents or foreign antigens. Interferons play significant roles in immunology and in tumor cells are involved in the downregulation of the cell cycle, induction of apoptosis increases expression of tumor antigens, and plays a role in the activation of T-lymphocytes (65). Recombinant interferon α-2b has been licensed as an adjuvant melanoma therapy by European Medicines Agency (EMA) since the year 2000 (66). Additionally, recombinant IL-2 has been approved and used in the United States for several decades in metastatic melanoma therapy with a 5-27 % response rate (67).

1.4.4.2. Immunotherapeutic effects of checkpoint inhibitors

The advent of checkpoint inhibitors contributed to a revolution in the treatment of metastatic melanoma. Cytotoxic T-lymphocyte-associated protein-4 (CTLA-4) is a prominent checkpoint protein that negatively regulates the activation of T-cell (Figure 4). The first checkpoint inhibitor to improve overall survival in metastatic melanoma was Ipilimumab, a monoclonal antibody that blocks CTLA-4 and thus increases the anti-tumor T-cell immunity. Programmed cell death-1 (PD-1) is another check-point protein *via* which tumor cells can escape the immune system. Tumor cells can associate with PD-1 on T-cells by expressing their ligands, programmed death-ligand 1 (PD-L1), and programmed death-ligand 2 (PD-L2), thereby inhibiting T-cell activation and proliferation (68) (Figure 4). Pembrolizumab and nivolumab are monoclonal antibodies that bind to and block PD-1 on lymphocytes and have been demonstrated to have a significant increase in survival when compared to chemotherapy. Both antibodies are approved for the treatment of metastatic melanoma by EMA since 2015 (69).

DOI:10.14753/SE.2022.2552

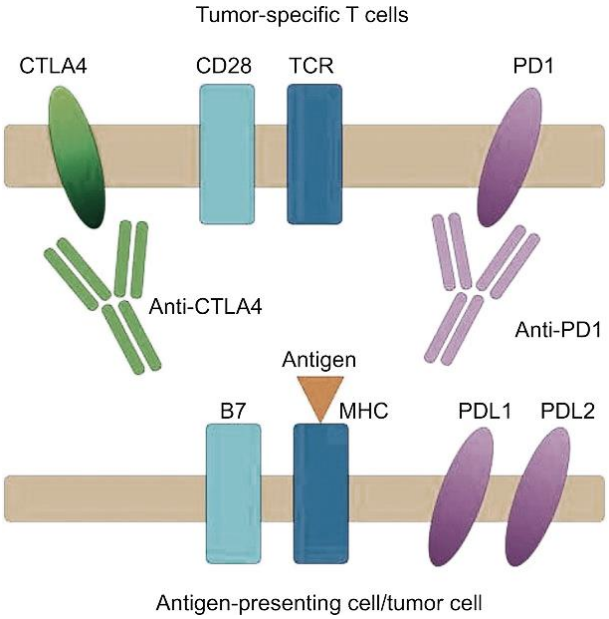

Figure 4. Checkpoint inhibitors and their mechanisms of action (CTLA4: cytotoxic T-lymphocyte-associated protein-4, CD28: cluster of differentiation 28, TCR: T-cell receptor, PD1: programmed cell death-1, Anti-CTLA4: anti-cytotoxic T-lymphocyte-associated protein-4, Anti-PD1: anti-programmed cell death-1, MHC: major histocompatibility complex, PDL1: programmed death-ligand 1, PDL2: programmed death-ligand 2). Modified from the original figure of Karlsson AK et al. (2017) (70)

1.4.5. Radiotherapy in the management of melanoma

Melanoma is traditionally regarded as radiation-resistant cancer (71). However, the risk of regional relapse following lymphadenectomy in high-risk stage III melanoma may be reduced by adjuvant radiation therapy (72-74). The effect is seemingly greater for cervical lymph nodes, with the highest risk of complications, such as lymphedema, delayed healing, and fibrosis, seen with irradiation to regional inguinal lymph nodes. While the majority of studies, including a recent randomized trial, have shown that adjuvant radiotherapy provides no survival benefit (72, 74), a retrospective study of > 600 patients revealed longer disease-specific survival (DSS) independently associated with radiation therapy (73). In a different retrospective study, improved survival was correlated only with a cumulative dose of > 50 Gy. Radiotherapy is also used in the palliative management of distant metastases. Furthermore, stereotactic radiosurgery is a viable alternative to surgical procedures for limited (<3 cm) metastasis and brain oligometastatic melanoma diseases (75).

1.4.6. Oncolytic viruses in the management of melanoma

Numerous viruses can infect tumor cells, resulting in the activation of tumor-specific T-cells. T-VEC (Talimogene laherparepvec) is a genetically modified herpes simplex virus, which can induce systemic and local antitumoral responses when injected into nodular melanoma metastases, cutaneous metastases, and subcutaneous metastases (76). A phase III randomized trial of 436 patients with unresectable type IIIB-IVM1c melanoma demonstrated a 26 % overall response rate and 11 % complete response in T-VEC treated patients. The sub-group analysis revealed that only patients with stage IIIBIVM1a disease exhibited a clinical benefit. In 2015, EMA approved T-VEC for unresectable stage III IVM1a melanoma (77).

1.4.7. Antigen-based active immunotherapy in the management of melanoma

Melanoma-associated antigens (MAGE) are a group of related proteins commonly found in tumor tissues but not in normal tissues except for testis and placenta (78). Over the past several years, studies have focused on developing immunotherapy composed of MAGE-A3, which is often present on the surface of melanoma cells, along with an immune-stimulant. The immunotherapy induces an antigen-specific immune response within the host. When 36 patients with MAGE-A3-positive, unresectable stage III-IVM1a melanoma were administered intramuscularly with recombinant MAGE-A3 and immunostimulant AS15 in a phase II trial, four patients (11 %) showed an objective response and superior overall survival compared to the control group (79).

1.4.8. Adoptive cell therapy in the management of melanoma

Adoptive cell therapy fundamentally involves the harvesting of the patient's tumor-specific T-cells, *in vitro* expansion of T-cell clones, and subsequent transfer of the cell back to the patient after treatment with a lymphocyte-depleting regiment. To increase the immunologic anti-tumor response, this is followed by a high dose of IL-2. In phase II trials, response rates of 38-50% were demonstrated in metastatic melanoma (80). Adoptive cell therapy is typically a promising method of treatment but it faces numerous challenges, amongst which the most evident is the need for resources and time (81).

1.5. Mechanism of apoptotic cell death and cell senescence

Apoptosis is a type of programmed cell death with caspases at the center of its mechanism, acting both as initiators and executioners of apoptosis. The processes that lead towards the activation of caspases are divided primarily into the intrinsic and extrinsic pathways as described in Figure 5 (82).

1.5.1. The extrinsic pathway

The extrinsic death receptor pathway begins with the binding of Fas ligand (FasL) and/or Tumor Necrotic Factor (TNF) to Fas (CD95) and type 1 TNF receptor (TNFR1) death receptor respectively (83). The binding of these ligands to their respective receptors initiates a cascade of intracellular events such as the recruitment of Fas-associated death domain (FADD), TNF receptor-associated death domain (TRADD), and caspase 8 (84). The ligand-death receptor interaction enables the binding of an adaptor protein, creating the ligand-death receptor-adaptor protein complex or the death-inducing signaling complex (DISC) (85). Formation of DISC results in pro-caspase 8 cleavage to produce activated caspase 8, an initiator caspase. Caspase 8 plays a significant role in the cleaving and activation of executioner and other downstream caspases thereby initiating the process of apoptosis (86).

1.5.2. The intrinsic pathway

Contrary to the extrinsic death receptor pathway, the intrinsic pathway is enabled *via* internal triggers coming from within the cells such as hypoxia, oxidative stress, irreversible DNA damage, and high calcium ion concentration (87). Each triggering factor results in increased mitochondrial permeability and the consequential release of cytochrome-c, a prominent pro-apoptotic molecule (88). The regulation of this pathway is mediated primarily by the Bcl-2 family proteins. Bcl-2 family proteins are further divided into the anti-apoptotic proteins such as Bcl-2, Bfl-1, Bcl-XL, Bcl-W, and Mcl-1 and the pro-apoptotic proteins such as Bax, Bcl-Xs, Bak, Bad, Bim, Bid, Bik, and Hrk. The release of cytochrome-c from the mitochondria is blocked by anti-apoptotic proteins, while pro-apoptotic proteins promote its release. The balance between pro-apoptotic and anti-apoptotic proteins determines the fate of the cell and whether apoptosis will be initiated (89). In the cytoplasm, caspase 3 is activated by cytochrome c resulting in the formation of a cytochrome c, caspase 9, and Apaf-1 complex known as apoptosome (90).

DOI:10.14753/SE.2022.2552

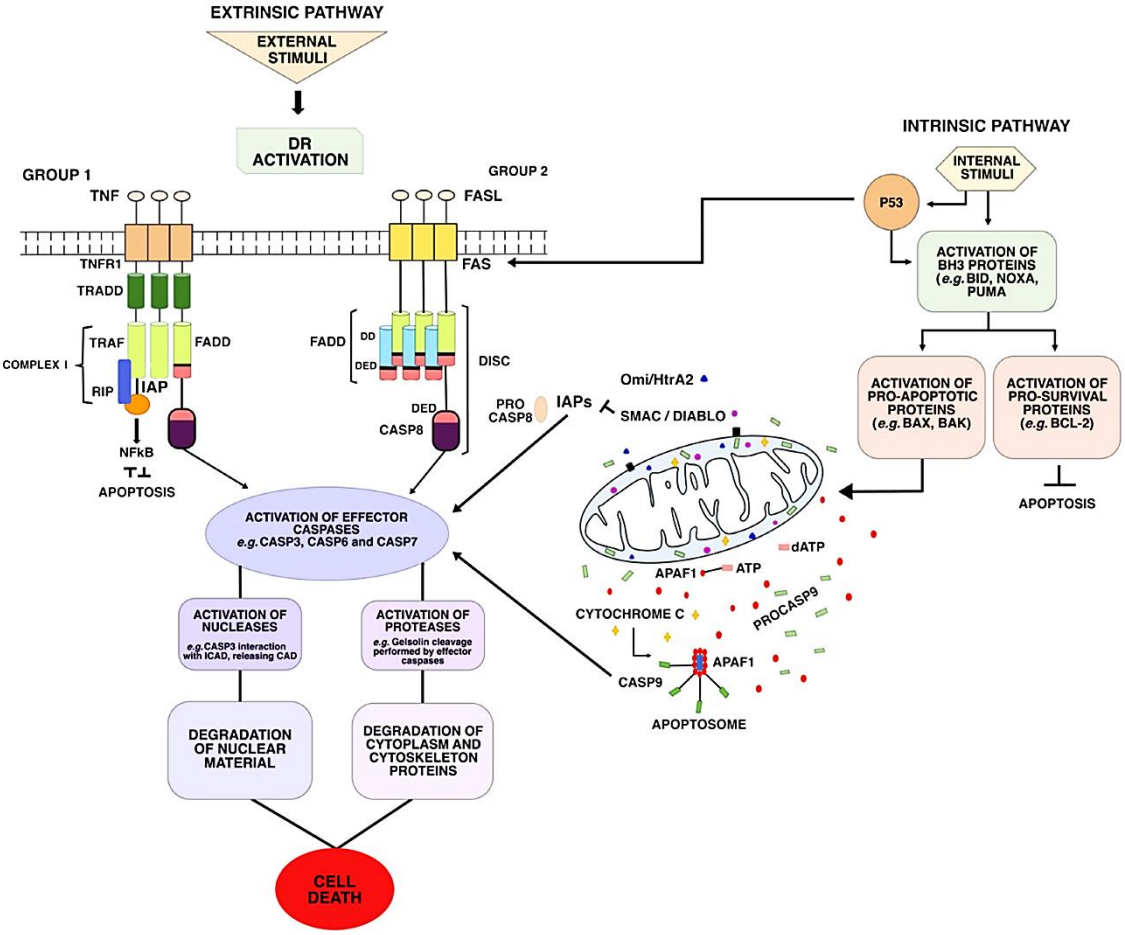

Figure 5. Extrinsic and intrinsic pathways of apoptosis (DR: direct, TNF: tumor necrotic factor, TNFR1: tumor necrotic factor receptor 1, TRADD: tumor necrosis factor receptor-associated death domain, TRAF: tumor necrosis factor receptor–associated factor, RIP: receptor-interacting protein, IAP: inhibitors of apoptosis proteins, FADD: Fas-associated death domain, NFkB: nuclear factor kappa-light-chain-enhancer of activated B cells, FASL: Fas-ligand, DD: death domain, DED: death effector domain, DISC: death-inducing signaling complex, PROCASP8: procaspase 8, PROCASP9: procaspase 9, CASP3: caspase 3, CASP6: caspase 6, CASP7: caspase 7, CASP8: caspase 8, CASP9: caspase 9, CAD: caspase-activated DNase , ICAD: inhibitor of caspase-activated DNase, SMAC: second mitochondria-derived activator of caspase, DIABLO: direct inhibitor of apoptosis-binding protein with low pI, APAF1: apoptotic protease activating factor 1, ATP: adenosine triphosphate, dATP: deoxyadenosine triphosphate, BID: BH3 interacting-domain death agonist, NOXA: phorbol-12-myristate-13-acetate-induced protein 1, PUMA: p53 upregulated modulator of apoptosis, BAX: Bcl-2 associated x-protein, BAK: Bcl-2 homologous antagonist killer, BCL-2: B-cell lymphoma 2). Modified from the original figure of Cavalcante GC et al. (2019) (82)

1.5.3. The common pathway of apoptosis

The extrinsic and intrinsic pathway of apoptosis results in the production of caspase 8 and caspase 9 respectively. Both pathways converge in the formation of caspase 3, an effector caspase. Cleavage of caspase-activated deoxyribonuclease inhibitor by caspase 3 results in nuclear apoptosis. Furthermore, protein kinases, DNA repair proteins, cytoskeletal proteins, and endonucleases family inhibitory subunits are cleaved by downstream caspases. Together, these affected proteins and their corresponding processes result in morphological changes that ultimately lead to apoptosis (91).

1.5.4. H2AX-mediated cell cycle arrest/apoptosis via the p53/p21 pathway

Cellular response to DNA damage includes a series of events that leads to either apoptosis or cell cycle arrest. One such event is the phosphorylation of histone 2AX (H2AX) (92). The serine 139 H2AX phosphorylation was first shown to be dependent on ataxia telangiectasia-mutative (ATM) kinase in mammalian cells treated with ionizing irradiation (91, 92) (Figure 6). Immediately after the generation of DNA breaks, H2AX phosphorylation occurs, mediating the formation of protein clusters at the damage site (93). The development of phosphorylated H2AX (γ-H2AX) foci has also been demonstrated after replication halting and single-stranded breaks of DNA (94-96). DNA damage results in either apoptosis or cell cycle arrest which allows for cellular repair. In both pathways, p53 is essential (96, 97) (Figure 6 and 7). Following DNA damage, p21 plays a critical role in the induction of G1 arrest *via* a p53-dependent process (98). p21 is a cyclin/cyclin-dependent kinases inhibitor that mediates the downstream effect of p53 on cell cycle arrest and senescence (99).

DOI:10.14753/SE.2022.2552

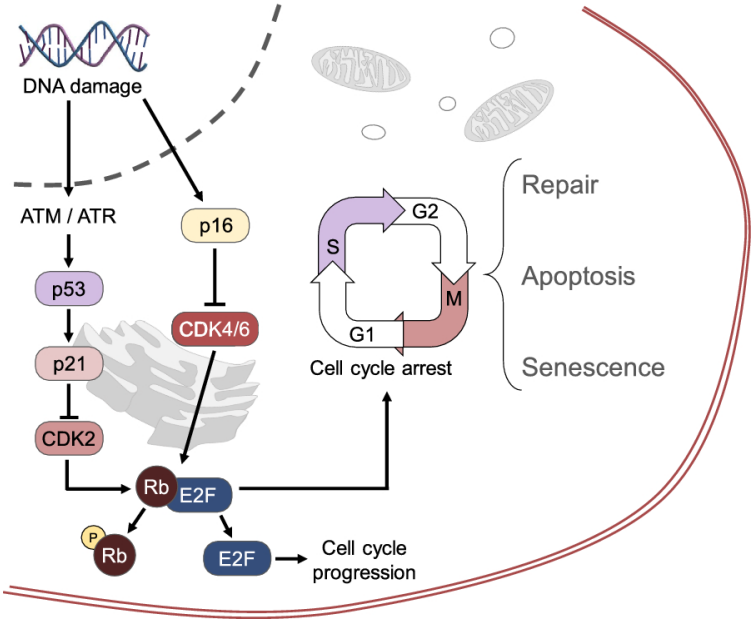

Figure 6. DNA damage pathway to cell cycle arrest (ATM: ataxia telangiectasia mutated, ATR: ataxia telangiectasia and rad3-related protein, CDK2: cyclin-dependent kinase 2, CDK4/6: cyclin-dependent kinase 4/6, Rb: retinoblastoma, P: phosphate, E2F: elongation factor 2). Modified from the original figure of Amaya-Montoya M et al. (2020) (98)

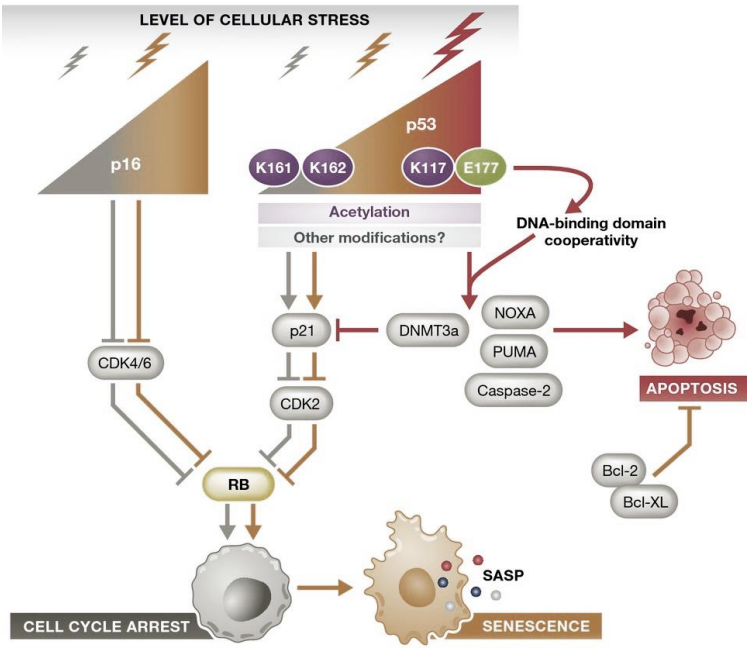

Figure 7. Signaling pathways involved in senescence, cell cycle arrest, and apoptosis (CDK2: cyclin-dependent kinase 2, CDK4/6: cyclin-dependent kinase 4/6, RB: retinoblastoma, DNA: deoxyribonucleic acid, NOXA: phorbol-12-myristate-13-acetate-induced protein 1, PUMA: p53 upregulated modulator of apoptosis, DNMT3a: DNA (cytosine-5)-methyltransferase 3a, Bcl-2: B-cell lymphoma 2, Bcl-XL: B-cell lymphoma-extra-large, SASP: senescence-associated secretory phenotype). Modified from the original figure of Childs BG et al. (2014) (100)

p21 blocks the cyclin-dependent kinases from phosphorylation by retinoblastoma protein (101) (Figure 6 and 7), or by binding to and inactivating the proliferating cell nuclear antigen (PCNA) (102) and elongation factor 2 (E2F) a cascade of processes are initiated which results in cell cycle arrest (102-104).

1.6. Tumor immunology

1.6.1. The microenvironment of tumors

The tumor microenvironment consists primarily of tumor cells, stromal cells, and non-malignant cells. The stroma is made up of specialized mesenchymal cell types, vasculature consisting of pericytes and endothelial cells, adaptive and innate immune cells, as well as, specialized proteins, structural proteins, and proteoglycans that makes up the extracellular matrix. Intercellular communication is enabled mainly *via* the release of chemokines and cytokines (105). The major components of the tumor microenvironment are B-cells, T-cells, NK-cells, NKT-cells, dendritic cells, myeloid-derived suppressor cells, tumor-associated macrophages, tumor-associated neutrophils, adipocytes, fibroblasts, lymphatic endothelial cells, pericytes, and vascular endothelial cells (106).

1.6.2. Cancer immunity cycle

Previously, Chen et al had described the cancer immunity cycle, reiterating the role that T-cell response plays in tumor growth suppression and destruction (107). The cancer immunity cycle can be categorized into seven major processes that culminate in the cytotoxic destruction of cancer cells. Each process involves the recruitment of several inhibitory and stimulatory factors. While inhibitory factors are involved in keeping checks and balances of the immune system and preventing over-stimulation or autoimmunity, the stimulatory factors are engaged in immune-activating processes. As a first step, necrotic cancer cells release antigens which are captured by dendritic cells for further processing. This is followed by processing of captured antigens, migration of the dendritic cells to regional lymph nodes, and presentation of the processed antigen on MHC class I to CD8+ T-lymphocytes and on MHC class II to CD4+ T-lymphocytes. The ability of dendritic cells to perform these functions depends on the status of their maturation. Several factors play an essential role in regulating the maturation of dendritic

cells such as inflammatory cytokines, bacterial-derived antigens, and whole bacteria, ligation of selected cell surface receptors, such as toll-like receptors, viral products, and CD40. During maturation, dendritic cells undergo several functional and phenotypical changes such as cytoskeleton reorganization and morphological changes, chemokines, proteases, and cytokines secretion, chemokine receptors and adhesion molecules surface expression, externalization of MHC molecules from intracellular compartments to the surface, and increase surface expressions of co-stimulatory molecules, such as CD80, CD40, and CD86 (108). The ability of dendritic cells to stimulate T-cells is dependent on the presence of inflammatory cytokines such as TNFα, IL1, IFNα, stimulatory factors, and costimulatory molecules (109). The third process involves priming and activation of effector T-lymphocyte responses with specificity against cancer cell antigens. At this stage, the ratio of T-cells versus T-regs determines the degree of the immune response to the activating cancer antigens. IL-2 and IL-12 are also essential for the activation of CD8+ T-cells, which are secreted by CD4+ T-helper cells and dendritic cells respectively. The next process involves the migration of effector CD8+ T-cells to the tumor site *via* special chemotactic chemokines, such as C-X-C motif chemokine ligand 5 (CCL5), C-X-C motif chemokine ligand 9 (CXCL9), and C-X-C motif chemokine ligand 10 (CXCL10). Next, extravasation of T-cells through the vascular endothelium towards the tumor is enabled *via* specific interactions between the T-cells and selectins, as well as, intercellular adhesion molecule 1 (ICAM-1). Upon arriving at the tumor site, as a next step, T-cells interact with the tumor cells *via* a CD8+ T-cell receptor (TCR) which binds with tumor antigen presented on major histocompatibility complex (MHC) class I of the cancer cells. This interaction results in the release of cytotoxic granules, cytokines and death receptors upregulation, such as Fas Ligand (FasL). This interaction results in the activation of caspase-dependent apoptosis and cell death of tumor cells, resulting in further release of tumor antigens that enhances the cancer-immunity cycle (109). Natural killer cells (NK-cells) also play a critical role as part of the immune surveillance *via* recognition and destruction of cells lacking in MHC class I (110). The function of NK-cells however is dependent on both lack of MHC class I as well as activating and inhibitory signals. Inhibitory receptors such as leukocyte inhibitory receptors (LIR) and killer immunoglobulin-like receptors (KIRs) are expressed on NK-cells. Likewise activating receptors such as CD16, Ly49 and natural killer group 2D (NKG2D) can be found on

NK-cells (111). The cytolytic killing of cells requires an appropriate balance between all activating and inhibiting signals to occur (112).

1.6.3. Cancer immunoediting

The immunoediting hypothesis describes the role of the immune system in protecting the host from tumor development as well as its role in the modulation of the tumor immunogenicity (113). Immunoediting consists of three phases which include elimination, equilibrium, and escape of tumor cells. The elimination phase describes the ability of the innate and adaptive immune system to identify and destroy tumor cells early on, before the development of a clinically significant tumor. The equilibrium phase describes the phase at which surviving cancer cells from the elimination phase still exist and thrive. While surviving cancer cells can escape the eliminating process of the immune system, they are primarily in a state of dormancy. However, changes in cancer immunity or intrinsic changes with the cancer cells may enable some cancer cells to propagate into the next phase of the immunoediting process, known as the escape phase. Progression into this phase leads to the formation of clinically significant tumors. Intrinsic changes in tumor cells such as the loss of tumor antigen expression especially due to genetic instability enable these cells to escape the immune system and continue developing irrespective of the presence of immune surveillance. Multiple mechanisms may affect the immunogenicity of cancer cells during the cancer-immunity cycle, leading to a decrease in recognition of tumor cells by T-cells, cytotoxic killing of cancer cells, T-cell tumor infiltration, and tumor antigen presentation to T-cells (114).

1.6.4. Tumor antigen presentation and activation of cytotoxic T-cells

Impairment of the ability of dendritic cells to present antigens, and activate T-cell response is one of the major important processes of tumor-induced immune suppression. The defect in dendritic cell function is common in cancers and is largely systemic which might be the result of an abnormal myeloid cell differentiation resulting in the accumulation of immature myeloid cells. These immature myeloid cells are termed “Myeloid-derived suppressor cells (MDSCs)”. Cancer cells secrete several factors, capable of inhibiting the differentiation of myeloid progenitors into dendritic cells such as transforming growth factor-beta (TGFβ), vascular endothelial growth factor (VEGF), Interleukin 6 (IL-6), Interleukin 10 (IL-10), granulocyte-macrophage colony-stimulating

factor (GM-CSF), and macrophage colony-stimulating factor (M-CSF). In addition to impairment in the differentiation of myeloid progenitors, the maturation process of these cells to dendritic cells can also be impaired, resulting in the formation of T-cell tolerance to cancer cells (115).

1.6.5. T-cell tumor infiltration

The homing of tumor-targeting effector T-cells is enabled *via* chemokine secretion that coordinates the migration of lymphocytes towards the tumor site. However, chemokines can suppress the tumor microenvironment (TME) by disrupting the normal chemokine signaling and may lead to infiltration of the TME by suppressive cell types such as regulatory T-cells (Tregs) and myeloid-derived suppressor cells (MDSCs) (116). The effect is the suppression of T-cell homing from the vascular endothelium to the tumor. Furthermore, tumor-derived angiogenic growth factors can inhibit the expression of adhesion molecules in vascular endothelial cells, thereby, limiting the ability of T-cells to extravasate and infiltrate tumors. In addition, TGFβ, IL-10, PD-L1 expressed by endothelial cells can have a negative suppressive effect on T-cells (117).

1.6.6. Tumor-infiltrating immunosuppressive cells

1.6.6.1. T-regulatory cells

T-regulatory cells (Tregs) are a subset of immune cells that functions primarily in the maintenance of self-tolerance by suppression of immune cell proliferation, activation and effector functions (118). In the tumor microenvironment, they function to suppress anti-tumor responses by immune cells. Increased infiltration of Tregs in tumors has been demonstrated in multiple solid tumors (119), as well as, malignancies of Hodgkin lymphoma (120). The increase in Tregs in solid tumors has a negative impact on prognosis in solid tumors. CD4+ and CD8+ Tregs have been described with the most extensively studied one being the CD4+CD25+FOXP3+ Tregs. The Tregs marker nuclear transcription factor Fork-head box P3 (FoxP3), plays an important function, not only as a marker of Tregs but also functions in modulating regulatory phenotype development (121). Two primary subsets of Tregs exist including induced Tregs (iTregs), which are induced T-regs produced under suppressive conditions, and natural Tregs (nTregs) which functions primarily in the suppression of innate and adaptive immune cells and are derived from the thymus (119). Thymus-derived Tregs migrate primarily to the periphery

and have a relatively homogeneous population. A sub-population of these thymus-derived Tregs has the capability of developing characteristics similar to effector T-cells and memory T-cells phenotypically. This enhances their ability to migrate into non-lymphoid and lymphoid tissues. Peripheral Tregs can develop from the conventional T-cells derived from the thymus, making them CD4+CD25-Foxp3- (114, 119). Evidence suggests that Tregs may express their suppressive functions based on multiple mechanisms, suggesting the possibility of functional specialization on these cells depending on the localization and type of immune response. One such mechanism is the ability of Tregs to secrete IL-10 which functions in the inhibition of effector T-cell response, directly or indirectly. TGFβ and IL-35 are also secreted by Tregs, which functions to enhance conventional CD4+ T-cell differentiation to Tregs, thereby increasing further the population of Tregs in respect to T-helper cells during an immune response. Furthermore, Tregs expression of CTLA4 enables binding to CD80 and CD86 co-stimulatory molecules on dendritic cells. This leads to a downregulation of CD80 and CD86 on dendritic cells, limiting their capacity to cause T-cell activation. Also, Tregs can have a direct cytotoxic effect on effector T-cells by induction of apoptosis or release of cytolytic mediators (115, 116).

1.6.6.2. Myeloid-derived suppressor cells

Myeloid-derived suppressor cells (MDSCs) are immature cell populations derived from a myeloid origin and capable of inducing suppression of T-cell responses. In healthy individuals, MDSCs functions primarily to regulate tissue repair and immune cell responses. Pathological conditions such as trauma, cancer, inflammation, and infection lead to the expansion of the MDSCs population due to a block in the differentiation of myeloid cells (115). In patients with primary solid tumors, the expansion of MDSCs has been demonstrated (122). In cancers, following the recruitment of MDSCs, increased production and secretion of MDSC-derived cytokines have been described and the increase in cell-cell interactions leads to tumor progression. The ability of MDSCs to limit T-cell responses and infiltration into the tumor microenvironment promotes tumor immune escape (123). Expansion of MDSCs is enabled *via* activation of the Janus tyrosine kinase (JTK) signaling and signal-transducer-and-activator-of-transcription-3 (STAT3) protein. STAT3 signaling can be activated by factors such as macrophage colony-stimulating factor (M-CSF), VEGF, IL-6, GM-CSF, prostaglandin, and stem cell factor (SCF). Activation of MDSCs *via* signal-transducer-and-activator-of-transcription-

6 (STAT6) and signal-transducer-and-activator-of-transcription-1 (STAT1) signaling pathway can lead to upregulation of nuclear factor (NF)-kappa B. This activation can be achieved by several factors, such as toll-like receptors (TLRs), IL-4, Interferon-gamma (IFNγ), IL-13, and TGFβ (115). NF-kappa B activation results in the suppression of MDSC activity through Arginase-1 and inducible nitric oxide synthase (iNOS) enzyme upregulation (118, 119). Activated NF-kappa B results in the production of suppressive cytokines such as TGFβ which promotes Tregs induction (124). Antigen-specific CD8+ T-cell tolerance can also be induced by MDSCs (125). For the design, development, and administration of effective therapies in cancer treatment, it is crucial to understand the processes involved in the activation, development, and effects of MDSCs.

1.7. Hyperthermia in cancer therapy

1.7.1. Overview of hyperthermia therapy

Alongside other treatment modalities such as radiotherapy, chemotherapy, immunotherapy, gene therapy, and surgery, hyperthermia is a widely used treatment modality in cancer therapy (126). In clinical settings, hyperthermia is mostly used in combination with other treatments, most especially radiotherapy and chemotherapy (127) which offers a much better synergistic therapeutic effect. In hyperthermia, thermal energy from an external heat source is applied to cancer cells which increases their temperature and leads to suppression of tumor growth (128). Higher temperature may have a direct damaging effect on cancer cells, augments chemotherapy and radiation therapy, or sensitize cancer cells to other treatment modalities. This confirms the use of hyperthermia as adjuvant therapy in cancer (129-131). Significant challenges exist in the application of hyperthermia clinically, such as the difficulty in achieving a homogenous dispersion of heat in treated tumors as well as failure in tumor-specific targeting without damage to adjacent normal tissues and organs (132).

1.7.2. Local hyperthermia

Local hyperthermia can be used to convey heat to the tumor, using intraluminal and superficial applicators, such as microwave, ultrasound, or radio waves (133). Local hyperthermia is used for relatively small tumors that arise superficially or in a cavity such as the rectum or esophagus. In local hyperthermia, different shapes and types of

superficial applicators, such as spiral, current sheet, or waveguide are positioned on the surface of tumors superficially. Water boluses are used simultaneously to maintain skin temperature at 37 °C to eliminate possible skin damage as an adverse effect (134). Intracavitary tumors, such as, esophageal, rectal, prostate, cervix, or vaginal tumors can be treated using intraluminal or intracavitary methods which apply heat directly into these organs (131).

1.7.3. Regional hyperthermia

Regional hyperthermia is a technique used mainly for the treatment of advanced tumors in the thighs, abdomen, and pelvic area. There are three primary methods of regional hyperthermia which include constant hyperthermic peritoneal perfusion (CHPP), thermal perfusion of limbs and organs, and intrinsic treatment (tumor heating *via* peripheral applicators) (135). Regional perfusion hyperthermia involves the temporary removal of the patient's blood, heating, and reperfusion back into the organ or limb of the patient, typically with anticancer agents. Regional hyperthermia can be applied as a therapeutic measure for malignancies of legs or arms (e.g., melanoma), and visceral organs such as the liver and lungs. In comparison to whole-body hyperthermia, regional hyperthermia shows significantly reduced adverse effects (135). Regional hyperthermia is, therefore, more complex than local heating, primarily because of substantial physical and physiological variations in tissue properties. More precise preparation, temperature control, and quality assurance are therefore needed. The treatment of cancers within the peritoneal cavity, such as gastric cancers, and primary peritoneal mesothelioma, has been indicated for Hyperthermic Intraperitoneal Chemotherapy (HIPEC). In HIPEC, a chemotherapeutic agent is introduced into the peritoneal cavity after heating to a temperature of 41 - 42 °C (136). Consistent temperature measurement in HIPEC is particularly challenging and as a result, makes the heating of upper abdominal tumors difficult. The procedure has been used in conjunction with radiotherapy in multiple regional hyperthermia clinical trials (137).

1.7.4. Whole-body hyperthermia

Whole-body hyperthermia refers to an increase in whole-body temperature using radiation or extracorporeal heating methods in the treatment of cancers. Radiant whole-body hyperthermia involves the use of inductive loops, hot blankets, and thermal

chambers to superficially heat the body (129, 138-140). On the other hand, extracorporeal whole-body hyperthermia is achieved by extraction of blood and heating it extracorporeally. In this case, the extracted blood is circulated through hot air or water bath and then recirculated into the main vein. Body temperature in this case is controlled by adjusting the volume flow of reinjected warmed blood (141). In whole-body hyperthermia, treatment can be conducted for 60 min at 42.0 °C or for 3 – 4 hr at 39.5 – 41.0 °C. Depending on the treatment type, deep sedation or general anesthesia may be administered during treatment (129, 138-140). Significant pressure is put on the heart during whole-body hyperthermia treatment, thus, it is necessary to preserve the patient's blood pressure to a systolic value of above 100 mmHg by injecting normal saline, following which the patient has to be checked weekly for any signs of adverse events (142). Significant, although temporary side effects often seen in whole-body hyperthermia include thermal pressure on the brain, lungs, heart, and liver, as well as, nausea, vomiting, and diarrhea (131).

1.7.5. Application of hyperthermia in cancer therapy

1.7.5.1. Hyperthermia as an isolated treatment

Although hyperthermia is used in combination with other treatment modalities in clinical settings, it can also be used as an isolated treatment in the therapeutic management of cancers. Tumor and normal tissue respond differentially to heat, thus making the application of hyperthermia in cancer treatment feasible (138, 139). Tumor tissue shows significant differences in pattern and type of vascular distribution from normal tissue. While normal tissue depicts a typical array of vascularization consisting of arterioles, capillaries, and veins, a chaotic network of capillaries, predominantly lacking innervation and smooth muscle layers are often seen in tumor tissues (143). The resulting vascular abnormality creates inefficiencies in blood supply, leading to intra-tumoral hypoxia. Although mild temperature increase (37°C - 42°C) can cause significant vascular dilation and improved perfusion in tumor (144), temperatures greater than 42°C can have a significant damaging effect on tumor vasculature, resulting in increased permeability of vessels, exudative and transudative changes with accompanying increase in interstitial fluid pressure, as well as resulting compression of vessels with further aggravation of reduced vascular perfusion (145).

1.7.5.2. Hyperthermia combined with chemotherapy

Combination of hyperthermia with chemotherapy can have a significant synergistic effect with enhanced drug cytotoxicity. An increase in tissue temperature accompanying hyperthermia treatment induces fluidity of the phospholipid bilayer of tumor cells, thereby, facilitating a decrease in membrane viscosity, increase permeability, and cellular uptake of drugs in cancer cells (144, 146). Furthermore, hyperthermia-induced changes in cellular metabolism, drug pharmacokinetics as well as excretion can enhance the cytotoxicity of some chemotherapeutic agents (147). The synergistic effect of hyperthermia with selected chemotherapeutic agents has well been described, especially in HIPEC. HIPEC is used primarily in combination with surgical therapy and involves the intraperitoneal administration and circulation of warmed chemotherapeutic agents in the peritoneal cavity for the treatment of advanced abdominal cancers. Significantly, improved therapeutic efficacy and index have been demonstrated with HIPEC in experimental studies. Higher thermal enhancement ratios are most evident with alkylating agents such as ifosfamide, melphalan, and cyclophosphamide (148). Peritoneal clearance of administered chemotherapeutic agents is relatively slow due to the existence of the peritoneal plasma barrier. This implies that higher intraperitoneal concentrations of the administered agent can be achieved, while systemic drug levels remain low (149). An additional advantage of HIPEC is that peritoneal blood drainage occurs through the portal vein leading to the liver. In the liver, detoxification of the drained blood (first-pass effect) occurs, furthermore decreasing the potential systemic side effect of these chemotherapeutic agents (150).

1.7.5.3. Hyperthermia combined with radiotherapy

As described in the previous section, chaotic vascularization of tumor tissue leads to hypoxia which results in the radioresistance of the tumor. Thus, improvement of the hypoxic condition with hyperthermia can improve radiosensitivity of tumor tissue. Hyperthermia can increase the sensitivity of tumor tissue to radiotherapy. This is attributed to the ability of mild hyperthermia especially at a temperature of 37°C - 42°C to increase vasodilation and increase blood flow to tumor cells, thereby, reducing the radioprotective effect of hypoxia (144). Higher treatment temperature however will result in blood vessel damage, leading to reduced blood perfusion and aggravating hypoxia. In

addition, thermal tolerance of cancer cells can be reduced by radiation therapy, thereby, improving the thermal effect of hyperthermia on tumor tissue (151).

1.8. Modulated electro-hyperthermia (mEHT)

1.8.1. Mechanism of mEHT specificity on tumor cells

Modulated electro-hyperthermia (mEHT) is a treatment modality in which a 13.56 MHz radiofrequency is used to generate an electric field that selectively accumulates and targets tumor cells (152). The metabolic and biophysical conditions of cancer cells are inherently different from normal cells, thus, enabling the selective targeting of cancer cells with electromagnetic energy of mEHT (153). Cancer cells exhibit the "Warburg effect" primarily due to their higher reliance on glycolysis than normal cells regardless of oxygen availability (154). The breakdown of glucose *via* glycolysis yields two ATP molecules in contrast to the 36 ATP molecules generated by normal cells from the complete oxidation of glucose (155). In addition, lactic acid production and other metabolites are significantly increased due to higher glucose uptake and glycolysis in cancer cells in comparison to normal cells (156). Low ATP in cancer cells creates insufficiencies necessary for the stabilization of the Na^+/ K^+ ATPase, which leads to a weakening of the pump function and the membrane potential (157). The cumulative effect of these changes results in the decreased efflux of Na^+ and water transport and increased efflux of K^+, Mg^{2+}, and Ca^{2+} ions observed. The resulting high lactate and ionic contents of tumor cells enable better coupling between electrodes of mEHT and the treated tumor (152).

1.8.2. Membrane raft heat stress localization with mEHT

One of the many benefits of mEHT treatment is that high thermal loads can be localized to only a small and specific area of the plasma membrane of the cancer cells (158), called lipid rafts which exists in a nanoscopic range and can absorb the energy load (159) (Figure 8). mEHT at 13.56 MHz frequency is incapable of penetrating the cell interior due to the excellent insulating property of the cell membrane (160). The energy generated from the amplitude-modulated radiofrequency current is absorbed primarily by the lipid raft and to a lesser extent by the extracellular matrix (161). Due to the different

DOI:10.14753/SE.2022.2552

electromagnetic properties of the lipid raft, it can absorb more radiofrequency energy compared to the cell membrane lipid bilayer (159).

This implies a higher energy absorption in the lipid raft leading to increase heat localization with continuous radiofrequency current delivery. Cell membranes of cancer cells are isolated electrically by a field strength that exceeds one million V/m. Thus, with radiofrequency treatment, this serves as an insulating layer, thereby directing the flow of current towards the extracellular electrolytes (153). The differences in permeability and conductivity between cancer cells and normal healthy cells enable precise distinguishing of both types of cells and enhance the cancer-specific effect of radiofrequency treatment (162-166).

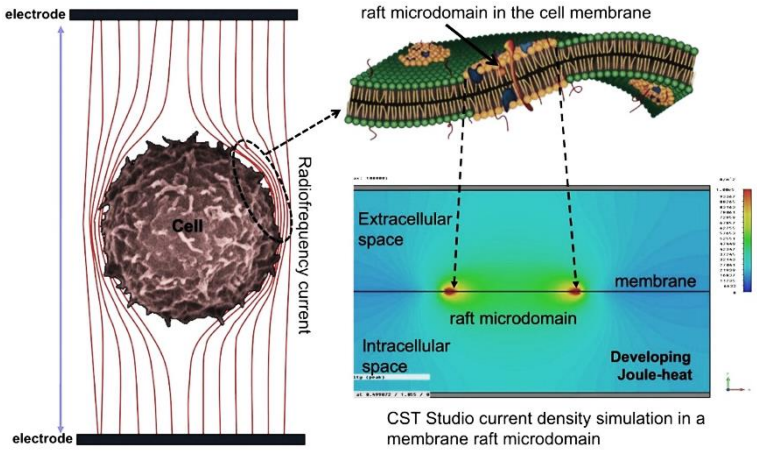

Figure 8. Schematic representation of the membrane raft-specific localized heat stress. Modified from the original figure of Andocs G et al. (2016) (153)

DOI:10.14753/SE.2022.2552

2. Objective

Although the efficacy of mEHT has been described extensively in multiple primary tumor models in mice, studies on the applicability and efficacy of mEHT as a viable treatment option in a pulmonary metastatic model have not been described before. This is probably due in part to the complexity of the thorax and the difficulty it poses to the application of mEHT as a treatment option. Additionally, the lack of adequate devices optimized for the targeted treatment of lung tumors presents a particular problem. Another challenging aspect of mEHT application in lung treatment is the difficulty of measuring lung temperature during treatment as direct measurement poses a significant risk of mechanical lung injury.

Therefore, in this study, we aimed at:

1. Developing a device-optimized-treatment-technique for targeted mEHT treatment of lung tumors.
2. Developing a minimally invasive method of indirect lung temperature measurement during mEHT treatment of lung tumors in mice.
3. Verifying the efficacy of mEHT on B16F10 melanoma in a subcutaneously induced primary tumor and pulmonary metastases model following the usual pattern of clinical dissemination of melanoma from the skin to the lungs.
4. Investigating the underlying molecular mechanisms of tumor growth inhibition by mEHT in a B16F10 melanoma pulmonary metastases model.
5. Investigating the capability of mEHT treatment-induced immune cells mobilization.
6. Investigating auxiliary lung damage as a potential adverse event following mEHT treatment of lungs in mice.

DOI:10.14753/SE.2022.2552

3. Materials and Methods

3.1. Animals and cell lines

All procedures were carried out according to the guidelines of the Hungarian Law of Animal Protection (28/1998) and were approved by the Government Office of Pest County (Permission number: PE/EA/50-2/2019 and PE/EA/51-2/2019). Animals tested in this study were the offspring of C57BL/6 colonies grown in the animal facility of the Semmelweis University. B16F10 mouse melanoma cell line (ATCC® CRL 6475™) was purchased from ATCC (Manassas, VA, USA). Cells were cultured in minimum essential medium (MEM) supplemented with 1% (v/v) MEM-vitamin solution, 5% (v/v) heat-inactivated HyClone fetal bovine serum, 1 mM sodium pyruvate, 2 mM L-glutamine and 1% (v/v) nonessential amino acids (NEAAs) purchased from Thermo Fisher Scientific (Waltham, MA, USA).

3.2. PET imaging and data analysis

In vivo positron emission tomography (PET) experiments were conducted at the Department of Biophysics and Radiation Biology, Semmelweis University. Animals were fasted before the experiment for 6 hours. Prior to PET imaging, 12-18 MBq radioactivity of [^{18}F]FDG (FDG-KEDOI® injection, Pet-Medicopus Ltd, Kaposvár, Hungary) in 0.2-0.3 mL was injected into the tail vein of the animals. After 90 min of post-injection awake [^{18}F]FDG uptake period, animals were anesthetized with 1.5% isoflurane in medical oxygen. During anesthesia, animals were placed in an immobilizing animal bed (MultiCell, Mediso, Budapest, Hungary). Static, 15 min PET whole-body scans of animals were performed using a microPET P4 scanner (Concorde Microsystems, US). Image volumes from the collected list mode data were then reconstructed using the instrument`s dedicated three-dimensional maximum a posteriori algorithm with a 1.56 mm voxel size. Data evaluation was carried out using two dedicated small animal image analysis software, Fusion (Mediso, Budapest, Hungary) and vivoQuant (inviCRO, MA, US). Three-dimensional lung regions of interest were drawn using a connected threshold algorithm, while blood regions of interest were manually drawn around the left ventricle of the heart. For the calculation of the Tumor Maximal Standardized Uptake Ratio (SURmax), and SUVmax, the standardized uptake values (SUV) were estimated by the

following equation: [tissue concentration (MBq/mL) x the body weight (g)]/injected dose (MBq). Thereafter, SURmax was obtained by time correcting the ratio of lung maximal SUV value in the lung region of interest (SUVmax) to blood SUV multiplied by the ratio of 75 min post-injection to 90 min post-injection, as described by Hofheinz et al. (167-169). After calculations, all mouse PET quantitative data were normalized to the respective lung mass (in grams) of each animal to account for initial size-related vascularization-derived differences in signal.

3.3. *In vivo* mEHT treatment

In the metastatic tumor model, pulmonary metastases of melanoma were established by injecting 10^5 B16F10 melanoma cells *via* tail vein into seven-to-nine-week-old female C57BL/6 mice. The animals were treated using the LabEHY-200 device (Oncotherm Ltd., Páty, Hungary) shown in Figure 9A. All animals were placed between the circuit's plane-parallel asymmetric electric condensers during treatment. The circuit consisted of a 72-cm^2 aluminum electrode which served also as a heating pad used to maintain the physiological temperature of the animal at approximately 37 °C (Figure 9B). The impedance was precisely matched, and the electromagnetic field was generated at 13.56 MHz radiofrequency using 1/f amplitude modulation. The upper conductive textile chest electrode (Figure 11A, 11B) was placed on the chest overlying the tumor-burdened lungs. Treatment with the lung-optimized chest electrode was repeated every third day for a total of six times for 30 min each starting from day 1. mEHT ability to induce heat-stress and DAMP signal release of B16F10 melanoma cells was verified in a primary solid B16F10 melanoma tumor model. In the primary tumor model, melanoma tumors were established by mixing 10^6 B16F10 cells with growth factor reduced matrigel (Trevigen, Gaithersburg, MD, USA) injected subcutaneously into seven-to-nine-week-old female C57Bl/6 mice in the right inguinal area. An upper pole electrode was positioned over the growing tumor in the right inguinal region (Figure 10A). The first mEHT treatment of 30 min was performed on day 4 after the implantation of the tumor cell/matrigel mixture and was repeated two more times with one day in between treatments. Animals were anesthetized with 2% isoflurane during treatment. Animals were housed separately, and treated control animals were maintained under similar conditions. Animals tested in this study were the offspring of C57BL/6 colonies grown in the animal facility of Semmelweis University,

Budapest, Hungary. All animal work conducted during this study was approved by the Governmental Ethical Committee under the permission number PE/EA/51-2/2019.

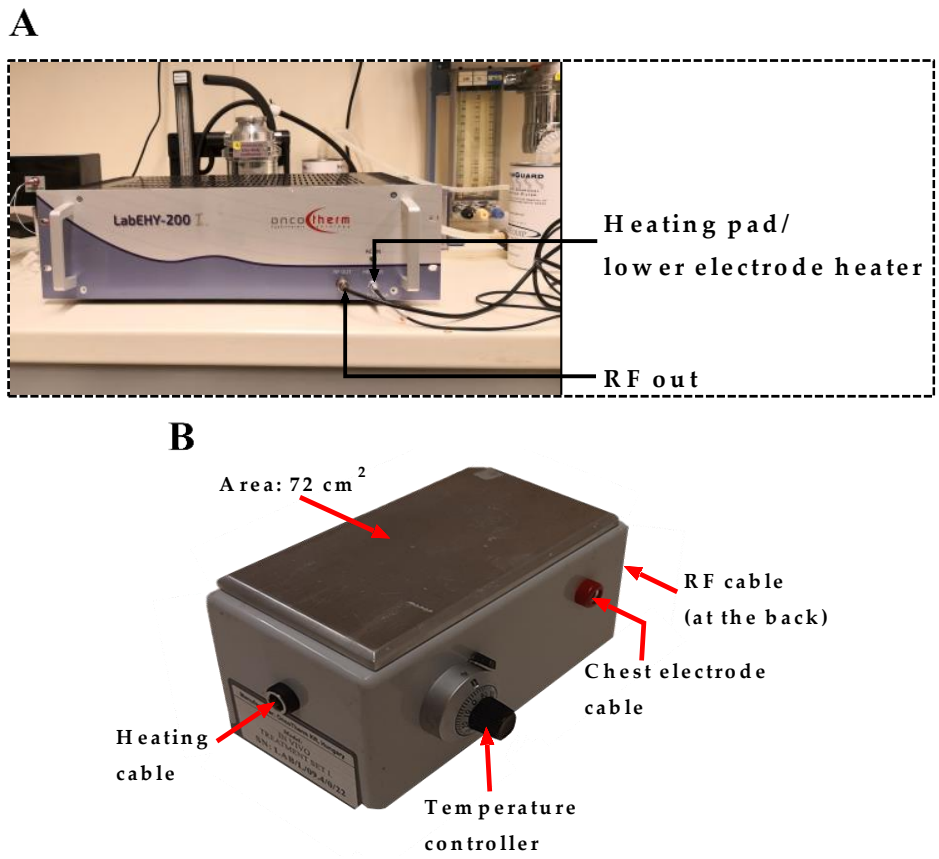

Figure 9. Treatment devices of modulated-electrohyperthermia. (A) LabEHY-200; (B) Heating pad/lower electrode. (RF: Radiofrequency)

3.4. Immunohistochemistry

Lung tissues fixed in 10% neutral buffered formalin were dehydrated and embedded in paraffin. 2.5 µm thick serial sections were cut, mounted on silanized glass slides, and kept in a thermostat at 65 °C for 1 hour. Sections were dewaxed and rehydrated for hematoxylin-eosin (H&E) staining, masson's trichrome staining, and immunohistochemistry (IHC). For antigen retrieval, sections were heated for 20 min in Tris-EDTA (TE) buffer pH 9.0 (0.1 M Tris_base and 0.01 M EDTA) using an avair electric pressure cooker (ELLA 6 LUX D6K2A, Bitalon Kft, Pécs, Hungary) followed by a 20 min cooling with an open lid. Endogenous peroxidases were blocked using 3% H_2O_2 in methanol while non-specific proteins were blocked with 3% bovine serum albumin (BSA, #82-100-6, Millipore, Kankakee, Illinois, USA) diluted in 0.1 M Tris-buffered saline (TBS, pH7.4) containing 0.01% sodium-azide, both for 15 min. The sections were

incubated with primary antibodies (Table 2) diluted in 1% BSA/TBS+TWEEN (TBST, pH 7.4) overnight in a humidified chamber. Peroxidase conjugated anti-rabbit & anti-mouse IgGs (HISTOLS-MR-T, micropolymer -30011.500T, Histopathology Ltd., Pécs, Hungary) were used for 40 min incubations and the enzyme activity was revealed by 3,3'-diaminobenzidine (DAB) chromogen/hydrogen peroxide kit (DAB Quanto, #TA-060-QHDX, Thermo, WA, USA) under microscopic control. All incubations were done at room temperature with samples washed between incubations in TBST buffer for 2 x 5 minutes. Digitalization of slides and evaluation of immune reactions were done using modules of the QuantCenter image analysis software tool pack (3DHISTECH, Budapest, Hungary). As multiple pulmonary melanoma nodules were noted in each lung sample, all tumors in each section were annotated for subsequent evaluations. The portion of p-H2Axγ(Ser139), CCasp3, and $p21^{waf1}$, Ki67(SP6), F4/80 (D2S9R), CD3, CD8α (D4W2Z) positive cells were quantified as a percentage of the total annotated tumor areas (HistoQuant module) while the portion of MPO positive cells and Masson's trichrome positive area was quantified as a percentage of the total lung area. Evaluation of histological lung injury was performed as described by Ehrentraut et al (170) taking into consideration scores of individual components of cellular inflammatory cell infiltrates in air space or vessel wall (1 = only wall; 2 = one to five cells (few cells) in air space; 3 = intermediate; 4 = severe (congestion of air space)), interstitial congestion and hyaline membrane formation (1 = normal lung; 2 = moderate (<25% of lung section); 3 = intermediate (25–50% of lung section); 4 = severe (>50% of lung section)), hemorrhage (0 = absent; 1 = present). From each animal, a total of six representative images were analyzed using a blinded semi-quantitative scoring system.

Table 2. Antibodies and conditions used for immunohistochemistry

Antigen	Type	Reference no.	Dilution	Antigen retrieval	Vendor
p-H2Axγ(Ser139)	Rabbit, mAb	#9718	1: 200	T-E	Cell Signaling
CCasp3	Rabbit, pAb	#9664	1:100	Citrate	Cell Signaling
$p21^{waf1}$	Rabbit, mAb	#ab188224	1:300	T-E	Abcam
Ki67 (SP6)	Rabbit, mAb	#MA5-14520	1:100	T-E	Thermo
F4/80 (D2S9R)	Rabbit, mAb	# 70076	1:300	T-E	Cell Signaling
CD3	Rabbit, pAb	#IS503	1:3	T-E	Dako
CD8α (D4W2Z)	Rabbit, mAb	#98941	1:500	T-E	Cell Signaling

(Vendor specification: Cell Signaling (Danvers, MA, USA); Thermo (Waltham, MA, USA); Dako (Glostrup, Denmark); Abcam (Cambridge, UK); Sino Biological (Beijing, China); T-E: Tris-EDTA, pH 9.0)

3.5. Measurement of extracellular hsp70, HMGB1, and ATP

The tumor interstitial fluid was obtained by digesting tumors as described above. After removing cells by centrifugation, the supernatant was further purified by centrifugation at maximum speed for 10 min and stored at -70 °C until use. The protein concentration of the tumor effusate was measured using Bradford reagent (Thermo Fisher Scientific, Waltham, MA). In the subsequent measurements, an equal amount of protein was used. The heat shock protein 70 (hsp70) concentration was measured using an hsp70 High-Sensitivity ELISA kit (Abcam, Cambridge, UK). The high-mobility group protein B1 (HMGB1) concentration was determined using a specific ELISA kit from Aviva Systems Biology (San Diego, CA, USA) following the manufacturer's protocol. Absorbance was measured at 450 nm with a PowerWave microplate spectrophotometer (BioTek, Winooski, VT). ATP content was evaluated using a luciferase-based ATP determination kit (Thermo Fischer Scientific) following the manufacturer's instructions. Luminescence was measured with a Varioskan Flash microplate reader (Thermo Fischer Scientific, Waltham, MA).

DOI:10.14753/SE.2022.2552

3.6. Statistical analysis

Statistical analysis was performed using GraphPad Prism software (v.6.07; GraphPad Software Inc., La Jolla, CA, USA). The normality of data distribution was assessed using the Kolmogorov-Smirnov test and an unpaired t-test or Mann-Whitney nonparametric test was performed accordingly for determination of significance. Data are expressed as mean ± SE, $p < 0.05$ were considered as significant.

DOI:10.14753/SE.2022.2552

4. Results

4.1. mEHT suppressed primary tumor growth of B16F10 melanoma

Prior to investigating the effect of mEHT on a pulmonary melanoma metastatic model, we first evaluated whether mEHT can have a significant tumor growth inhibition effect on B16F10 melanoma in a primary tumor model, primarily due to the simplicity of the model in comparison to the more complex pulmonary metastatic model. 10^6 B16F10 cells mixed with growth factor reduced matrigel (Trevigen, Gaithersburg, MD, USA) was subcutaneously injected into seven-to-nine-week-old female C57Bl/6 mice in the right inguinal area, simulating a primary tumor model. Before performing treatments, we set up conditions providing a standard 42 °C intra-tumoral temperature in a series of animals.

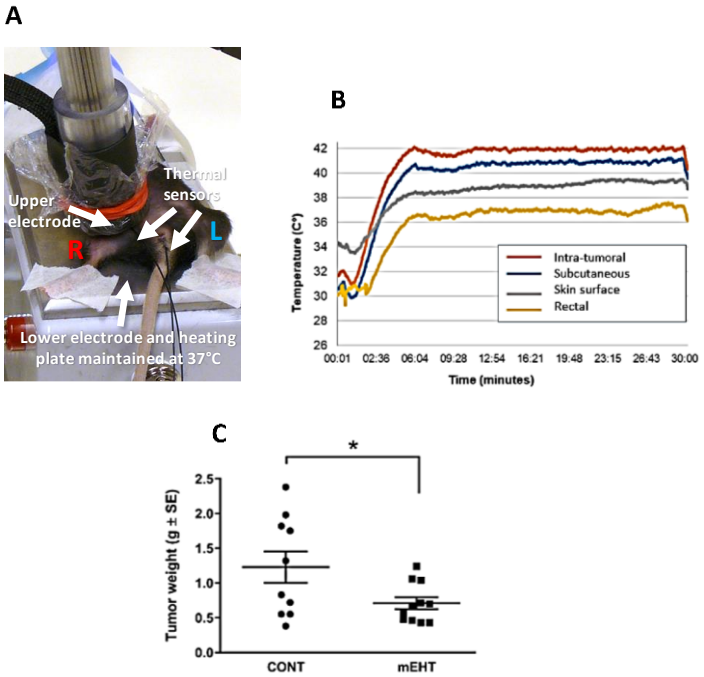

Figure 10. Modulated electrohyperthermia (mEHT) induced reduction of primary tumor growth. (A) Experimental setup of mEHT treatment using LabEHY-200. During treatment, mice were laid between plane-parallel asymmetric electric condensers of the circuit which consisted of the lower, 72-cm^2 aluminum electrode used as a heating plate (set to 37 °C) and the upper telescopic conductive textile electrode, which was placed on the tumor. (B) Temperature monitoring during mEHT treatment with optical thermo-sensors inserted into the tumor, subcutaneously, rectally, and on the skin surface directly below the upper electrode. (C) Tumor weights of the tumors harvested 48 h after the third mEHT treatment, n=10 for control (CONT) and n=11 for mEHT-treated tumors (mEHT). *$p \leq 0.05$, unpaired two-tailed t-test.

The temperature was monitored using optical thermo-sensors inside tumors, rectally, subcutaneously, and directly below the upper electrode (Figure 10A, 10B) to assess the thermal effect in and around treated tumors. The power adjustment profile allowed accurate maintenance of temperature around 42 °C in the center of the treated grafts. The subcutaneous temperature was 1 °C lower than the tumor center, while the skin surface was 39 °C, indicating a thermal gradient, with the highest value in the tumor core. The duration of the treatment was 30 min, following common clinical practice in mEHT application. This adjustment allowed us to avoid invasive temperature monitoring in the following experiments. Using this protocol, relying solely on the skin surface and rectal temperature measurements, we demonstrated that mEHT treatment resulted in significant tumor weight reduction after three-time treatments as demonstrated in Figure 10C.

4.2. mEHT induced localized temperature increase in mice lung

As mEHT has not been used before for interventions in the lung, our first objective was to develop a suitable chest electrode capable of inducing lung-specific hyperthermia without treatment-associated damage to nearby structures such as the heart, liver, and skin in mice. Because the impedance of the lung to transmitted energy is far higher than that of the neighboring tissues, the electrode needed to cover exclusively the target area, thereby avoiding the dissipation of energy to nearby structures. Based on these considerations, several chest electrodes were designed and tested for inducing lung-specific hyperthermia with a targeted treatment temperature range of 41.5 – 42.0 °C and the upper conductive textile chest electrode shown in Figure 11A (right panel) and 11B was found to be optimal for lung treatment. We demonstrated a localized increase in temperature over the target area on mice chest as represented by the externally measured thermal mapping shown in Figure 11A (left panel). Figure 11B depicts the dimensions of the conductive textile chest electrode used in this study for the targeted treatment of lung tumors in mice. Figure 11C shows the power adjustment profile of mEHT with measured lungs, pharyngeal, and rectal temperatures at different time points. A significant difference was observed between measured lung/pharyngeal and lung/rectal temperatures ($p<0.0001$) with mean temperature values of 41.6 ± 0.1 °C, 40.3 ± 0.1 °C, and 38.5 ± 0.5 °C measured in the lung, pharynx, and rectum respectively during treatment (Figure 11D). These results demonstrate that the targeted temperature range for mEHT treatment

of lungs could be achieved with the current chest electrode while maintaining limited dissipation of energy to nearby structures and the whole body.

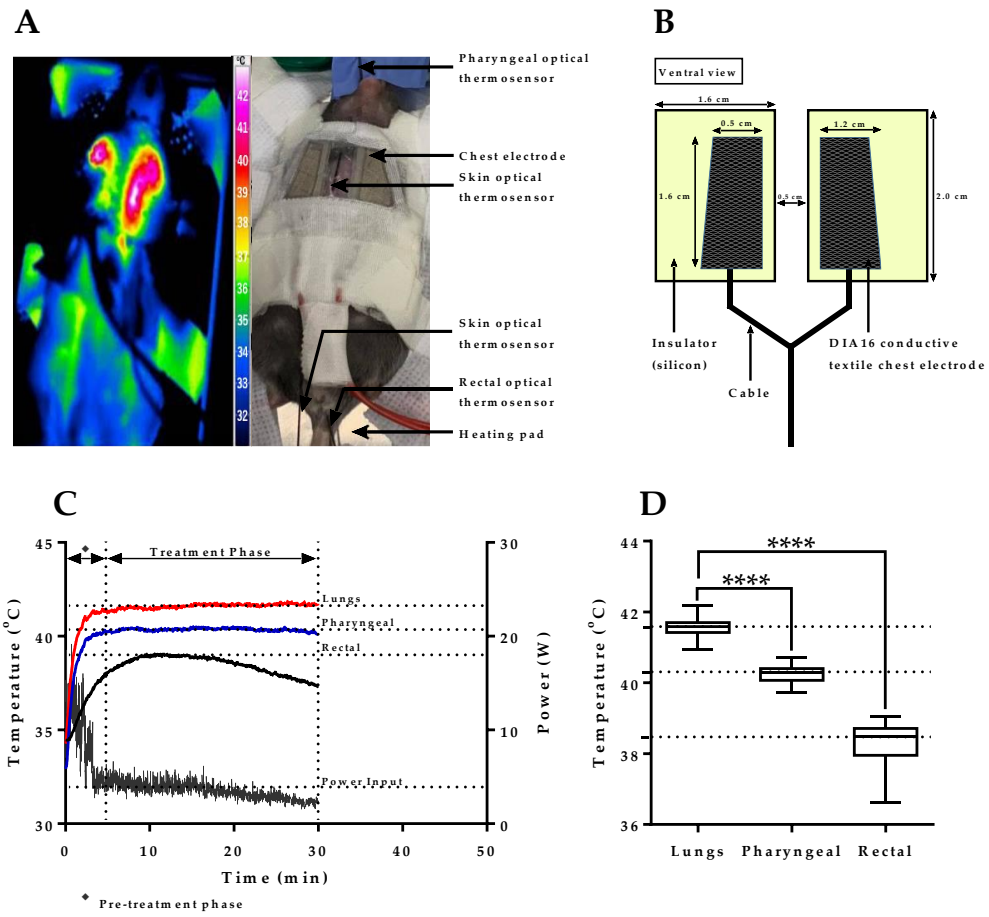

Figure 11. Localization of heat stress during targeted mEHT treatment of lungs. (A) Thermal image depicting a localized increase in temperature over target area on mice thorax (left panel) and treatment layout with the positioning of chest electrode and optical thermosensors (right panel); (B) Dimensions of conductive textile chest electrode for targeted lung treatment of tumors in mice; (C) Plot depicting temperature profiles of lungs, pharynx, and rectum with applied power settings; (D) Pharyngeal and rectal temperature versus lung temperature in treatment phase (n=4). Data represent average ± SEM. Mann-Whitney test, ****$p < 0.0001$.

DOI:10.14753/SE.2022.2552

4.3. Minimally invasive technique of lung temperature measurement in mEHT

The accurate measurement of lung temperature during repeated treatments with mEHT is highly essential to ensure that targeted treatment temperature is reached but not exceeded. Direct lung temperature measurement, however, is not feasible partly due to the high risk of mechanical lung injury. Therefore we sort out to develop a minimally invasive method of estimating lung temperature during mEHT treatment in mice. Optical thermosensors were advanced into the main bronchi, pharynx, and rectum of non-tumor-bearing animals and treated with mEHT for 30 min according to the experimental setup depicted in Figure 12A.

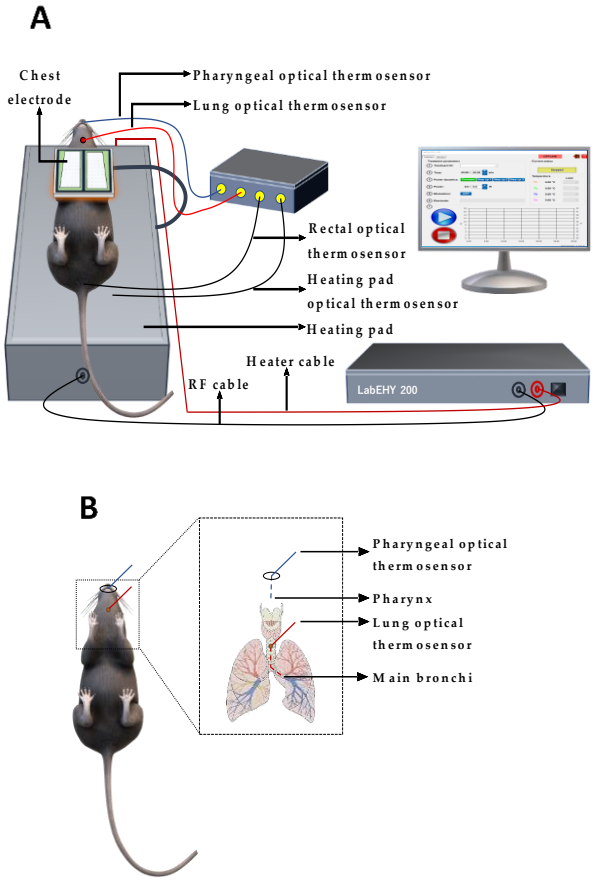

Figure 12. Experimental setup for investigation of quantitative relation between the lung and pharyngeal temperatures. (A) Schematic illustration of the experimental setup of mEHT for lung treatment of mice. Thermosensors are positioned in the lung (main bronchi), pharynx, rectum, and heating pad/lower electrode. (RF: Radiofrequency); (B) Schematic illustration depicting placement of pharyngeal and lung (main bronchi) optical thermosensors.

DOI:10.14753/SE.2022.2552

Access to mice trachea was enabled *via* puncture tracheotomy through which an optical thermosensor was advanced to the lung's main bronchi and *via* oral access, a pharyngeal optical thermosensor was placed in the pharynx of mice (Figure 12B). Lung temperature was maintained at 41.5 – 42.0 °C using the power adjustment profile of mEHT and the pharyngeal temperature was monitored simultaneously. The objective here was to assess if a quantitative relationship exists between the lung and pharyngeal temperature; in which case, if a relationship is established, lung temperature could be estimated indirectly in subsequent experiments by measuring the pharyngeal temperature only. Figure 13A shows a plot of the temperature difference between lungs and the pharynx or rectum with an observed minor deviation of the temperature difference seen in the pharynx. Major rectal temperature deviation from the lung temperature indicates its unsuitability as a parameter based on which lung temperature changes can be estimated. The minor deviation of temperature difference seen between the pharynx and lung indicates the existence of a quantitative relationship between the lung and the pharyngeal temperature based on which the lung temperature can be estimated from the pharyngeal temperature.

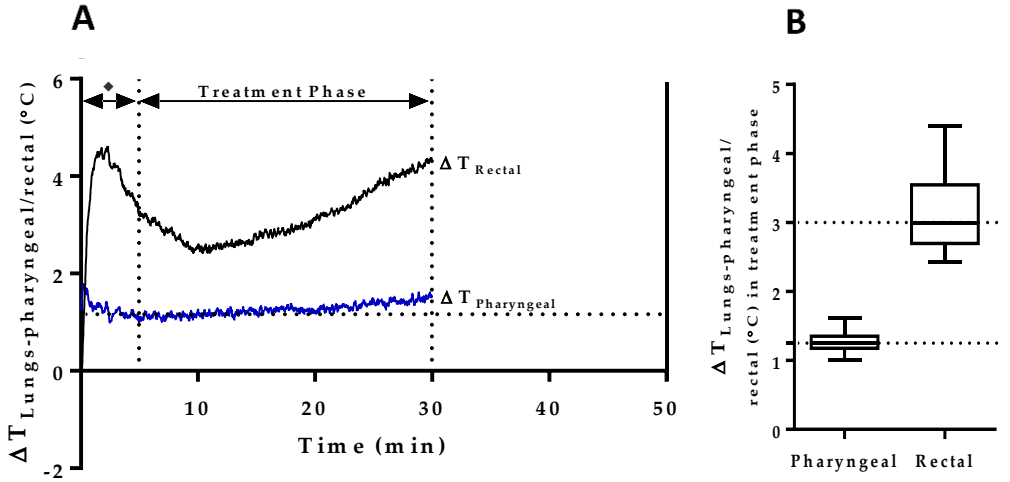

Figure 13. Quantitative relation of the lung (main bronchi) and pharyngeal temperatures during mEHT treatment. (A) Temperature gradient between the lung (main bronchi) and pharyngeal/rectal temperatures (n=4); (B) Plot of the mean difference between lungs (main bronchi) and pharyngeal/rectal temperatures (n=4). Data represent average ± SEM.

DOI:10.14753/SE.2022.2552

Following these experiments, subsequent treatment of tumor-bearing lungs was conducted by measurement of the pharyngeal temperature only eliminating the need for direct lung temperature measurement as depicted in Figure 14A. In sham-treated tumor-bearing animals, the chest electrode was placed on a coupling pad and pseudo-treated accordingly while all other conditions were maintained as same as mEHT-treated animals (Figure 14B). Figure 14C indicates a sample temperature profile measured during actual mEHT treatment of tumor-bearing lungs in mice.

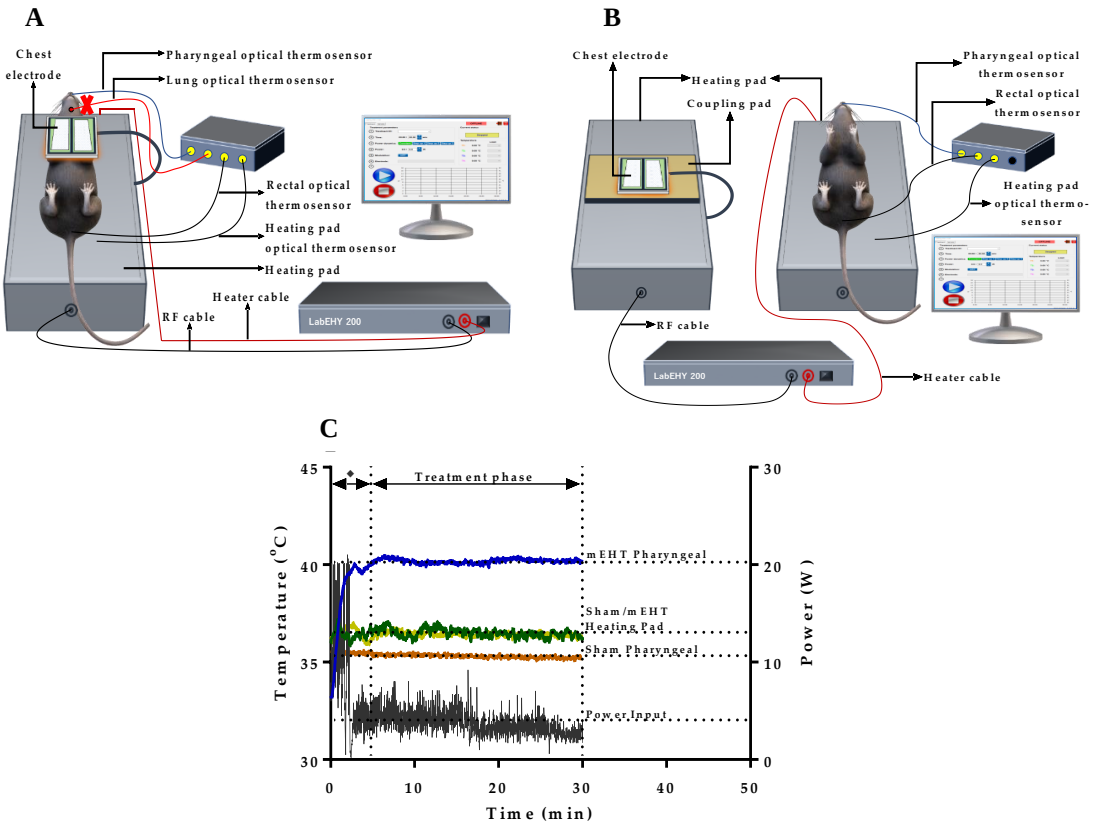

Figure 14. Experimental setup for mEHT treatment of tumor-bearing lungs in mice. (A) Schematic illustration of the experimental setup of mEHT for treatment of tumor-bearing lungs. Thermosensors were positioned in the pharynx, rectum, and heating pad/lower electrode only. As indicated (“X” sign), direct measurement of lung (main bronchi) temperature was eliminated. (RF: Radiofrequency); (B) Schematic illustration of sham treatment setup. (RF: Radiofrequency); (C) Plot depicting temperature profiles of the pharynx, and heating pad with applied power settings during mEHT treatment of tumor-bearing lungs. Data represent average ± SEM.

Taken together, these results demonstrate that pharyngeal temperature measurement during mEHT treatment is a viable method of estimating lung temperature and controlling heat stress generated in mice lung during mEHT treatment of tumors without any need for direct lung temperature measurement with the associated risk of mechanical injury.

4.4. mEHT induced reduction of pulmonary metastatic burden in mice lungs

To define the potential impact of mEHT in the host lung on the development of metastatic nodules, 10^5 B16F10 melanoma cells were injected into the tail vein of seven-to-nine-week-old female C57BL/6 mice. All animals were treated six times using mEHT. The first mEHT treatment of 30 min was performed one day after the tail vein injection of the animals with B16F10 melanoma cells. Treatment was repeated every third day for a total of six times as defined by the experimental protocol (Figure 15A).

Before sacrifice on day 18, PET imaging was performed on all animals to investigate the in vivo characteristics of mEHT-treated and sham-treated melanoma in mice lungs. Figure 15B shows representative PET images depicting [^{18}F]FDG uptake in sagittal and coronal sections of mEHT-treated and sham-treated control mice. As depicted by Figure 15C and 15D, significantly reduced SURmax ($p = 0.0169$) and SUVmax ($p = 0.0300$) were observed in the mEHT-treated lungs compared to the sham-treated ones.

Furthermore, a post-imaging sacrifice of all animals was performed to assess the gross pathological and metastatic burden of the lungs in both experimental groups. Visible tumor nodules were observed in the lungs of both mEHT-treated and sham-treated animals, indicating that metastatic tumors were successfully induced in mice lungs (Figure 16A). The pulmonary metastatic burden was assessed by counting the number of tumor nodules on the lung surface. Mice in the mEHT-treated group displayed a significantly lower number of tumor nodules (average of 17), whereas numerous distinguishable melanoma nodules (average of 60) were observed in the lungs of sham-treated animals ($p = 0.0049$, Figure 16B).

In addition, excised lungs were weighted to further characterize the difference in tumor burden between the treated and control group. As shown in Figure 16C, the mean lung weight in the mEHT-treated group was significantly reduced indicating the suppression of tumor growth compared to the control group ($p = 0.0090$).

DOI:10.14753/SE.2022.2552

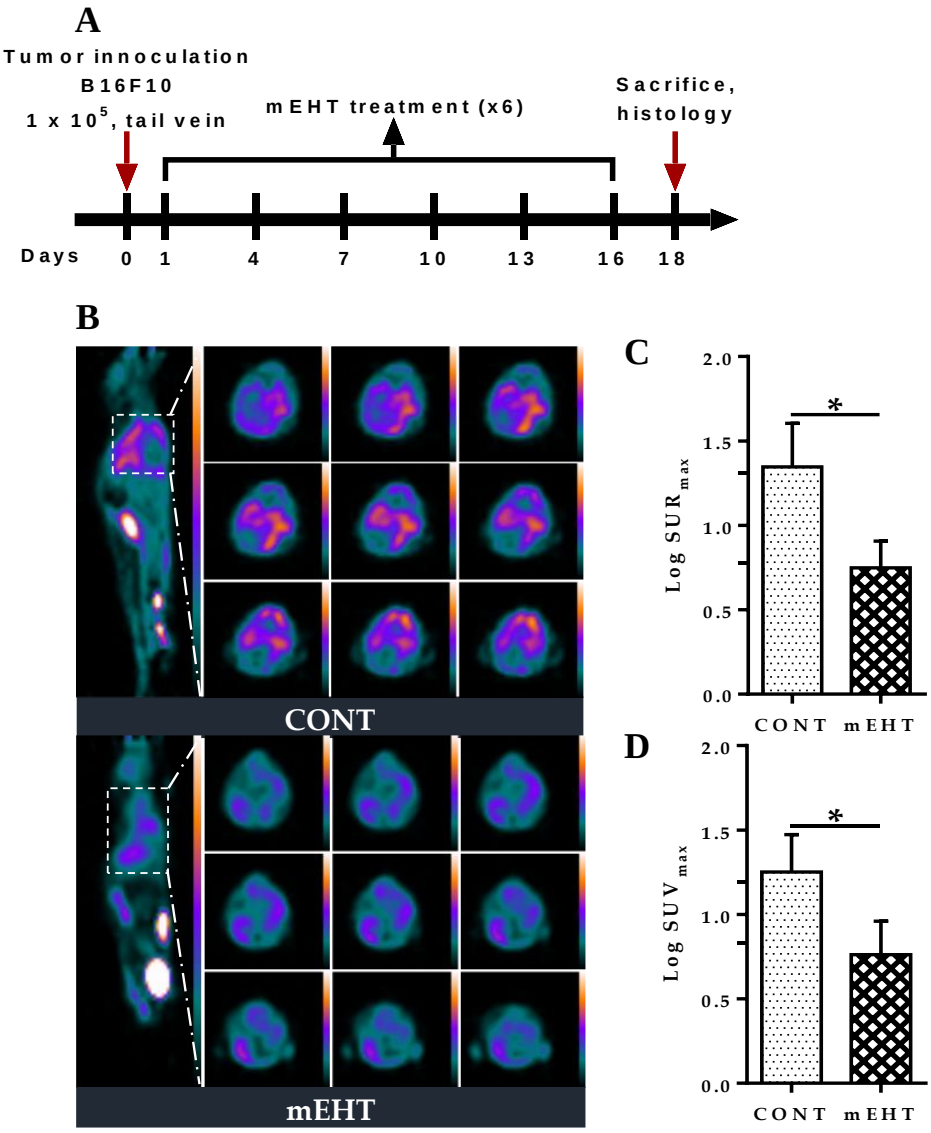

Figure 15. Effect of modulated-electrohyperthermia on tumor burden in mouse lungs. (A) Schematic representation of the experimental protocol; (B) Representative PET images depicting [^{18}F]FDG uptake in sagittal and coronal sections of CONT and mEHT; (C) Standardized uptake ratio (SURmax) of [^{18}F]FDG in CONT (n=4) and mEHT (n=3); (D) Standardized uptake value (SUVmax) of [^{18}F]FDG in CONT (n=4) and mEHT (n=3). Data represent average ± SEM. CONT vs mEHT, Mann-Whitney test. *$p < 0.05$.

DOI:10.14753/SE.2022.2552

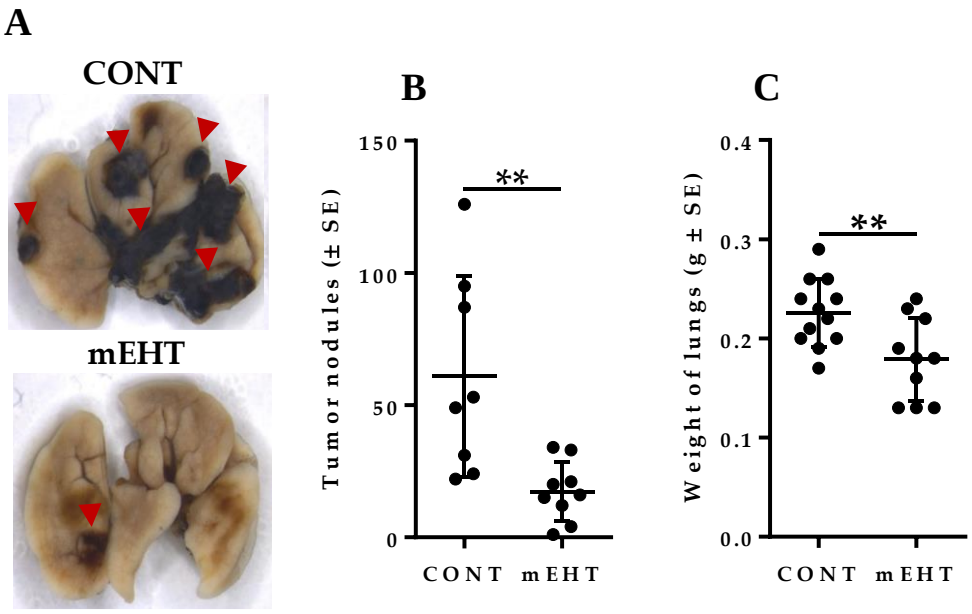

Figure 16. Effect of modulated-electrohyperthermia on tumor burden in mouse lungs. (A) Native lungs with pulmonary melanoma metastases in CONT and mEHT-treated animals; (B) Quantification of pulmonary melanoma metastatic nodules in CONT (n=8) and mEHT (n=9); (C) Quantification of lung weight in CONT (n=12) and mEHT (n=10). Data represent average ± SEM. CONT vs mEHT, unpaired t-test, **p < 0.01.

Furthermore, analysis of H&E stained sections was performed to characterize mEHT-related tumor growth suppression in the lungs including intra-parenchymal tumors with no surface visibility which often proves difficult to quantify by surface tumor nodules evaluation only. Multiple focal lesions with pleomorphisms and marked cellular atypia were observed in both mEHT-treated and sham-treated lungs (Figure 17A, 17B). Focal metastatic lesions in treated animals were significantly reduced in number especially for lesions < 0.1 mm^2 ($p = 0.0032$, Figure 17C). Likewise, the number of focal lesions > 0.1 mm^2 was significantly reduced in treated lungs compared to the sham-treated ones ($p = 0.0497$, Figure 17C). Additionally, counts per unit lung area of focal lesions showed a significant reduction in mEHT-treated animals compared to the sham-treated ones ($p = 0.0039$, Figure 17D). The total tumor area of focal metastatic melanoma lesions in mEHT-treated lungs was reduced significantly ($p = 0.0383$, Figure 17E), although the relative area occupied by these lesions per lung showed marked reduction without reaching a statistically significant value ($p = 0.0968$, Figure 17F).

DOI:10.14753/SE.2022.2552

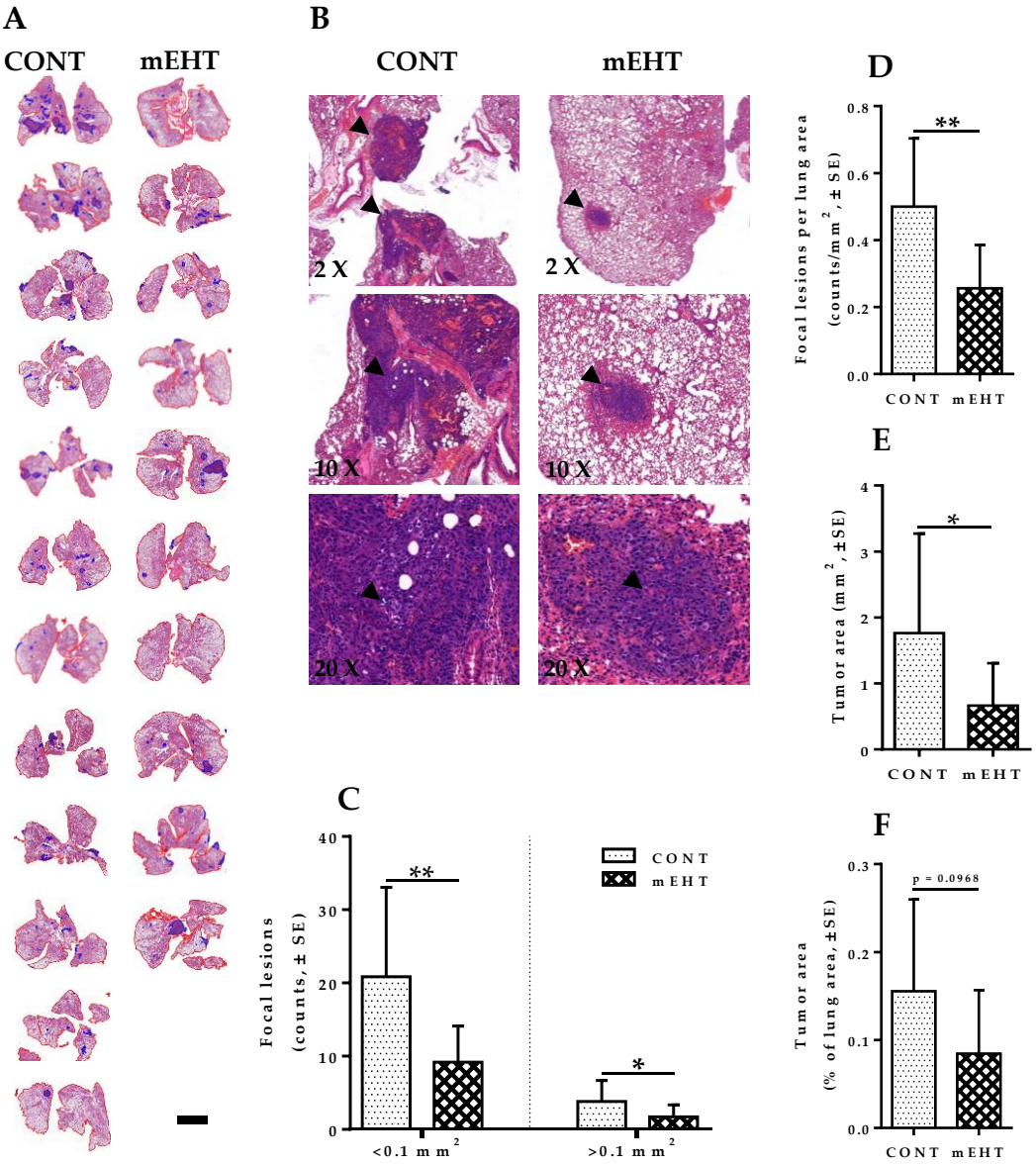

Figure 17. Inhibitory effect of modulated-electrohyperthermia on tumor growth and proliferation. (A) H&E stained lungs with pulmonary melanoma metastases in CONT and mEHT-treated animals; (B) H&E stained lungs with pulmonary melanoma metastases at higher magnification in CONT and mEHT-treated animals; (C) Cumulative counts of focal metastatic melanoma lesions in CONT (n=12) and mEHT (n=10) sorted based on size (<0.1 mm^2 and >0.1 mm^2); (D) Cumulative counts of focal metastatic melanoma lesions per total lung area in CONT (n=12) and mEHT (n=10); (E)Tumor area occupied by melanoma in lungs in CONT (n=12) and mEHT (n=10); (F) Tumor area per total lung area in CONT (n=12) and mEHT (n=10). Data represent average ± SEM. unpaired t-test, *$p < 0.05$, **$p < 0.01$. Scale bar on A represents 4000 μm.

DOI:10.14753/SE.2022.2552

4.5. mEHT induced reduction in Ki67 expression in B16F10 melanoma cells

The depletion of Ki67 in some human tumor cell lines and primary fibroblast cells has been demonstrated to slow entry into the S-phase and coordinately downregulate genes involved in DNA replication thereby slowing the proliferation of tumor cells (171). Therefore, we investigated whether Ki67 downregulation plays a role in mEHT-mediated inhibition of B16F10 melanoma growth in murine lungs. Ki67 expression was measured by immunohistochemistry with anti-Ki67 antibody in both mEHT-treated and sham-treated tumors (Figure 18A). Our investigation showed that Ki67 protein expression per unit tumor area was significantly reduced in mEHT-treated tumors compared to the control group ($p = 0.0085$, Figure 18B).

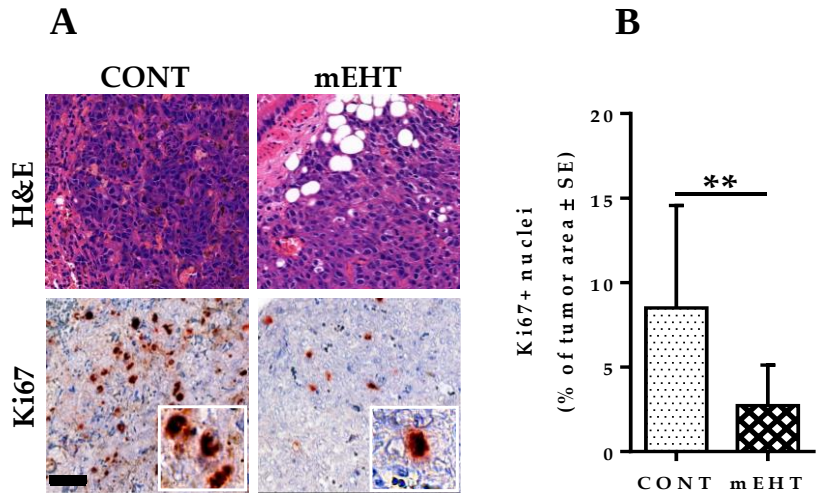

Figure 18. mEHT induced inhibition of tumor proliferation of B16F10 melanoma. (A) H&E and Ki67 staining of tumor area in CONT and mEHT; (B) Plot depicting Ki67 positive nuclei as a percentage of total tumor area in CONT (n=12) and mEHT (n=10). Data represent average ± SEM. CONT vs. mEHT, unpaired t-test, **$p < 0.01$. Scale bar on A represents 50 μm in low power images and 15 μm in their insets.

4.6. mEHT induced cell cycle arrest in B16F10 melanoma cells

$p21^{waf1}$ is a potent cyclin-dependent kinase inhibitor, the upregulation of which coincides with increased cell cycle arrest and senescence (172). Therefore, we investigated the effect of mEHT on the nuclear expression and localization of $p21^{waf1}$ in treated B16F10 melanoma cells. mEHT-treated and sham-treated samples were stained for $p21^{waf1}$ *via* immunohistochemistry and analyzed using modules of the QuantCenter image analysis software tool pack (3DHISTECH) for quantification. In mEHT-treated

tumors, significant upregulation in p21^{waf1} expression and nuclear localization was observed (Figure 19A). The fraction of p21^{waf1} positive cells as a percentage of tumor area was significantly increased in mEHT-treated tumors (p = 0.0206, Figure 19B) compared to the sham-treated group.

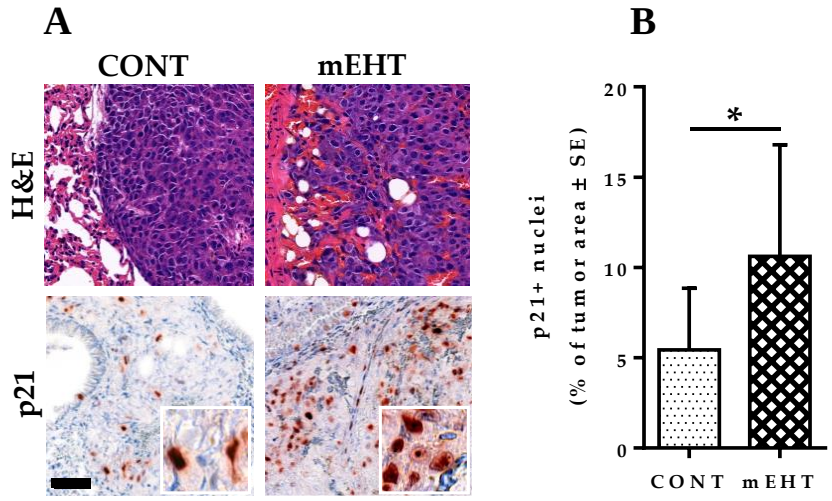

Figure 19. mEHT induced inhibition of tumor proliferation and cell cycle arrest. (A) H&E and p21^{waf1} staining of mouse lungs in CONT and mEHT; (B) Plot depicting counts of p21^{waf1} positive nuclei as a percentage of total tumor area in CONT (n=12) and mEHT (n=10). Data represent average ± SEM. CONT vs mEHT, Mann-Whitney test, *p < 0.05. Scale bar on A represents 50 μm on all low-power images and 15 μm in their insets.

4.7. mEHT induced DNA damage response in B16F10 melanoma tumor

Cellular response to DNA damage leads to a series of events, one of which is the phosphorylation of H2AX (173). H2AX phosphorylation typically occurs immediately after a DNA break formation, resulting in the recruitment of clusters of DNA damage response proteins at the site of damage, forming a DNA damage response focus (174). We tested the expression of phosphorylated H2AX (γ-H2AX) proteins to investigate whether mEHT induces significant DNA damage in treated tumors. While treated tumors showed marked DNA damage response to mEHT-treatment, adjacent normal lung tissue did not demonstrate any visible signs of DNA damage, reiterating that mEHT-associated DNA damage is confined only to the highly proliferating melanoma cells without associated damage to normal lung tissue (Figure 20A, 20B). In treated tumors, the expression of γ-H2AX was significantly increased after six-time treatment with mEHT compared to the sham-treated group (p = 0.0061, Figure 20C). Additionally, as DNA

damage may lead to either cell senescence or programmed cell death (173), we investigated the role of apoptosis in mEHT-mediated inhibition of tumor growth and proliferation. Treated B16F10 melanoma cells demonstrated a comparable level of cleaved caspase 3 expression per tumor area as sham-treated ones with no significant difference between both groups (p = 0.2331, Figure 20D, and 20E).

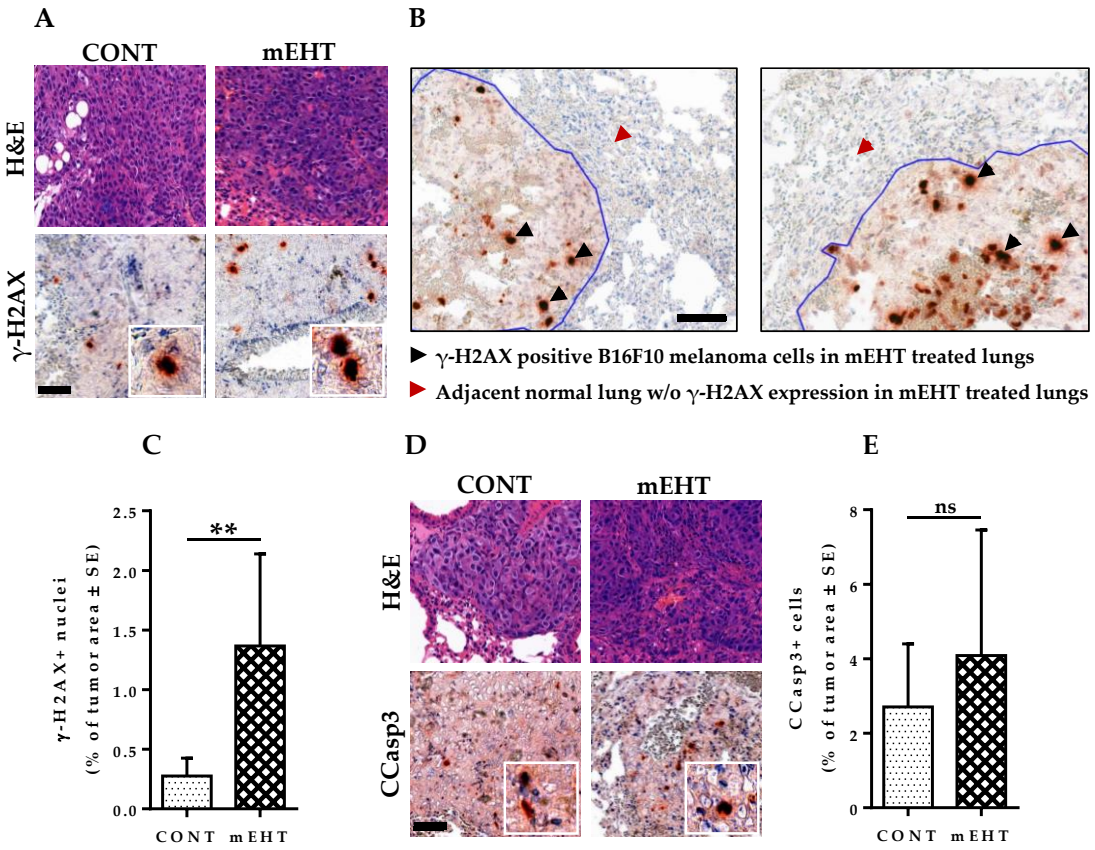

Figure 20. mEHT-related DNA damage response and apoptosis in metastatic B16F10 melanoma. (A) H&E and γ-H2AX staining of mouse lungs in CONT and mEHT; (B) Image depicting DNA damage response to mEHT treatment in tumor area but not in adjacent normal lung tissue; (C) Plot of γ-H2AX positive nuclei as a percentage of total tumor area in CONT (n=6) and mEHT (n=7); (D) H&E and CCasp3 staining of mouse lungs in CONT and mEHT; (E) Plot of CCasp3 positive cells as a percentage of total tumor area in CONT (n=12) and mEHT (n=9). Data represent average ± SEM. (C, E) CONT vs mEHT, unpaired t-test, ns = non-significant, **p < 0.01. Scale bar on A, D represents 50 μm on all low power images and 15 μm in their insets and 50 μm on B.

DOI:10.14753/SE.2022.2552

4.8. mEHT induced DAMP signal release in B16F10 melanoma cells

To assess the ability of mEHT to induce DAMP signal release from B16F10 melanoma tumor, we isolated tumor interstitial fluid derived from mEHT-treated primary tumors 48 hrs after the third mEHT treatment, which was used to detect the amount of hsp70, HMGB1 proteins, and ATP secretion. mEHT treatment resulted in a moderate but significant increase in secreted hsp70 ($p \leq 0.01$, Figure 21A), while HMGB1 showed approximately two-fold higher levels ($p \leq 0.004$, Figure 21B) and the concentration of ATP was five-fold higher ($p \leq 0.04$, Figure 21C) in the treated tumors.

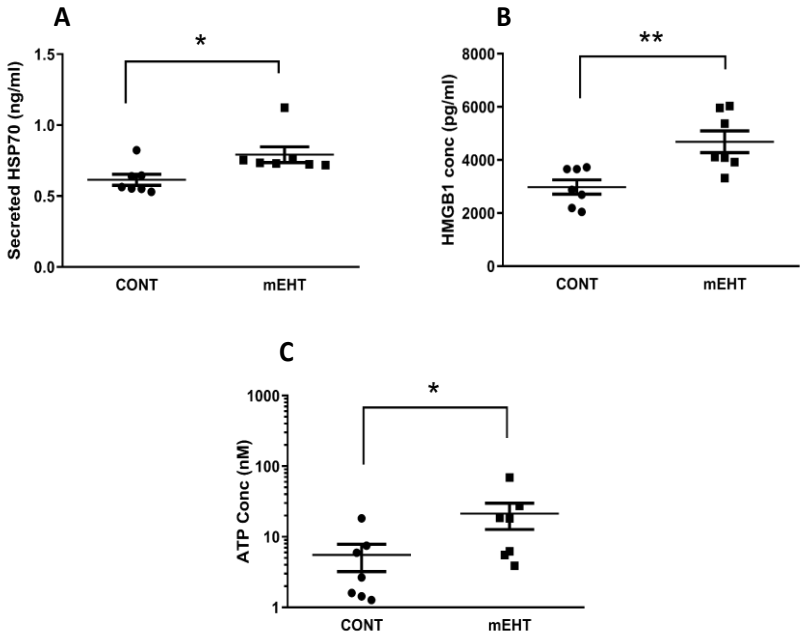

Figure 21. mEHT exposure of the tumors increased the release of damage-associated molecular patterns (DAMPs) into the tumor microenvironment. (A) hsp70, (B) HMGB1, and (C) ATP concentrations were determined in the tumor microenvironment 48 h after the last mEHT treatment using specific ELISA kits for hsp70 and HMGB1, and luciferase-based assay for ATP detection. n = 7; * $p < 0.01$ for hsp70, * $p < 0.04$ for ATP, ** $p < 0.004$, Mann–Whitney test.

4.9. T-cells and macrophages are increased in mEHT treated lungs

To study the putative contribution of immune cells to tumor growth inhibition by mEHT, we hypothesized that mEHT treatment might result in alteration in the immune status of the lungs and tumor microenvironment. Therefore, we analyzed the expansion of CD3+ T-cells, CD8+ T-cells, and F4/80+ macrophage in the lungs of tumor-bearing mice using immunohistochemistry in mEHT-treated and sham-treated animals. Significantly higher CD3+ T-cells infiltration into mEHT-treated tumors was observed compared to sham-treated ones ($p = 0.0252$, Figure 22A, 22B).

However, total lung CD3+ T-cells density was comparable between both groups with no statistically significant difference ($p = 0.6037$, Figure 22C). In contrast, the differences were significant for CD8+ T-cells, a prominent subtype of CD3+ cells with higher expression of positive cells seen in tumors of mEHT treated lungs ($p = 0.0221$, Figure 22D, 22E). The total lung CD8+ T-cell density was significantly increased as well in mEHT-treated mice ($p = 0.0238$, Figure 22F) compared to the control group. Furthermore, we investigated the density of F4/80+ macrophages in tumor and whole lung of mEHT-treated and sham-treated animals. A significantly higher density of F4/80+ macrophages was observed in tumors ($p = 0.0363$, Figure 22G, 22H) and whole lung ($p = 0.0007$, Figure 22I) of mice treated with mEHT compared to sham-treated animals.

DOI:10.14753/SE.2022.2552

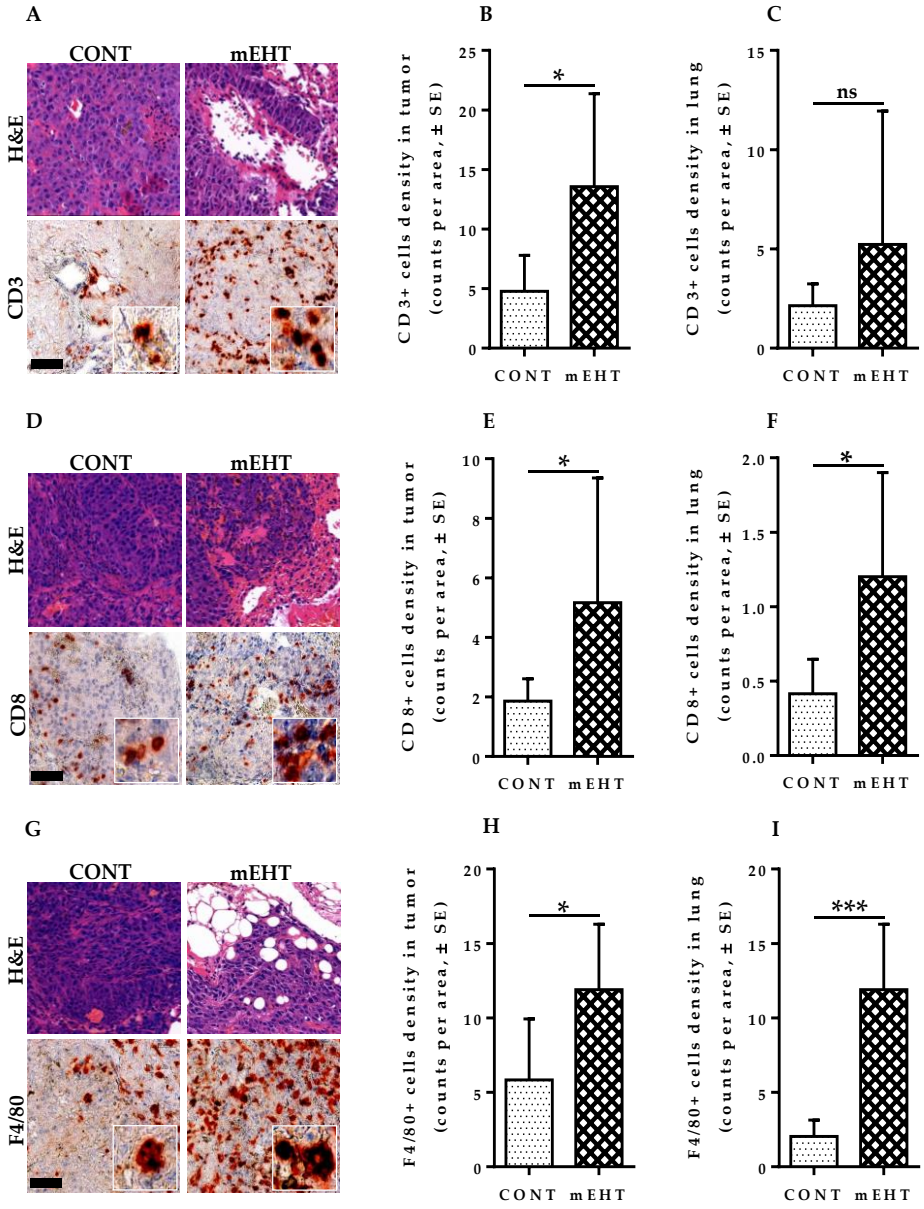

Figure 22. mEHT induced immune cell infiltration in focal metastatic melanoma lesions**.** (A) H&E and CD3 staining of mouse lungs in CONT and mEHT; (B) Plot depicting CD3 positive cell density in tumor area in CONT (n=6) and mEHT (n=7); (C) Plot depicting CD3 positive cell density in total lung area in CONT (n=6) and mEHT (n=7); (D) H&E and CD8 staining of mouse lungs in CONT and mEHT; (E) Plot depicting CD8 positive cell density in tumor area in CONT (n=6) and mEHT (n=7); (F) Plot depicting CD8 positive cell density in total lung area in CONT (n=6) and mEHT (n=7); (G) H&E and F4/80 positive cells staining of mouse lungs in CONT and mEHT; (H) Plot depicting F4/80 positive cell density in tumor area in CONT (n=5) and mEHT (n=6); (I) Plot depicting F4/80 positive cell density in total lung area in CONT (n=5) and mEHT (n=6). Data represent average ± SEM. (B, F, H, I) CONT vs mEHT, unpaired t-test, (C, E) CONT vs mEHT, Mann-Whitney test, ns = non-significant, *$p < 0.05$, **$p < 0.01$, ***$p < 0.001$. Scale bar represents 50 μm on all low-power images and 15 μm in their insets.

4.10. Auxiliary lung damage following six-times mEHT treatment

To study the potential adverse effect of mEHT treatment on the lungs, we investigated the capability of mEHT to induce significant inflammatory, lung injury, and fibrotic changes in the lungs in both acute and chronic conditions. All mice were treated a total of six times as described in the experimental protocol (Figure 23A) and sacrifice was performed accordingly on day 18 (2 days after last mEHT treatment) and on day 48 (32 days after last mEHT treatment) for acute and chronic cases respectively. To characterize the potential inflammatory effect of mEHT on treated lungs, lung samples were stained for myeloperoxidase (MPO) *via* immunohistochemistry in both mEHT-treated and sham-treated animals for quantification of MPO expressing cells (Figure 23B, 23C). mEHT induced a significant increase in MPO positive cells under acute conditions compared to the control group ($p = 0.0485$). However, chronic levels of MPO expressing cells measured on day 48, 32 days after the last treatment showed no significant difference between the groups ($p = 0.2730$), suggesting that the inflammatory impact of mEHT on the lungs is restricted to acute conditions only (Figure 23D).

Furthermore, to understand the full spectrum of potential mEHT related adverse effects on mice lungs, we investigated the degree of lung injury in both groups, taking into consideration the scores of each composing parameters, such as cellular infiltrate, alveolar over-distension, atelectasis, interstitial congestion, and hemorrhage (Figure 24B-24F).

The lung injury score was calculated as the sum of each composing parameters' score. Based on the scores of the composing parameters, we did not observe any significant increase in lung injury following mEHT treatment of mice lungs.

As inflammation can lead to fibrosis, especially under chronic conditions, we assessed the possibility of mEHT-induced fibrotic changes in the lungs by measuring the collagen contents in treated and sham-treated lungs. All samples were Masson's trichrome stained to characterize the collagen contents within the lungs (Figure 25A, 25B). As Figure 25C indicates, we did not find any evidence of increased collagen content in the lungs of mEHT-treated animals compared to sham-treated ones in both acute ($p = 0.5381$) and chronic conditions ($p = 0.8927$).

DOI:10.14753/SE.2022.2552

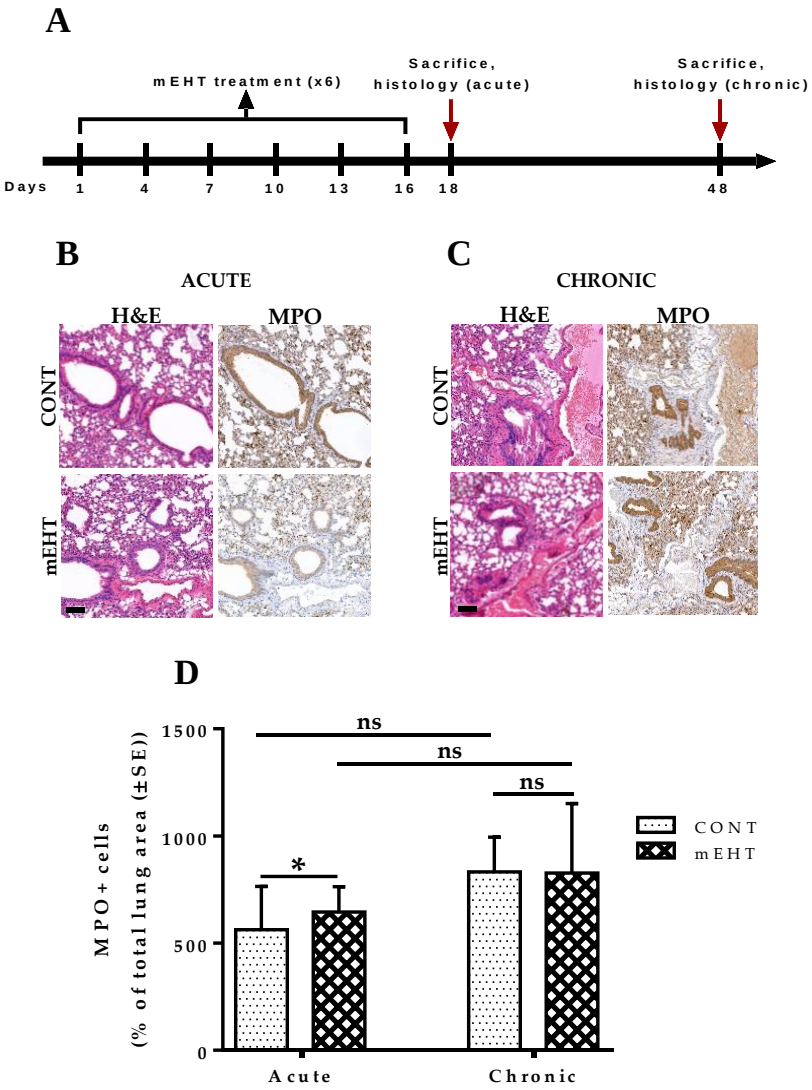

Figure 23. Acute and chronic implications of mEHT treatment on myeloperoxidase expression. (A) Experimental treatment protocol of non-tumor-bearing mice. (B, C) H&E and MPO staining of mice lungs 2 days (acute) and 32 days (chronic) after last mEHT treatment in CONT and mEHT; (C) Plot of MPO positive cells (fraction of total lung area) in CONT (n=5) and mEHT (n=5). Data represent average ± SEM. CONT vs mEHT, unpaired t-test, ns = non-significant, *$p < 0.05$. Scale bar in B and C represents 100 μm.

DOI:10.14753/SE.2022.2552

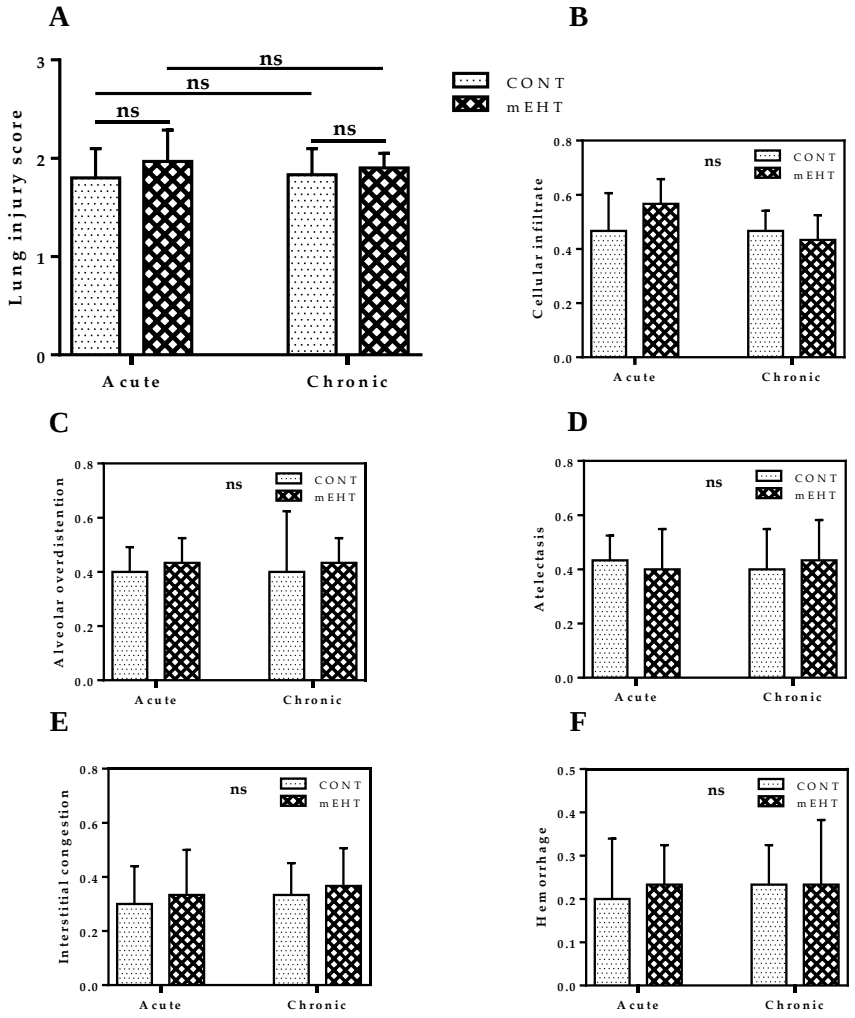

Figure 24. Acute and chronic implications of mEHT treatment on lung injury. (A) Cumulative lung injury score in CONT (n=5) and mEHT (n=5); (B, C, D, E, F) Component parameters of lung injury score which is a combined score of cellular infiltrate (0–4), alveolar over-distension (0–4), atelectasis (0–4), interstitial congestion (0–4), and hemorrhage (0 or 1). Data represent average ± SEM. (A) CONT vs. mEHT, unpaired t-test, (B, C, D, E, F) CONT vs mEHT, Mann-Whitney test, ns = non-significant.

DOI:10.14753/SE.2022.2552

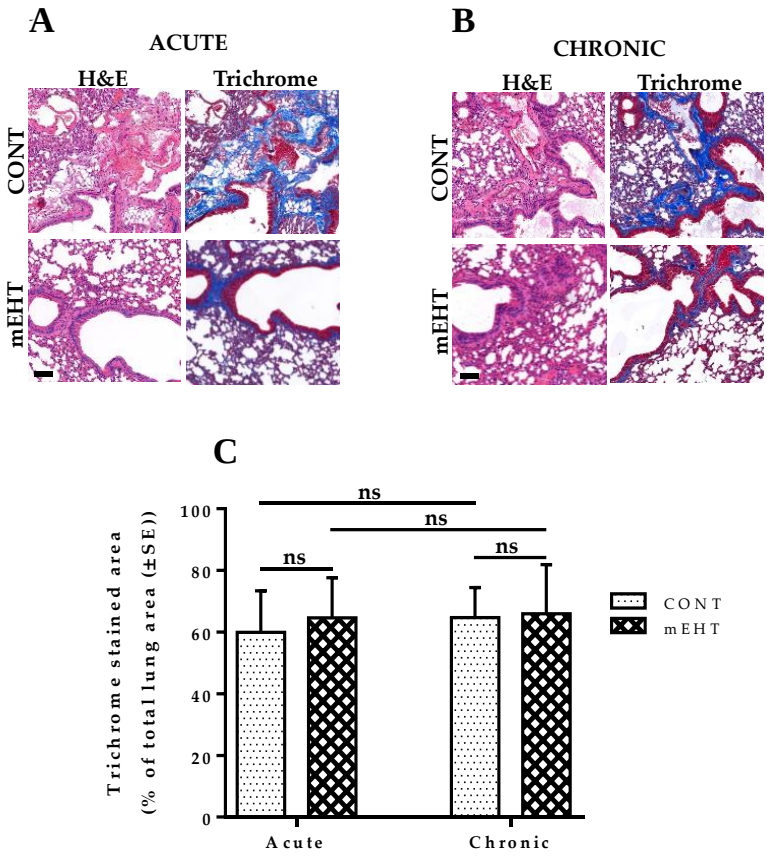

Figure 25. Acute and chronic implications of mEHT on pulmonary fibrosis. (A, B) H&E and Masson trichrome staining of mice lungs 2 days (acute) and 32 days (chronic) after last mEHT treatment in CONT and mEHT; (K) Plot of Masson's trichrome positive area (fraction of total lung area) in CONT (n=5) and mEHT (n=5). Data represent average ± SEM. CONT vs mEHT, unpaired t-test, ns = non-significant. Scale bar in A and B represents 100 μm.

DOI:10.14753/SE.2022.2552

5. Discussion

Our first priority in this study was to develop and optimize mEHT as a viable method of treating primary or metastatic lung tumors in mice. The difficulty of applying mEHT in lung oncology stems from the lack of adequate chest electrodes customized for localized induction of heat stress in lungs, as well as the lack of appropriate methods of measuring or estimating lung temperature for the duration of treatment non-invasively, or at the least minimally-invasively. Therefore, in this study, we first sort out to address these aforementioned issues. Multiple chest electrodes with different specifications were designed and successfully tested for the capability of inducing a targeted increase in lung temperature while minimizing energy dissipation to surrounding tissues and organs in the thorax. Next, we set up electric parameters to ensure a targeted treatment temperature of 41.5 – 42.0 °C in the lungs. During initial verification experiments, thermosensors were positioned in the main bronchi of lungs, pharynx, and rectum in non-tumor-bearing mice, and mEHT treated accordingly. A standard temperature gradient of 1.3 ± 0.1 °C was revealed between the lungs and pharyngeal temperature. Based on this, in subsequent experimental treatment of tumor-bearing mice, lung temperature was estimated by minimally invasive monitoring of the pharyngeal temperature only.

Serial treatment of the lungs with the newly developed method demonstrated significant tumor growth inhibition, leading to reduced tumor burden in the lungs of mEHT-treated animals. This was demonstrated by an apparent reduction in gross metastatic pulmonary nodules, lung weight, as well as tumor area, tumor counts, tumor counts (% of lung area), and decreased [^{18}F]FDG uptake in the lungs of treated animals as measured by PET. Lung SURmax and lung-to-blood SUVmean ratio are two quantitative parameters of [^{18}F]FDG uptake measured by PET. SURmax values reflect the metastatic lesion [^{18}F]FDG avidity in the lungs, while SUVmean ratio describes the dynamics of [^{18}F]FDG uptake from the blood by tumor cells, characterizing their metabolic difference from surrounding normal organ tissues. The decrease in these parameters suggests a “dampening” *in vivo* effect of mEHT on metastatic melanoma in the lungs.

Next, we investigated plausible molecular changes that may be responsible for the observed tumor growth inhibition following mEHT treatment of B16F10 melanoma in

the lungs. Ki67 is a tumor proliferation marker and its protein expression is consistent with the proliferative activity of malignant tumor cells (175). Following six-time treatments of melanoma with mEHT, significant downregulation of Ki67 protein expression was demonstrated in treated tumors which were accompanied by a comparable decrease in tumor size.

Furthermore, we investigated the role that $p21^{waf1}$ expression and nuclear localization may play as an anti-tumor effect of mEHT on melanoma tumors. The control of cell cycle progression is mediated by several factors in response to multiple stimuli amongst which $p21^{waf1}$, a potent cyclin-dependent kinase (CDK) inhibitor has been widely described. The nuclear localization of $p21^{waf1}$ in response to external or internal stimuli correlates with its inhibitory effect on cell cycle progression (176). Significant upregulation in $p21^{waf1}$ expression and nuclear localization was observed in treated tumors, suggesting that $p21^{waf1}$-mediated cell cycle arrest plays an important role in the anti-tumor effect of mEHT.

In addition, many events that cause either cell cycle arrest or apoptosis are associated with increased phosphorylation of H2AX in the cellular response to DNA damage. We measured the level of γ-H2AX in treated and sham-treated tumors to investigate the DNA damaging effect of mEHT. Treated tumors showed a significantly increased level of γ-H2AX expression in tumor cells compared to sham-treated control. Increased H2AX phosphorylation is linked to p53 protein upregulation associated with increased $p21^{waf1}$, a strong cyclin-dependent kinase inhibitor (173). We have also demonstrated previously that mEHT treatment mediated p53 stabilization by acetylation of p53 in B16F10 melanoma cells (177). Increased DNA damage and $p21^{waf1}$ as already described can induce apoptotic cell death in tumor cells. In this study, however, we did not observe any significant increase in apoptotic cell death of mEHT-treated tumor cells as demonstrated by the insignificant levels of CCasp3 expression. One plausible explanation for this observation is the possibility of a cellular level pro-survival gene mutation in mEHT-treated tumor cells.

Furthermore, we have demonstrated that mEHT induces significantly increased levels of DAMP signal proteins including secreted hsp70, HMGB1 proteins, and ATP in B16F10 melanoma. Damage-associated molecular patterns (DAMPs) release is associated with increased tissue injury or cellular stress and is capable of activating the innate immune system and stimulate anti-tumor immunity resulting in immunological cell

death (178). Therefore, we investigated whether mEHT treatment has the capability of mobilizing the immune system. As anti-tumor immunity is in most cases predominantly mediated by cellular immunity, we measured the density of CD3+- and CD8+-T cells in the whole lung and also in tumor tissue. We observed markedly increased CD3+-T cells in treated tumors, although an increase in CD3+-T cell density in the lung as a whole was statistically insignificant. An apparent increase in whole lung and tumor density of CD8+-T cells was observed in treated animals. Although mEHT treatment resulted in significantly increased T cells infiltration into treated tumors, it is yet to be investigated whether the infiltrating lymphocytes are actively involved in tumor destruction of B16F10 melanoma cells. In addition, we investigated the level of F4/80+ macrophage infiltrates in treated tumors to investigate the contribution of macrophages to the clearance of dead or senescent tumor cells. As expected, mEHT-treated lungs showed significantly increased F4/80+ macrophage density in both tumors and whole lungs indicating the critical role these cells may play in the efficacy of mEHT as a treatment modality.

Compared to conventional hyperthermia, mEHT can induce a significantly higher level of reactive oxygen species (ROS) in treated tumor cells (179). While this offers obvious therapeutic benefits such as ROS-mediated DNA damage of tumor cells (180), in normal lung tissues, ROS can activate NF-κB signal transduction leading to the expression of a variety of inflammatory genes for cytokines, IL-4, IL-5, IL-9, IL-15, and TNF-α with the potential of significant lung parenchymal damage (181). Therefore, we investigated whether mEHT treatment of lungs can induce significant treatment-related lung parenchymal injury under acute and chronic conditions. Heat stress was induced by exposing the anesthetized non-tumor-bearing mice to a lung temperature of 41.5 – 42.0 °C for 30 min with mEHT. Non-tumor-bearing mice were selected for this study to eliminate all potential influences that may affect the inflammatory status of the lungs. In two groups (sham-treated, mEHT-treated) of ten animals each, half of the animals in each group were sacrificed 48 h after the last mEHT treatment on day 18, and lungs were excised *en bloc* for further immunohistochemistry analysis. The remaining animals were kept under normal condition for an extended 30 days period, after which they were sacrificed and lungs excised for further analysis. All tissue samples were myeloperoxidase-stained. Myeloperoxidase (MPO) is a heme-containing protein found mostly in azurophilic

granules of neutrophils and to a lesser extent in monocytes (182). Neutrophils can undergo secondary necrosis during extensive inflammation, causing the release of MPO that may destroy resident lung cells and cause inflammation (182). mEHT treatment induced a significant increase in MPO positive cells under acute condition, although the measured levels of MPO positive cells in chronic condition was insignificant, demonstrating that this effect is non-long-lasting and limited to acute conditions only. The acute increase in MPO-positive cells did not result in any significant pathological damage to the lungs as demonstrated by the non-significant changes in lung injury score (LIS) in both acute and chronic conditions. The components measured as part of LIS included cellular infiltrate, alveolar over-distension, atelectasis, interstitial congestion, and hemorrhage, covering all major aspects of plausible lung injury. Furthermore, no signs of fibrosis, a potential consequence of chronic inflammation, was observed in this study. Based on these observations, it can be concluded that mEHT treatment alone did not induce any significant pathological changes in lungs of treated animals. The limitation of this study however, is that non-tumor bearing lungs was used, primarily to eliminate all other plausible cause of inflammation in mice lungs such as tumor presence as described earlier. Further investigation is needed on the potential adverse effect of mEHT in tumor-bearing lungs. Increase lymphocytic infiltration following mEHT treatment of lungs as previously described can potentially induce lung inflammation. Thus, the inflammatory status of mEHT-treated non-tumor bearing lungs is different from that of mEHT-treated tumor-bearing lungs and therefore deserves further investigation.

DOI:10.14753/SE.2022.2552

6. Conclusions

In this study, we have demonstrated the capability of mEHT to induce localized heat stress in the lungs, enabled *via* a customized chest electrode designed specifically for targeted treatment of lung tumors while minimizing the dissipation of energy to neighboring tissues and organs in the murine thorax. The verification of pharyngeal-lung temperature quantitative relation enabled the minimally invasive monitoring of lung temperature during treatment of tumor-bearing mice while avoiding any practical adverse effect of direct lung temperature measurement which may involve mechanical lung injury. This technique we believe could offer a particular advantage in clinical settings where accurate estimation of lung temperature is essential to eliminate over-heating or under-treating of primary or metastatic pulmonary cancers with a potential negative impact on treatment outcomes. We have demonstrated that repeated mEHT treatment (at 41.5 – 42.0 °C for 30 min) inhibits the growth of B16F10 melanoma in both primary tumor and pulmonary metastases models. A significant decrease in [^{18}F]FDG uptake and metastatic pulmonary melanoma nodules were observed in the lungs of treated animals. Upregulation of phosphorylated H2AX was demonstrated with mEHT treatment which led *via* the p53 pathway to upregulation and nuclear localization of p21^{waf1}, a potent cyclin-dependent kinase inhibitor responsible for tumor senescence and cell cycle arrest. The downregulating effect of mEHT on Ki67, a prominent tumor proliferation marker, reaffirms its ability to block cell cycle progression in treated tumor cells. Although several mechanisms have been described in this study to play a critical role in the tumor inhibitory effect of mEHT, apoptotic cell death was absent as demonstrated by the insignificant level of CCasp3 expression. As was verified previously in a primary tumor model of B16F10 melanoma, mEHT can induce significant DAMP signal release with the capability to stimulate the anti-tumor immunity that may result in the immunological death of tumor cells. Consequently, an increased density of infiltrating lymphocytes and macrophages was observed in mEHT-treated lungs compared to the sham-treated ones. The massive infiltration of tumors by CD3 and CD8 positive T-lymphocytes and by F4/80 positive macrophages indicated the mobilization of cellular anti-tumor immunity by mEHT. Furthermore, in non-tumor-bearing mice, mEHT treatment-induced lung infiltrating MPO positive cells (primarily neutrophils) was observed only in acute conditions, with

DOI:10.14753/SE.2022.2552

insignificant changes of MPO expressing cells observed in chronic conditions. This indicates absent inflammatory changes in the lungs in chronic conditions following mEHT treatment and explains the observed lack of fibrotic pathology in the lungs of treated animals. Despite the obvious therapeutic effects of mEHT treatment on the pulmonary metastases of melanoma as described in this paper, it remains to be evaluated whether synergistic advantages of combining mEHT with already existing treatment modalities may offer a better outcome for patients with primary or metastatic pulmonary cancers.

DOI:10.14753/SE.2022.2552

7. Summary

In this study, pulmonary metastases of melanoma were established by injecting B16F10 melanoma cells *via* tail vein into female C57BL/6 mice. Repeated treatment of tumor-bearing lungs with mEHT induced significant tumor growth inhibition demonstrated by the reduction in 2-Fluoro[18F]-2-Deoxy-D-Glucose uptake, decreased number of pulmonary metastatic nodules, decrease tumor area and decrease tumor counts as a fraction of the total lung area. The treatments provoked significant DNA double-strand breaks measured by the increased number of tumor cells displaying an elevated nuclear expression of phosphorylated H2AX protein. The mEHT-related significant increase in $p21^{waf1}$ positive tumor cells, besides the reduced Ki67 positive population, suggested that $p21^{waf1}$-mediated cell cycle arrest plays an important role in the anti-tumor effect of mEHT. Though mEHT did not induce major intratumoral cleaved/activated caspase-3 expression, the significantly elevated F4/80+ macrophage, and the enhanced CD3+ and CD8+ T-lymphocyte infiltration indicated the alerted anti-tumor cellular immunity in response to treatment. In conclusion, local mEHT can reduce the growth potential of pulmonary metastatic melanoma by dominantly inducing cell cycle arrest (senescence), inhibiting proliferation *via* downregulation of Ki67 expression, inducing DNA damage response, and mobilizing cellular immunity with potential tumor destructing effect, thus offering itself as a complementary partner of chemo- and/or radiotherapy.

DOI:10.14753/SE.2022.2552

8. Összefoglalás

Vizsgálatunkban a melanoma pulmonális metasztázisainak megjelenését nőstény C57BL/6 egerek farok vénájába injektált B16F10 melanoma sejtekkel idéztük elő. A metasztatikus tüdő ismételt mEHT-val való kezelése jelentős tumor növekedés gátlást váltott ki, amit a 2-Fluoro [18F]-2-Deoxy-D-Glucose felvétel mérséklődése, a pulmonális metasztázisok számának csökkenése és a daganat kiterjedésének zsugorodása jelzett. A kezelés kettős láncú DNS törések indukálása révén jelentős DNS károsodát váltott ki, melyet a fokozott foszforilált H2AX fehérje expressziót mutató tumorsejtek számának növekedésével igazoltunk. Az mEHT kezelés utáni p21waf1 pozitív tumorsejtek számának szignifikáns növekedése – csökkent Ki67 pozitív populáció mellett – rámutat, hogy a $p21^{waf1}$ mediált sejtciklus leállás fontos szerepet játszik az mEHT tumorellenes hatásában. Az mEHT nem indukált jelentős intratumorális hasított/aktivált kaszpáz-3 expressziót, ugyanakkor a szignifikánsan megemelkedett F4/80+ makrofág és CD3+/CD8+ T-limfocita infiltráció a kezelés által kiváltott tumor ellenes sejtes immunválasz aktiválódását jelezte. Összegzésképpen elmondható, hogy a lokális mEHT kezelés csökkentheti a pulmonális metasztatikus melanoma növekedési potenciálját azáltal, hogy a sejtciklus leállását (szeneszcenciát) és a Ki67 expresszió lecsökkenésén keresztül proliferáció gátlást okoz. Ezenkívül a kezelés által előidézett DNS károsodás és a tumor ellenes immunválasz indukálása révén potenciális daganat károsító hatása van, így alkalmas lehet kemo- és/vagy sugárterápia kiegészítésére.

DOI:10.14753/SE.2022.2552

9. References

1. Tsatmali M, Ancans J, Thody AJ. (2002) Melanocyte function and its control by melanocortin peptides. J Histochem Cytochem, 50: 125-133.

2. Abdel-Malek Z, Swope VB, Suzuki I, Akcali C, Harriger MD, Boyce ST, Urabe K, Hearing VJ. (1995) Mitogenic and melanogenic stimulation of normal human melanocytes by melanotropic peptides. Proceedings of the National Academy of Sciences of the United States of America, 92: 1789-1793.

3. Abdel-Malek Z, Suzuki I, Tada A, Im S, Akcali C. (1999) The melanocortin-1 receptor and human pigmentation. Ann N Y Acad Sci, 885: 117-133.

4. Erdei E, Torres SM. (2010) A new understanding in the epidemiology of melanoma. Expert Review of Anticancer Therapy, 10: 1811-1823.

5. Linos E, Swetter SM, Cockburn MG, Colditz GA, Clarke CA. (2009) Increasing burden of melanoma in the United States. Journal of Investigative Dermatology, 129: 1666-1674.

6. Guy GP, Thomas CC, Thompson T, Watson M, Massetti GM, Richardson LC, Centers for Disease C, Prevention. (2015) Vital signs: melanoma incidence and mortality trends and projections - United States, 1982-2030. MMWR. Morbidity and mortality weekly report, 64: 591-596.

7. Kosary CL, Altekruse SF, Ruhl J, Lee R, Dickie L. (2014) Clinical and prognostic factors for melanoma of the skin using SEER registries: Collaborative stage data collection system, version 1 and version 2. Cancer, 120: 3807-3814.

8. Rigel DS, Carucci JA. (2000) Malignant melanoma: prevention, early detection, and treatment in the 21st century. CA: A Cancer Journal for Clinicians, 50: 215-236.

9. Califano J, Nance M. (2009) Malignant Melanoma. Facial Plastic Surgery Clinics of North America, 17: 337-348.

10. Erdmann F, Lortet-Tieulent J, Schüz J, Zeeb H, Greinert R, Breitbart EW, Bray F. (2013) International trends in the incidence of malignant melanoma 1953-2008-are recent generations at higher or lower risk? International Journal of Cancer, 132: 385-400.

11. Whiteman DC, Green AC, Olsen CM. (2016) The Growing Burden of Invasive Melanoma: Projections of Incidence Rates and Numbers of New Cases in Six

Susceptible Populations through 2031. Journal of Investigative Dermatology, 136: 1161-1171.

12. Grigalavicius M, Moan J, Dahlback A, Juzeniene A. (2016) Daily, seasonal, and latitudinal variations in solar ultraviolet A and B radiation in relation to vitamin D production and risk for skin cancer. International Journal of Dermatology, 55: e23-e28.

13. Everett MA, Yeargers E, Sayre RM, Olson RL. (1966) PENETRATION OF EPIDERMIS BY ULTRAVIOLET RAYS. Photochemistry and Photobiology, 5: 533-542.

14. Li WQ, Cho E, Weinstock MA, Mashfiq H, Qureshi AA. (2016) Epidemiological assessments of skin outcomes in the nurses' health studies. American Journal of Public Health, 106: 1677-1683.

15. Brenner M, Hearing VJ. (2008) The protective role of melanin against UV damage in human skin. Photochemistry and Photobiology, 84: 539-549.

16. Moan J, Grigalavicius M, Baturaite Z, Dahlback A, Juzeniene A. (2015) The relationship between UV exposure and incidence of skin cancer. Photodermatology Photoimmunology and Photomedicine, 31: 26-35.

17. Martens MC, Seebode C, Lehmann J, Emmert S. (2018) Photocarcinogenesis and skin cancer prevention strategies: An update. Anticancer Research, 38: 1153-1158.

18. Estimated age-standardized incidence rates (World) in 2020, melanoma of skin, both sexes, all ages. https://gco.iarc.fr/today/online-analysis-map?v=2020&mode=population&mode_population=continents&population=900&populations=900&key=asr&sex=0&cancer=16&type=0&statistic=5&prevalence=0&population_group=0&ages_group%5B%5D=0&ages_group%5B%5D=17&nb_items=10&group_cancer=1&include_nmsc=1&include_nmsc_other=1&projection=natural-earth&color_palette=default&map_scale=quantile&map_nb_colors=5&continent=0&show_ranking=0&rotate=%255B10%252C0%255D (accessed June 4, 2021).

19. Crombie IK. (1979) Variation of melanoma incidence with latitude in North America and Europe. British Journal of Cancer, 40: 774-781.

20. Baade P, Meng X, Youlden D, Aitken J, Youl P. (2012) Time trends and latitudinal differences in melanoma thickness distribution in Australia, 1990-2006. International Journal of Cancer, 130: 170-178.

21. Seité S, del Marmol V, Moyal D, Friedman AJ. (2017) Public primary and secondary skin cancer prevention, perceptions and knowledge: an international cross-sectional survey. Journal of the European Academy of Dermatology and Venereology, 31: 815-820.

22. Jhappan C, Noonan FP, Merlino G. (2003) Ultraviolet radiation and cutaneous malignant melanoma. Oncogene, 22: 3099-3112.

23. Tripp MK, Watson M, Balk SJ, Swetter SM, Gershenwald JE. (2016) State of the science on prevention and screening to reduce melanoma incidence and mortality: The time is now. CA: A Cancer Journal for Clinicians, 66: 460-480.

24. Pollack LA, Li J, Berkowitz Z, Weir HK, Wu XC, Ajani UA, Ekwueme DU, Li C, Pollack BP. (2011) Melanoma survival in the United States, 1992 to 2005. Journal of the American Academy of Dermatology, 65: S78.e71-S78.e10.

25. Pfeifer GP, Besaratinia A. (2012) UV wavelength-dependent DNA damage and human non-melanoma and melanoma skin cancer. Photochem Photobiol Sci, 11: 90-97.

26. Rochette PJ, Therrien JP, Drouin R, Perdiz D, Bastien N, Drobetsky EA, Sage E. (2003) UVA-induced cyclobutane pyrimidine dimers form predominantly at thymine-thymine dipyrimidines and correlate with the mutation spectrum in rodent cells. Nucleic Acids Research, 31: 2786-2794.

27. Douki T, Reynaud-Angelin A, Cadet J, Sage E. (2003) Bipyrimidine photoproducts rather than oxidative lesions are the main type of DNA damage involved in the genotoxic effect of solar UVA radiation. Biochemistry, 42: 9221-9226.

28. Besaratinia A, Synold TW, Chen HH, Chang C, Xi B, Riggs AD, Pfeifer GP. (2005) DNA lesions induced by UV A1 and B radiation in human cells: Comparative analyses in the overall genome and in the p53 tumor suppressor gene. Proceedings of the National Academy of Sciences of the United States of America, 102: 10058-10063.

29. Kielbassa C, Roza L, Epe B. (1997) Wavelength dependence of oxidative DNA damage induced by UV and visible light. Carcinogenesis, 18: 811-816.

30. Kuluncsics Z, Perdiz D, Brulay E, Muel B, Sage E. (1999) Wavelength dependence of ultraviolet-induced DNA damage distribution: Involvement of direct or indirect mechanisms and possible artefacts. Journal of Photochemistry and Photobiology B: Biology, 49: 71-80.

31. Kvam E, Tyrrell RM. (1997) Induction of oxidative DNA base damage in human skin cells by UV and near visible radiation. Carcinogenesis, 18: 2379-2384.

32. Zhang X, Rosenstein BS, Wang Y, Lebwohl M, Mitchell DM, Wei H. (1997) Induction of 8-Oxo-7,8-Dihydro-2′-Deoxyguanosine by Ultraviolet Radiation in Calf Thymus DNA and HeLa Cells. Photochemistry and Photobiology, 65: 119-124.

33. Rossi M, Pellegrini C, Cardelli L, Ciciarelli V, di Nardo L, Fargnoli MC. (2019) Familial melanoma: diagnostic and management implications. Dermatology Practical & Conceptual, 9: 10-16.

34. Chudnovsky Y, Khavari PA, Adams AE. (2005) Melanoma genetics and the development of rational therapeutics. J Clin Invest, 115: 813-824.

35. Harland M, Petljak M, Robles-Espinoza CD, Ding Z, Gruis NA, van Doorn R, Pooley KA, Dunning AM, Aoude LG, Wadt KAW, Gerdes AM, Brown KM, Hayward NK, Newton-Bishop JA, Adams DJ, Bishop DT. (2016) Germline TERT promoter mutations are rare in familial melanoma. Familial Cancer, 15: 139-144.

36. Horn S, Figl A, Rachakonda PS, Fischer C, Sucker A, Gast A, Kadel S, Moll I, Nagore E, Hemminki K, Schadendorf D, Kumar R. (2013) TERT promoter mutations in familial and sporadic melanoma. Science, 339: 959-961.

37. Aoude LG, Pritchard AL, Robles-Espinoza CD, Wadt K, Harland M, Choi J, Gartside M, Quesada V, Johansson P, Palmer JM, Ramsay AJ, Zhang X, Jones K, Symmons J, Holland EA, Schmid H, Bonazzi V, Woods S, Dutton-Regester K, Stark MS, Snowden H, Van Doorn R, Montgomery GW, Martin NG, Keane TM, López-Otín C, Gerdes AM, Olsson H, Ingvar C, Borg A, Gruis NA, Trent JM, Jönsson G, Bishop DT, Mann GJ, Newton-Bishop JA, Brown KM, Adams DJ, Hayward NK. (2015) Nonsense mutations in the shelterin complex genes ACD and TERF2IP in familial melanoma. Journal of the National Cancer Institute, 107.

38. Shi J, Yang XR, Ballew B, Rotunno M, Calista D, Fargnoli MC, Ghiorzo P, Bressac-De Paillerets B, Nagore E, Avril MF, Caporaso NE, McMaster ML, Cullen M, Wang Z, Zhang X, Bruno W, Pastorino L, Queirolo P, Banuls-Roca J, Garcia-Casado Z, Vaysse A, Mohamdi H, Riazalhosseini Y, Foglio M, Jouenne

F, Hua X, Hyland PL, Yin J, Vallabhaneni H, Chai W, Minghetti P, Pellegrini C, Ravichandran S, Eggermont A, Lathrop M, Peris K, Scarra GB, Landi G, Savage SA, Sampson JN, He J, Yeager M, Goldin LR, Demenais F, Chanock SJ, Tucker MA, Goldstein AM, Liu Y, Landi MT. (2014) Rare missense variants in POT1 predispose to familial cutaneous malignant melanoma. Nature Genetics, 46: 482-486.

39. Robles-Espinoza CD, Harland M, Ramsay AJ, Aoude LG, Quesada V, Ding Z, Pooley KA, Pritchard AL, Tiffen JC, Petljak M, Palmer JM, Symmons J, Johansson P, Stark MS, Gartside MG, Snowden H, Montgomery GW, Martin NG, Liu JZ, Choi J, Makowski M, Brown KM, Dunning AM, Keane TM, López-Otín C, Gruis NA, Hayward NK, Bishop DT, Newton-Bishop JA, Adams DJ. (2014) POT1 loss-of-function variants predispose to familial melanoma. Nature Genetics, 46: 478-481.

40. Kanetsky PA, Rebbeck TR, Hummer AJ, Panossian S, Armstrong BK, Kricker A, Marrett LD, Millikan RC, Gruber SB, Culver HA, Zanetti R, Gallagher RP, Dwyer T, Busam K, From L, Mujumdar U, Wilcox H, Begg CB, Berwick M. (2006) Population-based study of natural variation in the melanocortin-1 receptor gene and melanoma. Cancer Research, 66: 9330-9337.

41. Newton RA, Roberts DW, Leonard JH, Sturm RA. (2007) Human melanocytes expressing MC1R variant alleles show impaired activation of multiple signaling pathways. Peptides, 28: 2387-2396.

42. Koludrovic D, Davidson I. (2013) MITF, the Janus transcription factor of melanoma. Future Oncol, 9: 235-244.

43. Yokoyama S, Woods SL, Boyle GM, Aoude LG, MacGregor S, Zismann V, Gartside M, Cust AE, Haq R, Harland M, Taylor JC, Duffy DL, Holohan K, Dutton-Regester K, Palmer JM, Bonazzi V, Stark MS, Symmons J, Law MH, Schmidt C, Lanagan C, O'Connor L, Holland EA, Schmid H, Maskiell JA, Jetann J, Ferguson M, Jenkins MA, Kefford RF, Giles GG, Armstrong BK, Aitken JF, Hopper JL, Whiteman DC, Pharoah PD, Easton DF, Dunning AM, Newton-Bishop JA, Montgomery GW, Martin NG, Mann GJ, Bishop DT, Tsao H, Trent JM, Fisher DE, Hayward NK, Brown KM. (2011) A novel recurrent mutation in MITF predisposes to familial and sporadic melanoma. Nature, 480: 99-103.

44. Bertolotto C, Lesueur F, Giuliano S, Strub T, De Lichy M, Bille K, Dessen P, D'Hayer B, Mohamdi H, Remenieras A, Maubec E, De La Fouchardière A, Molinié V, Vabres P, Dalle S, Poulalhon N, Martin-Denavit T, Thomas L, Andry-Benzaquen P, Dupin N, Boitier F, Rossi A, Perrot JL, Labeille B, Robert C,

Escudier B, Caron O, Brugières L, Saule S, Gardie B, Gad S, Richard S, Couturier J, Teh BT, Ghiorzo P, Pastorino L, Puig S, Badenas C, Olsson H, Ingvar C, Rouleau E, Lidereau R, Bahadoran P, Vielh P, Corda E, Blanché H, Zelenika D, Galan P, Aubin F, Bachollet B, Becuwe C, Berthet P, Jean Bignon Y, Bonadona V, Bonafe JL, Bonnet-Dupeyron MN, Cambazard F, Chevrant-Breton J, Coupier I, Dalac S, Demange L, D'Incan M, Dugast C, Faivre L, Vincent-Fétita L, Gauthier-Villars M, Gilbert B, Grange F, Grob JJ, Humbert P, Janin N, Joly P, Kerob D, Lasset C, Leroux D, Levang J, Limacher JM, Livideanu C, Longy M, Lortholary A, Stoppa-Lyonnet D, Mansard S, Mansuy L, Marrou K, Matéus C, Maugard C, Meyer N, Nogues C, Souteyrand P, Venat-Bouvet L, Zattara H, Chaudru V, Lenoir GM, Lathrop M, Davidson I, Avril MF, Demenais F, Ballotti R, Bressac-De Paillerets B. (2011) A SUMOylation-defective MITF germline mutation predisposes to melanoma and renal carcinoma. Nature, 480: 94-98.

45. Rauen KA. (2013) The RASopathies. Annual Review of Genomics and Human Genetics, 14: 355-369.

46. Knight T, Irving JA. (2014) Ras/Raf/MEK/ERK Pathway Activation in Childhood Acute Lymphoblastic Leukemia and Its Therapeutic Targeting. Front Oncol, 4: 160.

47. Santarpia L, Lippman SM, El-Naggar AK. (2012) Targeting the MAPKRASRAF signaling pathway in cancer therapy. Expert Opinion on Therapeutic Targets, 16: 103-119.

48. Gaggioli C, Robert G, Bertolotto C, Bailet O, Abbe P, Spadafora A, Bahadoran P, Ortonne JP, Baron V, Ballotti R, Tartare-Deckert S. (2007) Tumor-derived fibronectin is involved in melanoma cell invasion and regulated by V600E B-Raf signaling pathway. Journal of Investigative Dermatology, 127: 400-410.

49. Davies H, Bignell GR, Cox C, Stephens P, Edkins S, Clegg S, Teague J, Woffendin H, Garnett MJ, Bottomley W, Davis N, Dicks E, Ewing R, Floyd Y, Gray K, Hall S, Hawes R, Hughes J, Kosmidou V, Menzies A, Mould C, Parker A, Stevens C, Watt S, Hooper S, Jayatilake H, Gusterson BA, Cooper C, Shipley J, Hargrave D, Pritchard-Jones K, Maitland N, Chenevix-Trench G, Riggins GJ, Bigner DD, Palmieri G, Cossu A, Flanagan A, Nicholson A, Ho JWC, Leung SY, Yuen ST, Weber BL, Seigler HF, Darrow TL, Paterson H, Wooster R, Stratton MR, Futreal PA. (2002) Mutations of the BRAF gene in human cancer. Nature, 417: 949-954.

50. Akbani R, Akdemir KC, Aksoy BA, Albert M, Ally A, Amin SB, Arachchi H, Arora A, Auman JT, Ayala B, Baboud J, Balasundaram M, Balu S, Barnabas N,

Bartlett J, Bartlett P, Bastian BC, Baylin SB, Behera M, Belyaev D, Benz C, Bernard B, Beroukhim R, Bir N, Black AD, Bodenheimer T, Boice L, Boland GM, Bono R, Bootwalla MS, Bosenberg M, Bowen J, Bowlby R, Bristow CA, Brockway-Lunardi L, Brooks D, Brzezinski J, Bshara W, Buda E, Burns WR, Butterfield YSN, Button M, Calderone T, Cappellini GA, Carter C, Carter SL, Cherney L, Cherniack AD, Chevalier A, Chin L, Cho J, Cho RJ, Choi YL, Chu A, Chudamani S, Cibulskis K, Ciriello G, Clarke A, Coons S, Cope L, Crain D, Curley E, Danilova L, D'Atri S, Davidsen T, Davies MA, Delman KA, Demchok JA, Deng QA, Deribe YL, Dhalla N, Dhir R, Dicara D, Dinikin M, Dubina M, Ebrom JS, Egea S, Eley G, Engel J, Eschbacher JM, Fedosenko KV, Felau I, Fennell T, Ferguson ML, Fisher S, Flaherty KT, Frazer S, Frick J, Fulidou V, Gabriel SB, Gao J, Gardner J, Garraway LA, Gastier-Foster JM, Gaudioso C, Gehlenborg N, Genovese G, Gerken M, Gershenwald JE, Getz G, Gomez-Fernandez C, Gribbin T, Grimsby J, Gross B, Guin R, Gutschner T, Hadjipanayis A, Halaban R, Hanf B, Haussler D, Haydu LE, Hayes DN, Hayward NK, Heiman DI, Herbert L, Herman JG, Hersey P, Hoadley KA, Hodis E, Holt RA, Hoon DS, Hoppough S, Hoyle AP, Huang FW, Huang M, Huang S, Hutter CM, Ibbs M, Iype L, Jacobsen A, Jakrot V, Janning A, Jeck WR, Jefferys SR, Jensen MA, Jones CD, Jones SJM, Ju Z, Kakavand H, Kang H, Kefford RF, Khuri FR, Kim J, Kirkwood JM, Klode J, Korkut A, Korski K, Krauthammer M, Kucherlapati R, Kwong LN, Kycler W, Ladanyi M, Lai PH, Laird PW, Lander E, Lawrence MS, Lazar AJ, Łaźniak R, Lee D, Lee JE, Lee J, Lee K, Lee S, Lee W, Leporowska E, Leraas KM, Li HI, Lichtenberg TM, Lichtenstein L, Lin P, Ling S, Liu J, Liu O, Liu W, Long GV, Lu Y, Ma S, Ma Y, Mackiewicz A, Mahadeshwar HS, Malke J, Mallery D, Manikhas GM, Mann GJ, Marra MA, Matejka B, Mayo M, Mehrabi S, Meng S, Meyerson M, Mieczkowski PA, Miller JP, Miller ML, Mills GB, Moiseenko F, Moore RA, Morris S, Morrison C, Morton D, Moschos S, Mose LE, Muller FL, Mungall AJ, Murawa D, Murawa P, Murray BA, Nezi L, Ng S, Nicholson D, Noble MS, Osunkoya A, Owonikoko TK, Ozenberger BA, Pagani E, Paklina OV, Pantazi A, Parfenov M, Parfitt J, Park PJ, Park WY, Parker JS, Passarelli F, Penny R, Perou CM, Pihl TD, Potapova O, Prieto VG, Protopopov A, Quinn MJ, Radenbaugh A, Rai K, Ramalingam SS, Raman AT, Ramirez NC, Ramirez R, Rao U, Rathmell WK, Ren X, Reynolds SM, Roach J, Robertson AG, Ross MI, Roszik J, Russo G, Saksena G, Saller C, Samuels Y, Sander C, Sander C, Sandusky G, Santoso N, Saul M, Saw RP, Schadendorf D, Schein JE, Schultz N, Schumacher SE, Schwallier C, Scolyer RA, Seidman J, Sekhar PC, Sekhon HS, Senbabaoglu Y, Seth S, Shannon KF, Sharpe S, Sharpless NE, Shaw KRM, Shelton C, Shelton T, Shen R, Sheth M, Shi Y, Shiau CJ, Shmulevich I, Sica GL, Simons JV, Sinha R, Sipahimalani P, Sofia HJ, Soloway MG, Song X, Sougnez C, Spillane AJ, Spychała A, Stretch JR, Stuart J, Suchorska WM, Sucker A, Sumer SO, Sun Y, Synott M, Tabak B, Tabler TR, Tam A, Tan D, Tang J, Tarnuzzer R,

Tarvin K, Tatka H, Taylor BS, Teresiak M, Thiessen N, Thompson JF, Thorne L, Thorsson V, Trent JM, Triche TJ, Tsai KY, Tsou P, Van Den Berg DJ, Van Allen EM, Veluvolu U, Verhaak RG, Voet D, Voronina O, Walter V, Walton JS, Wan Y, Wang Y, Wang Z, Waring S, Watson IR, Weinhold N, Weinstein JN, Weisenberger DJ, White P, Wilkerson MD, Wilmott JS, Wise L, Wiznerowicz M, Woodman SE, Wu CJ, Wu CC, Wu J, Wu Y, Xi R, Xu AW, Yang D, Yang L, Yang L, Zack TI, Zenklusen JC, Zhang H, Zhang J, Zhang W, Zhao X, Zhu J, Zhu K, Zimmer L, Zmuda E, Zou L. (2015) Genomic Classification of Cutaneous Melanoma. Cell, 161: 1681-1696.

51. Munoz-Couselo E, Garcia JS, Perez-Garcia JM, Cebrian VO, Castan JC. (2015) Recent advances in the treatment of melanoma with BRAF and MEK inhibitors. Ann Transl Med, 3: 207.

52. Walia V, Mu EW, Lin JC, Samuels Y. (2012) Delving into somatic variation in sporadic melanoma. Pigment Cell Melanoma Res, 25: 155-170.

53. Jiang W, Jia P, Hutchinson KE, Johnson DB, Sosman JA, Zhao Z. (2015) Clinically relevant genes and regulatory pathways associated with NRASQ61 mutations in melanoma through an integrative genomics approach. Oncotarget, 6: 2496-2508.

54. Munoz-Maldonado C, Zimmer Y, Medova M. (2019) A Comparative Analysis of Individual RAS Mutations in Cancer Biology. Front Oncol, 9: 1088.

55. Roh MR, Eliades P, Gupta S, Tsao H. (2015) Genetics of melanocytic nevi. Pigment Cell and Melanoma Research, 28: 661-672.

56. Sharma R, Wu X, Rhodes SD, Chen S, He Y, Yuan J, Li J, Yang X, Li X, Jiang L, Kim ET, Stevenson DA, Viskochil D, Xu M, Yang FC. (2013) Hyperactive Ras/MAPK signaling is critical for tibial nonunion fracture in neurobromin-decient mice. Human Molecular Genetics, 22: 4818-4828.

57. Maertens O, Johnson B, Hollstein P, Frederick DT, Cooper ZA, Messiaen L, Bronson RT, McMahon M, Granter S, Flaherty K, Wargo JA, Marais R, Cichowski K, Affi. (2012) Elucidating Distinct Roles for NF1 in Melanomagenesis. doi:10.1158/2159-8290.CD-12-0313.

58. Hayward NK, Wilmott JS, Waddell N, Johansson PA, Field MA, Nones K, Patch AM, Kakavand H, Alexandrov LB, Burke H, Jakrot V, Kazakoff S, Holmes O, Leonard C, Sabarinathan R, Mularoni L, Wood S, Xu Q, Waddell N, Tembe V, Pupo GM, De Paoli-Iseppi R, Vilain RE, Shang P, Lau LMS, Dagg RA, Schramm SJ, Pritchard A, Dutton-Regester K, Newell F, Fitzgerald A, Shang CA,

Grimmond SM, Pickett HA, Yang JY, Stretch JR, Behren A, Kefford RF, Hersey P, Long GV, Cebon J, Shackleton M, Spillane AJ, Saw RPM, López-Bigas N, Pearson JV, Thompson JF, Scolyer RA, Mann GJ. (2017) Whole-genome landscapes of major melanoma subtypes. Nature, 545: 175-180.

59. Hodis E, Watson IR, Kryukov GV, Arold ST, Imielinski M, Theurillat JP, Nickerson E, Auclair D, Li L, Place C, Dicara D, Ramos AH, Lawrence MS, Cibulskis K, Sivachenko A, Voet D, Saksena G, Stransky N, Onofrio RC, Winckler W, Ardlie K, Wagle N, Wargo J, Chong K, Morton DL, Stemke-Hale K, Chen G, Noble M, Meyerson M, Ladbury JE, Davies MA, Gershenwald JE, Wagner SN, Hoon DSB, Schadendorf D, Lander ES, Gabriel SB, Getz G, Garraway LA, Chin L. (2012) A landscape of driver mutations in melanoma. Cell, 150: 251-263.

60. Haigh PI, DiFronzo LA, McCready DR. (2003) Optimal excision margins for primary cutaneous melanoma: A systematic review and meta-analysis. Canadian Journal of Surgery, 46: 419-426.

61. Testori A, Rutkowski P, Marsden J, Bastholt L, Chiarion-Sileni V, Hauschild A, Eggermont AMM. (2009) Surgery and radiotherapy in the treatment of cutaneous melanoma. Annals of Oncology, 20.

62. Luke JJ, Schwartz GK. (2013) Chemotherapy in the management of advanced cutaneous malignant melanoma. Clinics in Dermatology, 31: 290-297.

63. Holderfield M, Deuker MM, McCormick F, McMahon M. (2014) Targeting RAF kinases for cancer therapy: BRAF-mutated melanoma and beyond. Nature Reviews Cancer, 14: 455-467.

64. Hauschild A, Grob JJ, Demidov LV, Jouary T, Gutzmer R, Millward M, Rutkowski P, Blank CU, Miller WH, Kaempgen E, Martín-Algarra S, Karaszewska B, Mauch C, Chiarion-Sileni V, Martin AM, Swann S, Haney P, Mirakhur B, Guckert ME, Goodman V, Chapman PB. (2012) Dabrafenib in BRAF-mutated metastatic melanoma: A multicentre, open-label, phase 3 randomised controlled trial. The Lancet, 380: 358-365.

65. Akira S, Uematsu S, Takeuchi O. (2006) Pathogen recognition and innate immunity. Cell, 124: 783-801.

66. Di Trolio R, Simeone E, Di Lorenzo G, Buonerba C, Ascierto PA. (2015) The use of interferon in melanoma patients: A systematic review. Cytokine and Growth Factor Reviews, 26: 203-212.

67. Petrella T, Quirt I, Verma S, Haynes AE, Charette M, Bak K. (2007) Single-agent interleukin-2 in the treatment of metastatic melanoma: A systematic review. Cancer Treatment Reviews, 33: 484-496.

68. Bardhan K, Anagnostou T, Boussiotis VA. (2016) The PD1: PD-L1/2 pathway from discovery to clinical implementation. Frontiers in Immunology, 7.

69. Weber JS, D'Angelo SP, Minor D, Hodi FS, Gutzmer R, Neyns B, Hoeller C, Khushalani NI, Miller WH, Lao CD, Linette GP, Thomas L, Lorigan P, Grossmann KF, Hassel JC, Maio M, Sznol M, Ascierto PA, Mohr P, Chmielowski B, Bryce A, Svane IM, Grob JJ, Krackhardt AM, Horak C, Lambert A, Yang AS, Larkin J. (2015) Nivolumab versus chemotherapy in patients with advanced melanoma who progressed after anti-CTLA-4 treatment (CheckMate 037): A randomised, controlled, open-label, phase 3 trial. The Lancet Oncology, 16: 375-384.

70. Karlsson AK, Saleh SN. (2017) Checkpoint inhibitors for malignant melanoma: A systematic review and meta-analysis. Clinical, Cosmetic and Investigational Dermatology, 10: 325-339.

71. Espenel S, Vallard A, Rancoule C, Garcia MA, Guy JB, Chargari C, Deutsch E, Magné N. (2017) Melanoma: Last call for radiotherapy. Critical Reviews in Oncology/Hematology, 110: 13-19.

72. Guadagnolo BA, Zagars GK. (2009) Adjuvant radiation therapy for high-risk nodal metastases from cutaneous melanoma. The Lancet Oncology, 10: 409-416.

73. Agrawal S, Kane JM, Guadagnolo BA, Kraybill WG, Ballo MT. (2009) The benefits of adjuvant radiation therapy after therapeutic lymphadenectomy for clinically advanced, high-risk, lymph node-metastatic melanoma. Cancer, 115: 5836-5844.

74. Henderson MA, Burmeister BH, Ainslie J, Fisher R, Di Iulio J, Smithers BM, Hong A, Shannon K, Scolyer RA, Carruthers S, Coventry BJ, Babington S, Duprat J, Hoekstra HJ, Thompson JF. (2015) Adjuvant lymph-node field radiotherapy versus observation only in patients with melanoma at high risk of further lymph-node field relapse after lymphadenectomy (ANZMTG 01.02/TROG 02.01): 6-year follow-up of a phase 3, randomised controlled trial. The Lancet Oncology, 16: 1049-1060.

75. Bibault JE, Dewas S, Mirabel X, Mortier L, Penel N, Vanseymortier L, Lartigau E. (2011) Adjuvant radiation therapy in metastatic lymph nodes from melanoma. Radiation Oncology, 6: 12-12.

76. Bommareddy PK, Patel A, Hossain S, Kaufman HL. (2017) Talimogene Laherparepvec (T-VEC) and Other Oncolytic Viruses for the Treatment of Melanoma. American Journal of Clinical Dermatology, 18.

77. Andtbacka RHI, Kaufman HL, Collichio F, Amatruda T, Senzer N, Chesney J, Delman KA, Spitler LE, Puzanov I, Agarwala SS, Milhem M, Cranmer L, Curti B, Lewis K, Ross M, Guthrie T, Linette GP, Daniels GA, Harrington K, Middleton MR, Miller WH, Zager JS, Ye Y, Yao B, Li A, Doleman S, Van Der Walde A, Gansert J, Coffin RS. (2015) Talimogene laherparepvec improves durable response rate in patients with advanced melanoma. Journal of Clinical Oncology, 33: 2780-2788.

78. Jungbluth AA, Busam KJ, Kolb D, Iversen K, Coplan K, Chen YT, Spagnoli GC, Old LJ. (2000) Expression of MAGE-antigens in normal tissues and cancer. International Journal of Cancer, 85: 460-465.

79. Kruit WHJ, Suciu S, Dreno B, Mortier L, Robert C, Chiarion-Sileni V, Maio M, Testori A, Dorval T, Grob JJ, Becker JC, Spatz A, Eggermont AMM, Louahed J, Lehmann FF, Brichard VG, Keilholz U. (2013) Selection of immunostimulant AS15 for active immunization with MAGE-A3 protein: Results of a randomized phase II study of the European organisation for research and treatment of cancer melanoma group in metastatic melanoma. Journal of Clinical Oncology, 31: 2413-2420.

80. Nguyen LT, Saibil SD, Sotov V, Le MX, Khoja L, Ghazarian D, Bonilla L, Majeed H, Hogg D, Joshua AM, Crump M, Franke N, Spreafico A, Hansen A, Al-Habeeb A, Leong W, Easson A, Reedijk M, Goldstein DP, McCready D, Yasufuku K, Waddell T, Cypel M, Pierre A, Zhang B, Boross-Harmer S, Cipollone J, Nelles M, Scheid E, Fyrsta M, Lo CS, Nie J, Yam JY, Yen PH, Gray D, Motta V, Elford AR, DeLuca S, Wang L, Effendi S, Ellenchery R, Hirano N, Ohashi PS, Butler MO. (2019) Phase II clinical trial of adoptive cell therapy for patients with metastatic melanoma with autologous tumor-infiltrating lymphocytes and low-dose interleukin-2. Cancer Immunology, Immunotherapy, 68: 773-785.

81. Bernatchez C, Radvanyi LG, Hwu P. (2012) Advances in the treatment of metastatic melanoma: Adoptive T-cell therapy. Seminars in Oncology, 39: 215-226.

82. Cavalcante GC, Schaan AP, Cabral GF, Santana-da-Silva MN, Pinto P, Vidal AF, Ribeiro-Dos-Santos A. (2019) A Cell's Fate: An Overview of the Molecular Biology and Genetics of Apoptosis. Int J Mol Sci, 20.

83. Hengartner MO. (2001) Apoptosis: corralling the corpses. Cell, 104: 325-328.

84. Schneider P, Tschopp J. (2000) Apoptosis induced by death receptors. Pharm Acta Helv, 74: 281-286.

85. Walczak H. (2013) Death receptor-ligand systems in cancer, cell death, and inflammation. Cold Spring Harb Perspect Biol, 5: a008698.

86. Dickens LS, Boyd RS, Jukes-Jones R, Hughes MA, Robinson GL, Fairall L, Schwabe JWR, Cain K, MacFarlane M. (2012) A Death Effector Domain Chain DISC Model Reveals a Crucial Role for Caspase-8 Chain Assembly in Mediating Apoptotic Cell Death. Molecular Cell, 47: 291-305.

87. Zhou DR, Eid R, Miller KA, Boucher E, Mandato CA, Greenwood MT. (2019) Intracellular second messengers mediate stress inducible hormesis and Programmed Cell Death: A review. Biochim Biophys Acta Mol Cell Res, 1866: 773-792.

88. Danial NN, Korsmeyer SJ. (2004) Cell death: critical control points. Cell, 116: 205-219.

89. Kale J, Osterlund EJ, Andrews DW. (2018) BCL-2 family proteins: changing partners in the dance towards death. Cell Death Differ, 25: 65-80.

90. Kroemer G, Galluzzi L, Brenner C. (2007) Mitochondrial membrane permeabilization in cell death. Physiol Rev, 87: 99-163.

91. Ghobrial IM, Witzig TE, Adjei AA. (2005) Targeting Apoptosis Pathways in Cancer Therapy. CA: A Cancer Journal for Clinicians, 55: 178-194.

92. Fernandez-Capetillo O, Lee A, Nussenzweig M, Nussenzweig A. (2004) H2AX: the histone guardian of the genome. DNA Repair (Amst), 3: 959-967.

93. Fernandez-Capetillo O, Celeste A, Nussenzweig A. (2003) Focusing on foci: H2AX and the recruitment of DNA-damage response factors. Cell Cycle, 2: 426-427.

94. Rao VA, Fan AM, Meng L, Doe CF, North PS, Hickson ID, Pommier Y. (2005) Phosphorylation of BLM, Dissociation from Topoisomerase IIIα, and Colocalization with γ-H2AX after Topoisomerase I-Induced Replication Damage. Molecular and Cellular Biology, 25: 8925-8937.

95. Ward IM, Chen J. (2001) Histone H2AX Is Phosphorylated in an ATR-dependent Manner in Response to Replicational Stress. Journal of Biological Chemistry, 276: 47759-47762.

96. Furuta T, Takemura H, Liao ZY, Aune GJ, Redon C, Sedelnikova OA, Pilch DR, Rogakou EP, Celeste A, Chen HT, Nussenzweig A, Aladjem MI, Bonner WM, Pommier Y. (2003) Phosphorylation of histone H2AX and activation of Mre11, Rad50, and Nbs1 in response to replication-dependent DNA double-strand breaks induced by mammalian DNA topoisomerase I cleavage complexes. Journal of Biological Chemistry, 278: 20303-20312.

97. Bartek J, Lukas J. (2001) Mammalian G1- and S-phase checkpoints in response to DNA damage. Curr Opin Cell Biol, 13: 738-747.

98. Amaya-Montoya M, Perez-Londono A, Guatibonza-Garcia V, Vargas-Villanueva A, Mendivil CO. (2020) Cellular Senescence as a Therapeutic Target for Age-Related Diseases: A Review. Adv Ther, 37: 1407-1424.

99. El-Deiry WS, Kern SE, Pietenpol JA, Kinzler KW, Vogelstein B. (1992) Definition of a consensus binding site for p53. Nature Genetics, 1: 45-49.

100. Childs BG, Baker DJ, Kirkland JL, Campisi J, Deursen JM. (2014) Senescence and apoptosis: dueling or complementary cell fates? EMBO reports, 15: 1139-1153.

101. Levine AJ, Hu W, Feng Z. (2006) The P53 pathway: what questions remain to be explored? Cell Death Differ, 13: 1027-1036.

102. Afshari CA, Nichols MA, Xiong Y, Mudryj M. (1996) A role for a p21-E2F interaction during senescence arrest of normal human fibroblasts. Cell Growth and Differentiation, 7: 979-988.

103. Li R, Waga S, Hannon GJ, Beach D, Stillman B. (1994) Differential effects by the p21 CDK inhibitor on PCNA-dependent DNA replication and repair. Nature, 371: 534-537.

104. Waga S, Hannon GJ, Beach D, Stillman B. (1994) The p21 inhibitor of cyclin-dependent kinases controls DNA replication by interaction with PCNA. Nature, 369: 574-578.

105. Balkwill FR, Capasso M, Hagemann T. (2012) The tumor microenvironment at a glance. Journal of Cell Science, 125: 5591-5596.

106. Peltanova B, Raudenska M, Masarik M. (2019) Effect of tumor microenvironment on pathogenesis of the head and neck squamous cell carcinoma: a systematic review. Mol Cancer, 18: 63.

107. Chen DS, Mellman I. (2013) Oncology meets immunology: the cancer-immunity cycle. Immunity, 39: 1-10.

108. Spel L, Boelens J-J, Nierkens S, Boes M. (2013) Antitumor immune responses mediated by dendritic cells: How signals derived from dying cancer cells drive antigen cross-presentation. OncoImmunology, 2: e26403-e26403.

109. Gabrilovich D. (2004) Mechanisms and functional significance of tumour-induced dendritic-cell defects. Nat Rev Immunol, 4: 941-952.

110. Ljunggren HG, Kärre K. (1990) In search of the 'missing self': MHC molecules and NK cell recognition. Immunology Today, 11: 237-244.

111. Lopez-Botet M, Moretta L, Strominger J. (1996) NK-cell receptors and recognition of MHC class I molecules. Immunol Today, 17: 212-214.

112. Vivier E, Tomasello E, Baratin M, Walzer T, Ugolini S. (2008) Functions of natural killer cells. Nat Immunol, 9: 503-510.

113. Schreiber RD, Old LJ, Smyth MJ. (2011) Cancer immunoediting: integrating immunity's roles in cancer suppression and promotion. Science, 331: 1565-1570.

114. Dunn GP, Old LJ, Schreiber RD. (2004) The immunobiology of cancer immunosurveillance and immunoediting. Immunity, 21: 137-148.

115. Gabrilovich DI, Nagaraj S. (2009) Myeloid-derived suppressor cells as regulators of the immune system. Nat Rev Immunol, 9: 162-174.

116. Franciszkiewicz K, Boissonnas A, Boutet M, Combadiere C, Mami-Chouaib F. (2012) Role of chemokines and chemokine receptors in shaping the effector phase of the antitumor immune response. Cancer Res, 72: 6325-6332.

117. Motz GT, Coukos G. (2013) Deciphering and reversing tumor immune suppression. Immunity, 39: 61-73.

118. Mougiakakos D, Choudhury A, Lladser A, Kiessling R, Johansson CC. (2010) Regulatory T cells in cancer. Adv Cancer Res, 107: 57-117.

119. Zou W. (2006) Regulatory T cells, tumour immunity and immunotherapy. Nat Rev Immunol, 6: 295-307.

120. Schreck S, Friebel D, Buettner M, Distel L, Grabenbauer G, Young LS, Niedobitek G. (2009) Prognostic impact of tumour-infiltrating Th2 and regulatory T cells in classical Hodgkin Lymphoma. Hematological Oncology, 27: 31-39.

121. Sakaguchi S. (2004) Naturally arising CD4+ regulatory t cells for immunologic self-tolerance and negative control of immune responses. Annu Rev Immunol, 22: 531-562.

122. Almand B, Clark JI, Nikitina E, van Beynen J, English NR, Knight SC, Carbone DP, Gabrilovich DI. (2001) Increased Production of Immature Myeloid Cells in Cancer Patients: A Mechanism of Immunosuppression in Cancer. The Journal of Immunology, 166: 678-689.

123. Khaled YS, Ammori BJ, Elkord E. (2013) Myeloid-derived suppressor cells in cancer: recent progress and prospects. Immunol Cell Biol, 91: 493-502.

124. Tadmor T, Attias D, Polliack A. (2011) Myeloid-derived suppressor cells--their role in haemato-oncological malignancies and other cancers and possible implications for therapy. Br J Haematol, 153: 557-567.

125. Nagaraj S, Schrum AG, Cho H-I, Celis E, Gabrilovich DI. (2010) Mechanism of T Cell Tolerance Induced by Myeloid-Derived Suppressor Cells. The Journal of Immunology, 184: 3106-3116.

126. Lutgens L, van der Zee J, Pijls-Johannesma M, De Haas-Kock DF, Buijsen J, Mastrigt GA, Lammering G, De Ruysscher DK, Lambin P. (2010) Combined use of hyperthermia and radiation therapy for treating locally advanced cervical carcinoma. Cochrane Database Syst Rev, doi:10.1002/14651858.CD006377.pub2: CD006377.

127. Tabuchi Y, Wada S, Furusawa Y, Ohtsuka K, Kondo T. (2012) Gene networks related to the cell death elicited by hyperthermia in human oral squamous cell carcinoma HSC-3 cells. International Journal of Molecular Medicine, 29: 380-386.

128. Hegyi G, Szigeti GP, Szasz A. (2013) Hyperthermia versus Oncothermia: Cellular Effects in Complementary Cancer Therapy. Evid Based Complement Alternat Med, 2013: 672873.

129. Wust P, Hildebrandt B, Sreenivasa G, Rau B, Gellermann J, Riess H, Felix R, Schlag PM. (2002) Hyperthermia in combined treatment of cancer. Lancet Oncol, 3: 487-497.

130. Sharif-Khatibi L, Kariminia A, Khoei S, Goliaei B. (2007) Hyperthermia induces differentiation without apoptosis in permissive temperatures in human erythroleukaemia cells. International Journal of Hyperthermia, 23: 645-655.

131. van der Zee J. (2002) Heating the patient: a promising approach? Ann Oncol, 13: 1173-1184.

132. Krishnan S, Diagaradjane P, Cho SH. (2010) Nanoparticle-mediated thermal therapy: evolving strategies for prostate cancer therapy. Int J Hyperthermia, 26: 775-789.

133. Habash RW, Bansal R, Krewski D, Alhafid HT. (2006) Thermal therapy, part 2: hyperthermia techniques. Crit Rev Biomed Eng, 34: 491-542.

134. Falk MH, Issels RD. (2001) Hyperthermia in oncology. Int J Hyperthermia, 17: 1-18.

135. Behrouzkia Z, Joveini Z, Keshavarzi B, Eyvazzadeh N, Aghdam RZ. (2016) Hyperthermia: How Can It Be Used? Oman Med J, 31: 89-97.

136. Bijelic L, Sugarbaker PH, Stuart OA. (2012) Hyperthermic intraperitoneal chemotherapy with melphalan: a summary of clinical and pharmacological data in 34 patients. Gastroenterol Res Pract, 2012: 827534.

137. Neuwirth MG, Alexander HR, Karakousis GC. (2016) Then and now: cytoreductive surgery with hyperthermic intraperitoneal chemotherapy (HIPEC), a historical perspective. J Gastrointest Oncol, 7: 18-28.

138. Prosnitz LR, Maguire P, Anderson JM, Scully SP, Harrelson JM, Jones EL, Dewhirst M, Samulski TV, Powers BE, Rosner GL, Dodge RK, Layfield L, Clough R, Brizel DM. (1999) The treatment of high-grade soft tissue sarcomas with preoperative thermoradiotherapy. International Journal of Radiation Oncology Biology Physics, 45: 941-949.

139. Song CW, Patten MS, Chelstrom LM, Rhee JG, Levitt SH. (1987) Effect of multiple heatings on the blood flow in RIF-1 tumours, skin and muscle of c3h mice. International Journal of Hyperthermia, 3: 535-545.

140. Valdagni R, Amichetti M. (1994) Report of long-term follow-up in a randomized trial comparing radiation therapy and radiation therapy plus hyperthermia to metastatic lymphnodes in stage IV head and neck patients. International Journal of Radiation Oncology, Biology, Physics, 28: 163-169.

141. Wiedemann GJ, Robins HI, Gutsche S, Mentzel M, Decken M, Katschinski DM, Eleftheriadis S, Crahé R, Weiss C, Storer B, Wagner T. (1996) Ifosfamide, Carboplatin and Etoposide (ICE) combined with 41.8°C whole body hyperthermia in patients with refractory sarcoma. European Journal of Cancer, 32: 888-892.

142. Issels RD, Abdel-Rahman S, Wendtner C, Falk MH, Kurze V, Sauer H, Aydemir U, Hiddemann W. (2001) Neoadjuvant chemotherapy combined with regional hyperthermia (RHT) for locally advanced primary or recurrent high-risk adult soft-tissue sarcomas (STS) of adults: long-term results of a phase II study. Eur J Cancer, 37: 1599-1608.

143. Shchors K, Evan G. (2007) Tumor angiogenesis: cause or consequence of cancer? Cancer Res, 67: 7059-7061.

144. Bicher HI, Hetzel FW, Sandhu TS, Frinak S, Vaupel P, O'Hara MD, O'Brien T. (1980) Effects of hyperthermia on normal and tumor microenvironment. Radiology, 137: 523-530.

145. Fajardo LF, Schreiber AB, Kelly NI, Hahn GM. (1985) Thermal sensitivity of endothelial cells. Radiation research, 103: 276-285.

146. Kerner T, Deja M, Ahlers O, Hildebrandt B, Dieing A, Riess H, Wust P, Gerlach H. (2002) Monitoring arterial blood pressure during whole body hyperthermia. Acta Anaesthesiologica Scandinavica, 46: 561-566.

147. de Bree E, Tsiftsis DD. (2007) Principles of perioperative intraperitoneal chemotherapy for peritoneal carcinomatosis. Recent results in cancer research. Fortschritte der Krebsforschung. Progrès dans les recherches sur le cancer, 169: 39-51.

148. Takemoto M, Kuroda M, Urano M, Nishimura Y, Kawasaki S, Kato H, Okumura Y, Akaki S, Kanazawa S, Asaumi J, Joja I, Hiraki Y. (2003) The effect of various chemotherapeutic agents given with mild hyperthermia on different types of tumours. International Journal of Hyperthermia, 19: 193-203.

149. Flessner MF. (2005) The transport barrier in intraperitoneal therapy. Am J Physiol Renal Physiol, 288: F433-442.

150. Valle SJ, Alzahrani NA, Liauw W, Sugarbaker PH, Bhatt A, Morris DL. (2016) Hyperthermic Intraperitoneal Chemotherapy (HIPEC) Methodology, Drugs and Bidirectional Chemotherapy. Indian Journal of Surgical Oncology, 7: 152-159.

151. Song CW, Park HJ, Lee CK, Griffin R. (2005) Implications of increased tumor blood flow and oxygenation caused by mild temperature hyperthermia in tumor treatment. Int J Hyperthermia, 21: 761-767.

152. Krenacs T, Meggyeshazi N, Kovago C, Kiss E, Forika G, Balogh A, Vancsik T. (2019) [Mechanism of action of modulated electro- hyperthermia (mEHT) induced tumor damage in colorectal adenocarcinoma models]. Magy Onkol, 63: 359-364.

153. Andocs G, Rehman MU, Zhao QL, Tabuchi Y, Kanamori M, Kondo T. (2016) Comparison of biological effects of modulated electro-hyperthermia and conventional heat treatment in human lymphoma U937 cells. Cell Death Discovery, 2: 1-10.

154. Vander Heiden MG, Cantley LC, Thompson CB. (2009) Understanding the Warburg effect: the metabolic requirements of cell proliferation. Science, 324: 1029-1033.

155. Devic S. (2016) Warburg Effect - a Consequence or the Cause of Carcinogenesis? J Cancer, 7: 817-822.

156. Cardone RA, Casavola V, Reshkin SJ. (2005) The role of disturbed pH dynamics and the Na+/H+ exchanger in metastasis. Nat Rev Cancer, 5: 786-795.

157. Alevizopoulos K, Calogeropoulou T, Lang F, Stournaras C. (2018) Na+/K+ ATPase Inhibitors in Cancer. Current Drug Targets, 15: 988-1000.

158. Wust P, Ghadjar P, Nadobny J, Beck M, Kaul D, Winter L, Zschaeck S. (2019) Physical analysis of temperature-dependent effects of amplitude-modulated electromagnetic hyperthermia. International Journal of Hyperthermia, 36: 1245-1253.

159. Papp E, Vancsik T, Kiss E, Szasz O. (2017) Energy Absorption by the Membrane Rafts in the Modulated Electro-Hyperthermia (mEHT). Open Journal of Biophysics, 07: 216-229.

160. Vincze G, Szigeti G, Andócs G, Szász A. (2015) Nanoheating without artificial nanoparticles. Biology and Medicine, 7.

161. Krenacs T, Meggyeshazi N, Forika G, Kiss E, Hamar P, Szekely T, Vancsik T. (2020) Modulated Electro-Hyperthermia-Induced Tumor Damage Mechanisms Revealed in Cancer Models. Int J Mol Sci, 21.

162. Andocs G, Renner H, Balogh L, Fonyad L, Jakab C, Szasz A. (2009) Strong synergy of heat and modulated electromagnetic field in tumor cell killing. Strahlentherapie und Onkologie, 185: 120-126.

163. Blad B, Baldetorp B. (1996) Impedance spectra of tumour tissue in comparison with normal tissue; a possible clinical application for electrical impedance tomography. Physiol Meas, 17 Suppl 4A: A105-115.

164. Blad B, Wendel P, Jönsson M, Lindström K. (1999) An electrical impedance index to distinguish between normal and cancerous tissues. Journal of Medical Engineering and Technology, 23: 57-62.

165. Fiorentini G, Szasz A. (2006) Hyperthermia today: Electric energy, a new opportunity in cancer treatment. Journal of Cancer Research and Therapeutics, 2: 41-41.

166. Zou Y, Guo Z. (2003) A review of electrical impedance techniques for breast cancer detection. Med Eng Phys, 25: 79-90.

167. Hofheinz F, Li Y, Steffen IG, Lin Q, Lili C, Hua W, van den Hoff J, Zschaeck S. (2019) Confirmation of the prognostic value of pretherapeutic tumor SUR and MTV in patients with esophageal squamous cell carcinoma. European Journal of Nuclear Medicine and Molecular Imaging, 46: 1485-1494.

168. Shin S, Pak K, Kim IJ, Kim BS, Kim SJ. (2017) Prognostic Value of Tumor-to-Blood Standardized Uptake Ratio in Patients with Resectable Non-Small-Cell Lung Cancer. Nuclear Medicine and Molecular Imaging, 51: 233-239.

169. Hofheinz F, Apostolova I, Oehme L, Kotzerke J, Van Den Hoff J. (2017) Test–retest variability in lesion SUV and lesion SUR in18F-FDG PET: An analysis of data from two prospective multicenter trials. Journal of Nuclear Medicine, 58: 1770-1775.

170. Ehrentraut H, Clambey ET, McNamee EN, Brodsky KS, Ehrentraut SF, Poth JM, Riegel AK, Westrich JA, Colgan SP, Eltzschig HK. (2013) CD73+ regulatory T cells contribute to adenosine-mediated resolution of acute lung injury. FASEB Journal, 27: 2207-2219.

171. Sun X, Bizhanova A, Matheson TD, Yu J, Zhu LJ, Kaufman PD. (2017) Ki-67 Contributes to Normal Cell Cycle Progression and Inactive X Heterochromatin in p21 Checkpoint-Proficient Human Cells. Molecular and Cellular Biology, 37.

172. Al Bitar S, Gali-Muhtasib H. (2019) The Role of the Cyclin Dependent Kinase Inhibitor p21(cip1/waf1) in Targeting Cancer: Molecular Mechanisms and Novel Therapeutics. Cancers (Basel), 11.

173. Fragkos M, Jurvansuu J, Beard P. (2009) H2AX Is Required for Cell Cycle Arrest via the p53/p21 Pathway. Molecular and Cellular Biology, 29: 2828-2840.

174. Podhorecka M, Skladanowski A, Bozko P. (2010) H2AX Phosphorylation: Its Role in DNA Damage Response and Cancer Therapy. J Nucleic Acids, 2010.

175. Sun X, Kaufman PD. (2018) Ki-67: more than a proliferation marker. Chromosoma, 127: 175-186.

176. Karimian A, Ahmadi Y, Yousefi B. (2016) Multiple functions of p21 in cell cycle, apoptosis and transcriptional regulation after DNA damage. DNA Repair (Amst), 42: 63-71.

177. Besztercei B, Vancsik T, Benedek A, Major E, Thomas MJ, Schvarcz CA, Krenács T, Benyó Z, Balogh A. (2019) Stress-induced, p53-mediated tumor growth inhibition of melanoma by modulated electrohyperthermia in mouse models without major immunogenic effects. International Journal of Molecular Sciences, 20.

178. Roh JS, Sohn DH. (2018) Damage-Associated Molecular Patterns in Inflammatory Diseases. Immune Netw, 18: e27.

179. Yang KL, Huang CC, Chi MS, Chiang HC, Wang YS, Hsia CC, Andocs G, Wang HE, Chi KH. (2016) In vitro comparison of conventional hyperthermia and modulated electro-hyperthermia. Oncotarget, 7: 84082-84092.

180. Yang H, Villani RM, Wang H, Simpson MJ, Roberts MS, Tang M, Liang X. (2018) The role of cellular reactive oxygen species in cancer chemotherapy. J Exp Clin Cancer Res, 37: 266.

181. Park HS, Kim SR, Lee YC. (2009) Impact of oxidative stress on lung diseases. Respirology, 14: 27-38.

182. Haegens A, Vernooy JHJ, Heeringa P, Mossman BT, Wouters EFM. (2008) Myeloperoxidase modulates lung epithelial responses to pro-inflammatory agents. European Respiratory Journal, 31: 252-260.

DOI:10.14753/SE.2022.2552

10.Bibliography of Candidate's Publications

Publications related to the dissertation

Thomas MJ, Major E, Benedek A, Horváth I, Máthé D, Bergmann R, Szász AM, Krenács T, Benyó Z. (2020) Suppression of metastatic melanoma growth in lung by modulated electro-hyperthermia monitored by a minimally invasive heat stress testing approach in mice. Cancers, 12: 1-24.

Besztercei B, Vancsik T, Benedek A, Major E, **Thomas MJ**, Schvarcz CA, Krenács T, Benyó Z, Balogh A. (2019) Stress-induced, p53-mediated tumor growth inhibition of melanoma by modulated electrohyperthermia in mouse models without major immunogenic effects. International Journal of Molecular Sciences, 20.

Dank M, Balogh A, Benedek A, Besztercei B, Danics LEA, Forika G, Garay T, Hamar P, Karászi Á, Kaucsár T, Kiss É, Krenács T, Major E, Mohácsi R, Portörő I, Ruisanchez É, Schvarcz C, Szász AM, **Thomas JM**, Vancsik T, Zolcsák Z, Benyó Z. (2019) Preclinical and clinical investigation and development of electromag-netic oncological device – experience with solid tumors. Magyar Onkologia, 63: 354-358.

Publications not related to the dissertation

Gaál A, Garay TM, Horváth I, Máthé D, Szöllősi D, Veres DS, **Mbuotidem J**, Kovács T, Tóvári J, Bergmann R, Streli C, Szakács G, Mihály J, Varga Z, Szoboszlai N. (2020) Development and in vivo application of a water-soluble anticancer copper ionophore system using a temperature-sensitive liposome formulation. Pharmaceutics, 12: 466-466.

DOI:10.14753/SE.2022.2552

11.Acknowledgment

I am grateful to Éva Mátrainé Balogh of the 1st Department of Pathology and Experimental Cancer Research, Semmelweis University, Budapest, Hungary for her expert technical assistance. I also thank the *in vivo* Imaging Advanced Core Facility of the Hungarian Center of Excellence for Molecular Medicine and Dr. Domokos Máthé, Dr. Ildikó Horváth, of the Department of Biophysics and Radiation Biology, Semmelweis University, Budapest, Hungary for their help with *in vivo* imaging. I also thank Prof. Ralf Bergmann of Helmholtz-Zentrum Dresden Rossendorf, Institute of Radiopharmaceutical Cancer Research, Dresden, Germany for his expert advice in the PET studies and analysis. I am also thankful to all of my former and recent colleagues: Dr. Andrea Balogh, Dr. Enikő Major, Balázs Besztercei, and Anett Benedek, for their support. I am also grateful to all members of the Institute of Translational Medicine, Semmelweis University, Budapest, Hungary who helped me in any aspect of my doctorate studies. Many thanks to Dr. Tibor Krenács for his support and to Prof. Zoltán Benyó, my supervisor, for his motivation and professional support throughout every aspect of my doctorate work. Finally, I am truly grateful to my beloved family and friends who gave me all the support and motivation I needed throughout my doctorate studies.